

Habilitation à Diriger des Recherches

Présentée par

Sawako Nakamae

Service de Physique de l'État Condensé IRAMIS/DSM/CEA-Saclay

Magnetic Nanoparticles: from Superspin Glass, Superferromagnetism to Energy Applications

Soutenue le 20 novembre 2013 devant le jury compose de:

- Hamid Kachkashi, Université de Perpignan Via Domitia, France (rapporteur)
- Dino Fiorani, Institute of Structure of Materials, CNR-Rome; Italy (rapporteur)
- Christophe Goupil, Ecole Nationale Supérieure d'Ingénieurs de CAEN France (rapporteur)
- André Thiaville, Université Paris-Sud, Orsay, France
- Claude Pasquier, Université Paris-Sud, Orsay, France
- Isabelle Lisiecki, Université Pierre et Marie Curie, Paris, France
- Philippe Monod, Ecole Supérieure de Physique et de Chimie Industrielle de la Ville de Paris, France

Table of contents

1. Introduction	1
2. Magnetic Nanoparticles and Supermagnetism	2
2.1. Single Particle Magnetism	3
2.1.1 Critical Size	3
2.1.2 Magnetic Anisotropy	3
2.1.2.1 Magnetocrystalline Anisotropy	4
2.1.2.2 Surface Anisotropy	4
2.1.3 Superparamagnetism and Blocking Phenomenon	5
2.1.4 Size Polydispersity	7
2.2. Interacting Magnetic Nanoparticles	7
2.2.1 Weakly vs. Strongly Interacting Nanoparticles	8
2.2.2 Collective State at Low Temperature : Superspin Glass	9
2.3. Concluding Remarks	10
3. Spin Glass	11
3.1. Spin Glass Theory	12
3.2. Experiments	13
3.2.1 Glass Transition Temperature	13
3.2.2 Slow and Out-of-Equilibrium Dynamics	15
3.2.2.1 DC Measurements	15
3.2.2.2 AC Measurements	16
3.2.2.3 Noise Measurements	17
3.3. Why Study Superspin Glass?	18
4. Superspin Glass: Experimental Investigations	20
4.1. Dynamic Correlation Length Growth in Superspin Glasses	20
4.1.1 Anisotropy-axis Orientation effect on the magnetization of γ - Fe_2O_3 Frozen Ferrofluid (published work)	23
4.1.2 Dynamic Correlation Length Growth in Superspin Glass: Bridging experiments and simulations (published work)	32
4.2. Violation of Fluctuation-Dissipation Theorem in a Superspin Glass	38
4.2.1 Background	38
4.2.2 Noise Measurements using MicroHall Probes	39
4.2.3 A Local Noise Measurement Device for Magnetic Physical Systems (published work)	40
4.2.4 Experimental Evidence for Violation of the Fluctuation-Dissipation Theorem in a Superspin Glass (published work)	48
5. Perspectives	53
5.1. The Quest for Superferromagnetism	53
5.1.1 Superferromagnetism: Dipolar Ferromagnetism of Superspines?	53
5.1.2 Magnetism of Supracrystals and Nanocrystallinity Effect	55
5.1.2.1 Cobalt Nanoparticles and Supracrystals	55

5.1.2.2	Nanocrystallinity Effect on the Magnetic Property of Co-Supracrystals	56
5.1.3	Superferromagnetism in Co-Supracrystals	57
5.1.3.1	In-situ Magnetic Property Measurements using SQUID magnetometer	58
5.1.3.2	Magnetization Measurements of Supracrystalline Nanorods Using microHall Probes	59
5.1.4	Beyond Superferromagnetism	60
5.2.	Magnetic Nanoparticles for Energy Applications:	
	Magnetothermoelectric effect in Ferrofluids	61
5.2.1	Background	62
5.2.2	Current and Future Research in Liquid Thermoelectric Materials	63
5.2.2.1	Thermoelectric Effects in Nonaqueous Electrolytes and Ionic Liquids	64
5.2.2.2	Thermoelectric and Magnetothermoelectric Effects in Ferrofluids	65
5.2.3	Future Applications	66
5.2.4	Concluding Remarks	67
References		68
Annex I: Research Statement (Projet de Recherche)		73
Annex II: List of Publications		76
Annex III : Curriculum Vitae		81

1. Introduction

Since my arrival to the SPEC/CEA Saclay in 2005, my main research focus has been on the out-of-equilibrium magnetic state of interacting ferromagnetic nanoparticles, now widely known as “superspin glass” (SSG). The aim of this manuscript is to present; 1) the summary of results obtained through the experimental investigations on superspin glasses; and 2) the perspectives on my future research that will continue to be centered around the physics and the applications of magnetic nanoparticles.

The magnetic nanoparticles have been the lodestone in many fields of applied research because they possess attractive and tunable properties that are usable near room temperature. The superparamagnetic blocking phenomena and its associated high coercive field had been suggested for their use in information storage since its discovery [1]. More recently, magnetic nanoparticles have been exploited in biomedical applications where we have witnessed numerous technological breakthroughs [2]. For example, the magnetic nanoparticle thermotherapy, or hyperthermia (where magnetic nanoparticles are injected directly into tumors and subsequently heated in an alternating magnetic field to treat tumor cells) has already entered clinical trials [3]. But since before all these applications became available, the fundamental ‘magnetism’ of nanoparticles has captivated the minds of many scientists, and we continue to discover their interesting new properties. “Superspin Glass” presented in the present manuscript is one such example, characterized by collective and out-of-equilibrium behavior of highly interacting magnetic nanoparticles that bear much resemblance to atomic spin glasses.

The manuscript is organized as follows. Chapter 2 highlights the salient features of magnetic nanoparticle properties and interaction effects. As the focus of the present manuscript is on the interacting systems, certain important topics on the single-particle magnetism of nanoparticles are intentionally omitted, such as surface/interface effects. For readers seeking more in-depth knowledge on the magnetic nanoparticle physics, there are several comprehensive reviews in literature [4-7]. (For those interested in the surface/interface effects, excellent reviews and articles can be found in [8, 9].) Chapter 3 introduces some of the main theoretical models and experimental results from spin glasses (great many books and reviews on spin glasses are available in literature [10-14]). The topics and examples presented here were chosen according to their relevance to the two experimental studies on interacting magnetic nanoparticles in the superspin glass state, presented in Chapter 4. Chapter 5 describes my current research activities and perspectives for the future. They are divided into two categories; namely, “Quest for Superferromagnetism” and “Magnetic Nanoparticle for Energy Science”. In Annex sections, the summary of my past, present and future research works (including studies that do not involve magnetic nanoparticles) as well as the list of publications and CV are included. These works are, and will be, produced in collaboration with the members of SPHYNX/SPEC as well as with external collaborators from PECSA and LM2N at University of Pierre et Marie Curie in Paris, France. Among them, I owe special thanks to Dr. François Ladieu, Dr. Katsuyoshi Komatsu (post-doc 2008-2010) and Dr. Denis L’Hôte who passed away prematurely in 2011.

2. Magnetic Nanoparticles and Supermagnetism

Magnetic nanoparticles are, as the name suggests, a class of nanoparticles (less than $1\mu\text{m}$ in diameter) made of magnetic elements such as iron, nickel and cobalt and their alloys and chemical compounds [15, 16]. A quick internet search on “magnetic nanoparticles + research” reveals a plethora of current research efforts involving magnetic nanoparticles for their potential (and some current) use in biomedicine [17], magnetic resonance imaging [18], magnetic particle imaging [19], data storage [1], nanofluids [20] etc. While their unique and tunable physical properties (most generally that of superparamagnetism) make them attractive for technological applications, the magnetism of magnetic nanoparticles (individually or collectively) by itself has also been a focus of active fundamental research since the original works by Néel [21], Stoner and Wolfarth [22] in the 1940s.

In macroscopic sized magnetic materials, regions of uniform magnetization are separated by domain walls. The domain wall formation is a process driven by the balance between the magnetostatic energy and the domain-wall energy. The magnetostatic energy is proportional to the volume of the material, while the domain wall energy to the interfacial surface area. Therefore a critical size can be reached, below which it becomes energetically more costly to form domain walls than to resist the external magnetostatic energy of a uniformly magnetized single-domain state. Within a single-domained nanoparticle, all atomic spins are aligned in the same direction (uniformly magnetized) and thus the particle in question can be considered as a small permanent magnet with a large magnetic moment (also known as a ‘superspin’ [23]), typically in the order of 10^3 – $10^5\mu_B$, where μ_B is the Bohr magneton. The magnetization reversal of one superspin requires the collective rotation of *all* atomic spins inside, giving rise to the very high coercivity observed in nanoparticles. The magnetization reversal mechanism in single-domain particles has been intensively studied both theoretically and experimentally in the last six decades, the majority of such studies relying heavily on the pioneering theoretical work by Stoner and Wohlfarth [22].

Some remarkable phenomena have been observed in magnetic nanoparticles arising from the intricate balance between the materials’ intrinsic properties, the finite-size effects and the interparticle interactions. If nanoparticles are widely spaced and hence non-interacting, then the magnetic moments of individual particles act independently. Their rotational dynamics is governed solely by thermal agitation, each behaving like a paramagnetic atom but with a much larger magnetic moment (superspins) leading to the phenomenon widely known as *superparamagnetism*. As there is no interaction between particles, the dynamic and static properties of superparamagnetism are controlled by the intrinsic material property and the finite-size effects which influence the anisotropy energy barrier (coercivity) of individual nanoparticles.

Although in an assembly of isolated particles (not touching), direct exchange interactions between them may be negligible, the magnetic properties can be greatly controlled by the dipole field energy in addition to the magnetic anisotropy and thermal energies. Indeed, it has been found that at sufficiently high concentrations the inter-particle dipolar interactions* have profound effects on the dynamical properties of the particle assembly. They modify the energy barrier arising from the anisotropy contributions of individual particle; *i.e.*, the reversal of one superspin can change the

* In certain cases where magnetic nanoparticles are in physical contact with one another, super-exchange interactions can also play a role.

energy barriers of surrounding nanoparticles. In strongly interacting nanoparticle systems, low temperature collective states are observed. These collective states, now widely known as “*superspin glasses*” show many of the phenomenology found in atomic spin glasses [24]. By further increasing the particle concentration, it may even be possible to create a long-range ordered state; i.e., *superferromagnetic (SFM)* state. Together, these magnetic states created by magnetic nanoparticles now form a new branch of magnetism called “Supermagnetism” [5].

2.1. Single Particle Magnetism

2.1.1. Critical Size

As discussed above, when a ferromagnetic particle is smaller than the typical size of the magnetic domains in the corresponding bulk material, it becomes single domained. The critical size below which a single domained state exists depends strongly on the material itself. The values of critical diameter D_c (in the case of spherical particles) can be approximated by [25]

$$D_c \approx 18 \frac{(AK_u)^{1/2}}{\mu_0 M_s^2} \quad (2.1)$$

where A is the exchange integral and K_u the uniaxial anisotropy density, μ_0 the vacuum permeability and M_s the particle's saturation magnetization. The critical size limit is material dependent and influenced by various anisotropy energy contributions, but generally occurs in the 10–800 nm range. Typical values of D_c for commonly used magnetic materials are listed in Table 1. [6, 26-28].

Table1: Approximate critical diameter values for different magnetic nanoparticles

Material	D_c [nm]
hcp Co	15
fcc Co	7
Fe	15
Ni	55
SmCo ₅	750
Fe ₃ O ₄	128
γ -Fe ₂ O ₃	30
CoFe ₂ O ₄	40

2.1.2. Magnetic Anisotropy

Inside a single-domain particle, all spins are aligned in the same direction (uniformly magnetized). The direction along which the atomic spins tend to align is called the ‘magnetic easy-axis’ or the ‘magnetic anisotropy axis’ and the energy that holds them together is called ‘anisotropy energy.’ The anisotropy energy has several origins; the most important are the magnetocrystalline anisotropy and surface anisotropies, which are described below. The shape anisotropy can also make significant contribution to the total anisotropy energy in non-spherical shaped nanoparticles [29]; however, it is not discussed here as the experimental studies presented in the present manuscript use γ -Fe₂O₃ and

Co nanoparticles which are both spherical. Generally, the anisotropy energy densities of typical magnetic nanoparticles are found in the order of 10^2 – 10^7 Jm⁻³.

2.1.2.1. Magnetocrystalline Anisotropy

The magnetocrystalline anisotropy axis lies along the crystal symmetry of the material and thus can be *uniaxial* (in a hexagonal lattice) as well as *cubic* (in the case of a cubic lattice) and the total anisotropy energy is proportional to the particle's volume. Most studied magnetic nanoparticles have uniaxial anisotropy because they are simpler to model and understand. In this case, the anisotropy energy E_a can be expressed as:

$$E_a(\theta) = K_u V \sin^2(\theta) \quad (2.2)$$

where K_u is again the (magnetocrystalline) anisotropy energy density, V the particle volume and θ is the angle between the magnetization and the easy-axis. It is easy to see that $E_a(\theta)$ has local energy minima at $\theta = 0$ and π , separated by an energy barrier equal to KV at $\theta = \pi/2$. (see figure 2.1). The KV values of 5 - 10 nm (diameter) nanoparticles can easily reach 1000 K or higher, giving rise to the very high coercivity observed in nanoparticles.

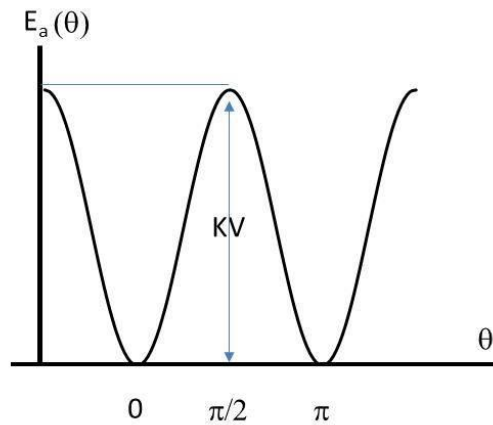


Figure 2.1: Schematic illustration of the energy of a single-domain nanoparticle with uniaxial anisotropy as a function of the angle between the magnetization direction and the anisotropy axis.

2.1.2.2. Surface Anisotropy

As the particle size becomes smaller, a larger proportion of atoms are found on the particle surface, therefore it is rather intuitive to expect that the surface and Interface effects are more prominent in smaller particles [30]. Surface atoms have fewer nearest neighbors than inner atoms, and this broken symmetry leads to changes in the band structure and the lattice constant. For example, in face-centered cubic Co particles with diameter of the order of 1.6 nm, nearly 60% of spins reside on the surface [25]. Such reduction in size leads to anisotropy energy density to increase by more than one order of magnitude from the bulk value [31]. The enhancement in the total anisotropy due to surface spins has been observed in various magnetic nanoparticles [32, 33] and in certain cases, becomes even dominant [34]. Together with the surface spin contribution, the total effective anisotropy density K_{eff} can be written as:

$$K_{eff} = K_V + \frac{S}{V} K_S \quad (2.3)$$

where $S = \pi d^2$ and $V = \pi d^3/6$ are the particle's surface area and volume (d = particle diameter), respectively [35]. Strictly speaking, K_v and K_s are both temperature dependent parameters, but at temperatures well below the materials' Curie temperature (usually several hundred K), they can be taken as constants.

2.1.3. Superparamagnetism and Blocking Phenomenon

The magnetization reversal of a single-domain nanoparticle refers to the flipping of particle magnetization (superspin) from one magnetic easy axis to another by overcoming a large (or small) anisotropy energy barrier (Figure 2.1). As temperature increases (or conversely, the particle size decreases), the thermal energy ($k_B T$) becomes larger than the anisotropy energy barrier E_a . Then the particle magnetic moment will become thermally activated and fluctuates between the two energy minima positions as described above. The rate at which the magnetic moments fluctuate, τ , is given by the famous Néel-Brown equation [21, 36, 37], although a qualitative idea of such dynamics had been proposed a decade earlier by Thellier [38] who had studied the ferromagnetic transition temperature of Earth's magnetic rocks (for a recent review on the subject, see [39]):

$$\tau = \tau_0 \exp\left(\frac{E_a}{k_B T}\right) \quad (2.4)$$

With τ_0 treated as a constant (within the experimental temperature range of interest, this is approximation is valid) in the order of $10^{-9} \sim 10^{-11}$ s. As can be understood from this equation, τ is strongly dependent on temperature and the particle size. For example, with $E_a = 1000$ K and $\tau_0 = 10^{-9}$ s, τ increases from 10^{-8} s at 300K to 10^{12} s at 20 K!! A slight change in the particle diameter can also induce a large change in τ .

At high enough temperature, the superspins can fluctuate very rapidly and thus the system behaves like a paramagnet. The corresponding magnetic regime is called *superparamagnetism* (SPM) [40]. In the SPM regime, the magnetization shows no hysteresis and it follows the usual paramagnetic behavior: $\mu_0 m H = m \mathcal{L}(x)$ where m is the single particle magnetic moment, H applied magnetic field and $\mathcal{L}(x)$ is the Langevin function [$\mathcal{L}(x) = \coth(x) - 1/x$] with $x = \mu_0 m H / k_B T$. At sufficiently low field, the temperature dependence of the SPM magnetization can be described, approximately, by the Curie law. Instead, if an experiment is performed at a temperature T with an observation time window shorter than $\tau(T)$, the superspin appears 'blocked'. The temperature that separates the freely rotating and blocked superspin regimes (for a given τ , of course) is called the blocking temperature, T_B and its definition is highly dependent on the choice of experiment. For a typical experimental measuring time of a SQUID magnetometer of ~ 100 s, T_B is roughly $E_a / 25 k_B T$, while in Mossbauer measurements where the characteristic measurement time is about 10^{-8} s, T_B is close to $E_a / 2.3 k_B$.

Due to the blocking of magnetic moments, the temperature dependent magnetization of SPM systems (in low field limit) shows bifurcation at T_B as illustrated in Figure 2.2. Here, magnetization is measured 1) after being cooled in zero applied field (zero-field cooled, ZFC) then applying a small probing field and 2) after cooling in the presence of a probing field (field cooled, FC). Similar effect is observed in various magnetic systems where irreversibility exists.

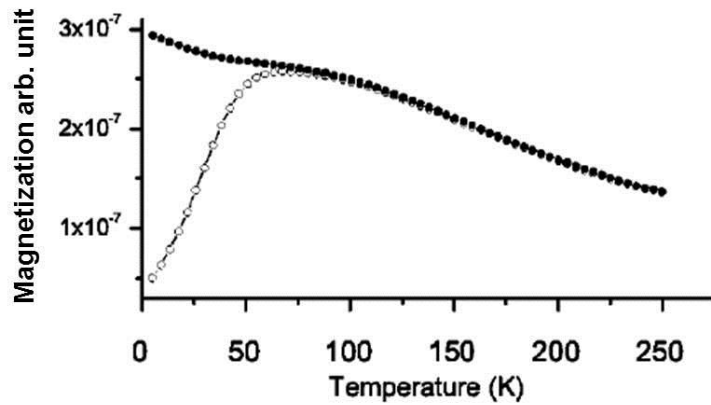


Figure 2.2: Temperature dependence of field-cooled (solid circles) and zero-field-cooled (open circles) of dilute $\gamma\text{-Fe}_2\text{O}_3$ nanoparticle ($d_{\text{ave}} = 8.6\text{nm}$) dispersed in water [41]. 40 Oe was applied as a probing field.

Below T_B , blocked-nanoparticle magnetization show hysteresis with a coercive field H_c corresponding to the field value necessary for reversing the magnetization [4]. The magnetization hysteresis loops of non-interacting magnetic nanoparticle assemblies have been calculated by Stoner and Wohlfarth [22] and presented in Figure 2.3. In nanoparticles with a uniaxial anisotropy direction parallel to the external magnetic field, $H_c = 2K_{\text{eff}}/M_s$ is expected.

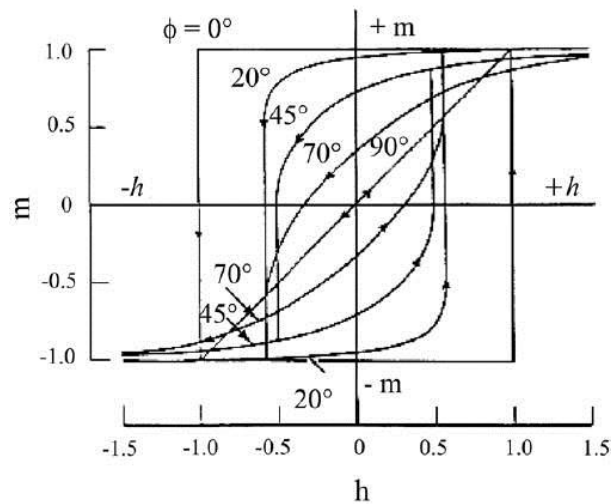


Figure 2.3: Magnetization hysteresis loops of a spherical nanoparticle for different angles ϕ between the anisotropy easy-axis and the external magnetic field. Reduced magnetization $m = M/M_s$ where M_s is the saturation magnetization and $h = H/H_c$ where H_c is the coercive field at $\phi = 0$. (Image reproduced from [22])

The magnetization reversal mechanism in single-domain particles has been studied extensively both theoretically and experimentally in the last six decades in various nanoparticle types and sizes. The possibility to control the coercivity of magnetic nanoparticles, *i.e.*, switching field, has spurred numerous technological applications, particularly in the field of data storage.

It needs to be emphasized that the appearance of the ‘blocking’ phenomenon is very much observation time dependent; *i.e.*, given enough time $t > \tau(T)$, superspins do rotate, albeit very slowly. Furthermore, unlike model systems used for calculations, real nanoparticle assemblies invariably

present size polydispersity. As seen above, a small size difference in particle sizes causes a large change in the characteristic time constant of nanoparticles. Thus a real nanoparticle assembly shows a wide τ distribution with larger particle magnetization relaxing much slower than the smaller ones. These are very important factors in interpreting the slow magnetization relaxation effects.

2.1.4. Size polydispersity

Alas, real magnetic nanoparticle ensembles are never truly monodisperse. There is always a size distribution that can be quite large and random. But, to be able to extract any meaningful information, we generally choose nanoparticle assemblies whose size (diameter, d) distribution follows a lognormal distribution centered about an average value:

$$P(d) = \frac{1}{\sqrt{2\pi}s d_0} \exp \left[-\frac{1}{2s^2} \ln^2 \left(\frac{d}{d_0} \right) \right] \quad (2.5)$$

where d_0 is the mean particle diameter and s is the standard deviation of $\ln(d)$. The size distribution is often determined by taking images (for example by TEM, see figure 2.4 below) from a selected area (or a volume) of a sample, but can also be accessed indirectly by other methods such as: Small Angle Neutron Scattering (SANS) [34] and magnetization measurements as a function of temperature in the SPM regime, where the total magnetization is simply a superposition of individual nanoparticle magnetization, each following the Langevin function. An example image of a nanoparticle assembly with a large size polydispersity is shown in Figure 2.4.

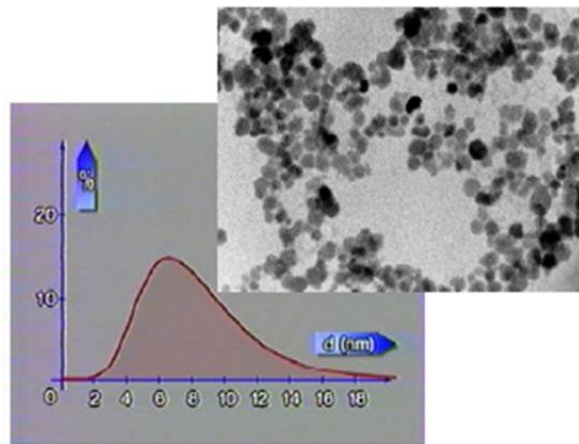


Figure 2.4: TEM micrograph image of maghemite nanoparticles with a mean diameter of 7 nm and the corresponding log-normal size distribution. (Image courtesy of E. Dubois, PECSA UPMC)

2.2. Interacting Magnetic Nanoparticles:

In the SPM regime described above, the interparticle interactions are considered negligibly small. This situation applies to dilute superparamagnetic particle assemblies. Upon increasing the concentration and therefore the interparticle distance, individual particles start to ‘feel’ the local magnetic field created by the neighbors. For isolated superparamagnetic nanoparticles, *i.e.*, no direct contact between the particles, by far the most dominant interaction is the dipole-dipole interaction.

The dipolar interaction energy between two magnetic dipole moments (superspins, in this case) \mathbf{m}_1 and \mathbf{m}_2 separated by \mathbf{r} can be expressed as:

$$E_{dip} = \frac{\mu_0}{4\pi r^3} \left[\mathbf{m}_1 \cdot \mathbf{m}_2 - \frac{3}{r^2} (\mathbf{m}_1 \cdot \mathbf{r})(\mathbf{m}_2 \cdot \mathbf{r}) \right] \quad (2.6)$$

This is a long-range interaction whose strength falls as r^{-3} . In magnetic materials where atomic dipolar moments are small ($\sim 1\mu_B$), the corresponding dipolar energy is typically less than 1 K. Between superparamagnetic nanoparticles, a typical dipolar moment is in the 10^3 - $10^5\mu_B$ range, and thus the dipolar interaction energy can become comparable to the anisotropy energy. The interaction energy is added to the anisotropy energy of each nanoparticle to define new total barrier energy E_B , which is different from that for a single particle:

$$E_B = K_{eff}V + E_{int} \quad (2.7)$$

where E_{int} must include dipolar interaction energy from all its neighbours [42].

Other possible, but less frequent interparticle interactions include:

1. Direct exchange interactions: when particles are touching
2. Super-exchange interactions: when nanoparticles are embedded in an insulating matrix (and are very close), or with insulating magnetic nanoparticles in contact, super-exchange interactions are believed to occur via intermediate ions [43, 44].
3. Tunnelling exchange interaction: This particular type of exchange interaction is said to take place between particles in extreme proximity [45]
4. RKKY interactions: When both nanoparticles and the surrounding matrix are metallic, RKKY (Ruderman-Kittel-Kasuya-Yoshida) interactions should become possible.

2.2.1. Weakly vs. Strongly Interacting Nanoparticles

Magnetic interactions modify the total energy barrier E_B , of each nanoparticle and thus all their dynamic properties governed by E_B such as the (collective) blocking temperature and the relaxation time constants. Shtrikman and Wohlfarth [46] first described the interparticle interaction effect in the weak-interaction limit using the Vogel-Fulcher law [47]:

$$\tau = \tau_0 \exp \left[-\frac{E_B}{k_B(T_B - T_0)} \right] \quad (2.8)$$

where the effective temperature, T_0 is related, but not equal to the interparticle interaction energy strength. The V-F model is valid if the ratio between the dipolar interaction energy density ($M_s^2 a$; M_s is the saturation magnetization per particle and a is roughly the average distance between nearest neighbor particles) and the anisotropy energy density (K) is less than 0.03. A more rigorous approach was introduced by Dormann, Bessais and Fiorani [4], using Boltzmann statistics to calculate the interaction energy between fluctuating particle moments. Their model and its approximated forms were able to quantitatively reproduce the T_B variation found experimentally in various nanoparticle systems (Fe particles in alumina matrix and γ - Fe_2O_3 in a polymer, see [4] and the references therein) with both weak and strong interaction strengths. Not surprisingly, the model predicts that T_B increases upon increasing the interparticle interaction strength. However, in certain very weakly interacting systems, the blocking temperature values determined via Mössbauer experiments were found to *decrease* with increasing strength of interactions [48, 49]. To explain the observed phenomena, Mørup has proposed a model that distinguishes two magnetic regimes. In a weakly-interacting regime, T_B decreases with increasing interaction while in a strongly-interacting regime,

the opposite holds [50]. It is explained that at high interaction strength, the magnetic moment freezing occurs at an *ordering* temperature T_p , indicating a transition to a collective state, rather than a modified blocking temperature of individual moments. The phase diagram corresponding to this effect is shown in Figure 2.5, and its main features have been reproduced experimentally by de Toro *et al.*, who examined the T_B evolution as a function of nanoparticle concentration via magnetization measurements [44].

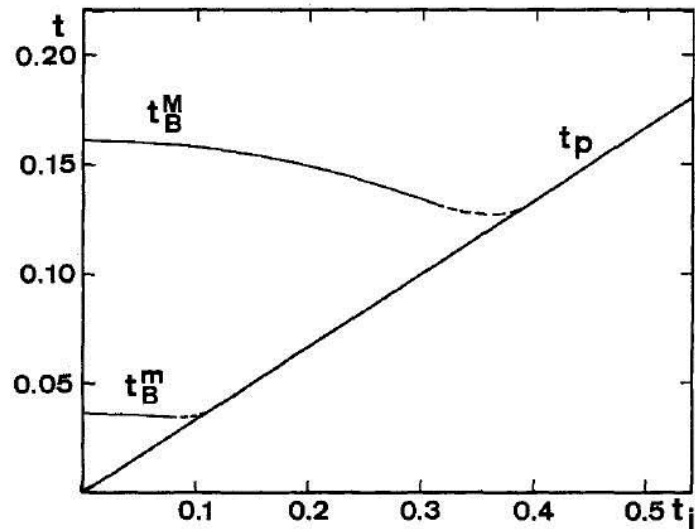


Figure 2.5: Schematic phase diagram showing the T_B evolution as a function of interaction strength. Both temperature (t) and the interaction strength (t_i) are presented in reduced units; $t = k_B T / KV$ and $t_i = E_{int} / KV$. The curve marked t_p is the reduced ordering temperature. t_B^M and t_B^m refer to the reduced blocking temperatures obtained from Mssbauer and magnetization measurements, respectively. (Image reproduced from [50])

Numerical simulations (Monte Carlo simulations) [51] also produced results that are compatible with experimentally observed magnetization hysteresis behaviour (e.g., H_c reduction in randomly oriented magnetic particle systems) [52].

2.2.2. Collective State at Low Temperature: Superspin Glass

In the previous section, the notion of “collective state” in strongly interacting magnetic nanoparticle systems below an ordering temperature was evoked. There is now ample experimental evidence indicating such a collective state in dense nanoparticle assemblies. All laboratory-made nanoparticle assemblies till this day contain a certain degree of irregularities such as size polydispersity and random distribution of particles in space, which are unfavourable for the formation of a ferromagnetic-like long-range ordered state. Not surprisingly, collective states observed in strongly-interacting nanomagnetic systems (frozen ferrofluids and granular multilayers) invariably show out-of-equilibrium dynamics with marked similarities with atomic spin-glasses [24, 41, 53-65]. The critical slowing down near the transition temperature, the waiting time (or age) dependent magnetization relaxation, and memory effects are just a few examples of spin-glass like magnetic behaviours that have been extensively studied in the past 15 years. Such disordered collective states in nanoparticle assemblies are now widely known as *superspin glasses* (SSG). However, there are some fundamental differences between atomic spin glasses and nanoparticle superspin glasses. For example: 1) in SSG, long-range dipolar interactions dominate while in most atomic spin glasses, interactions are of short-

range nature (exchange and RKKY interactions); 2) relaxation time of superspins is much longer than atomic spins and also strongly temperature dependent; and 3) due to the size polydispersity, large particle magnetic moment are 'blocked' at the SSG temperature range and thus are excluded from the collective dynamics. Despite these differences, theoretical models developed for atomic spin-glass have so far succeeded in describing many aspects of SSG dynamics.

2.3. Concluding remarks

In Chapter 4, experimental works on the out-of-equilibrium dynamics of interacting magnetic nanoparticles in the SSG state will be presented. These experiments were performed on concentrated frozen ferrofluids comprised of γ -Fe₂O₃ nanoparticles. In particular, we have examined 1) how the superspin correlation length grows with time and 2) violation of the Fluctuation Dissipation Theorem in strongly ageing regime of SSG phase. The observed phenomena are interpreted in terms of existing *spin glass* models, which are outlined in the next Chapter.

In addition to *superparamagnetism* and *superspin glass* phases, there is another supermagnetic phase; namely, *superferromagnetism* (SFM). Superferromagnetism was first introduced by Mørup [66] and it describes mesoscopic 'domains' of interacting magnetic nanoparticles that are all ferromagnetically coupled. The SFM state has rarely been observed in three dimensional magnetic nanoparticle systems [44] and the pure dipolar-SFM is yet to be found. This is indeed one of the subjects, and a quest, of my future research. The theoretical background and how the dipolar-SFM state may be achieved in 3D magnetic nanoparticle assemblies will be discussed in detail in Chapter 5.

3. Spin Glasses:

As discussed briefly in the previous section, strongly interacting (dipolar) magnetic nanoparticles at low temperature quite often exhibit collective, out-of-equilibrium behavior resembling atomic spin glasses. These systems are now widely known as “Superspin Glasses (SSG)” and a large part of my recent research at SPEC, CEA-Saclay was concentrated on the experimental investigation of such out-of-equilibrium SSG dynamics. A full account of spin glass theory and experimental findings are too voluminous to be reproduced here, thus only a brief summary of the underlying principles and selected examples on experiments are given, intended to facilitate the discussion on SSG dynamics presented in later Chapters. For readers interested in spin glasses, many comprehensive (ex. Mydosh [10], Binder and Young [11] and Fischer and Hertz [12]) as well as shorter reviews (ex. Stein, mostly theoretical [13] and Vincent, mostly experimental [14]) are available in literature.

“Spin Glass (SG)” refers to a metastable magnetic state created by quenched (frozen) and randomly interacting magnetic moments. In reality, such a system is produced by random inclusion of magnetic impurities in a non-magnetic medium (see figure 3.1). The randomness (or disorder) induces competing interactions among magnetic moments such that it is difficult to find a global spin configuration that minimizes the system’s energy, resulting in a multitude of ground states that are highly degenerate. Therefore, the magnetization of spin glasses evolves slowly with time with spins forever searching for a true ground state. This out-of-equilibrium description is analogous to an ordinary glass which is indeed a frozen solid with translational disorder without any crystal structure or long-range order in the atomic arrangement.

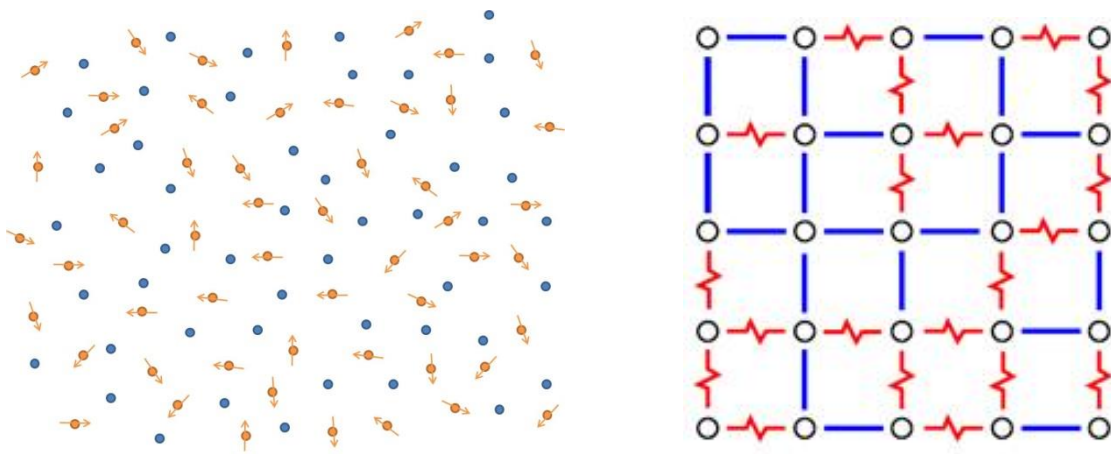


Figure 3.1: (left) Amorphous spin glass where orange atoms represent randomly embedded magnetic ions on disordered lattice sites. (right) Random-bond spin glasses where red zigzag lines represent antiferromagnetic coupling and blue straight lines correspond to ferromagnetic coupling (figure taken from [67])

The first observation of an SG state was in dilute CuMn and AuFe alloys, where a small amount of magnetic atoms were introduced as random impurities inside a nonmagnetic metallic lattice. Here, the random interactions responsible for the spin glass state are the RKKY (Ruderman-Kittel-Kasuya-Yoshida) interactions among the localized magnetic moments mediated by conduction electrons. Slightly later, spin glass states were reported in insulators such as $\text{Eu}_x\text{Sr}_{1-x}\text{S}$ ($0.1 < x < 0.5$) where the competition between the ferromagnetic nearest-neighbors interactions and the antiferromagnetic next-nearest-neighbor exchange interactions govern the SG phase. Much less common, but dipolar

spin-glasses have also been found in some insulators (*e.g.*, dilute magnetic semiconductors and insulators).

3.1 Spin Glass theory

Standard phase transitions are accompanied by a symmetry breaking at the critical temperature. In a ferromagnetic material, for example, above the transition temperature the spins are randomly oriented (paramagnetic state). Below the transition temperature, all spins point either in up or down direction. In a spin glass, no such obvious symmetry appears at the transition temperature. Instead, the spins freeze into a disordered state. Thus a multitude of stable minima can exist in the free energy surface, each corresponding to a different and disordered spin configuration.

One natural question is then: is it possible to construct a universal model describing *all* spin glasses that are, by definition, random and disordered? The fact that different types of materials (metallic alloys, insulators and semiconductors) produce spin glasses suggests the existence of ‘universality’ (to a certain degree) in these systems. There have been various theoretical and phenomenological models proposed to explain the SG phenomena over the last 40 years, the first of which being that of Edwards and Anderson (EA) [68] which starts with a simple Hamiltonian:

$$H_J = - \sum_{\langle i,j \rangle} J_{ij} s_i s_j - h \sum_i s_i \quad (3.1)$$

where $s_i = \pm 1$ is the spin at site i , h is an external magnetic field and J_{ij} is a random interaction (spin coupling) between nearest neighbors. A Gaussian distribution is considered for the J_{ij} strength which is a function of the distance between the interacting spins. (J_{ij} can be exchange, RKKY or dipolar interactions.) If only s_i^z enters the Hamiltonian, then the system is that of an “Ising” spin glass, while if all $s^{x,y,z}$ are considered, it describes a “Heisenberg” system. The RKKY spin glass systems, such as AuFe alloys, are Heisenberg spin glasses while systems with strong uniaxial anisotropy, such as a single crystal $\text{Fe}_x\text{Mn}_{1-x}\text{TiO}_3$ are Ising spin glasses. In the case of strongly interacting magnetic nanoparticles such as frozen ferrofluids, they can be considered as a Heisenberg system with a randomly distributed anisotropy axis.

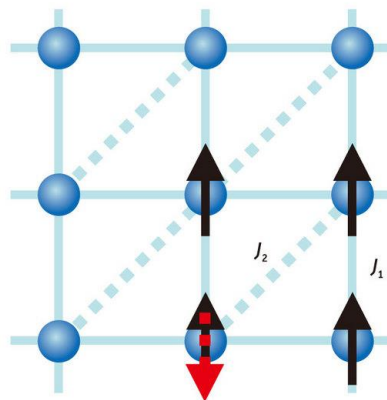


Figure 3.2: Frustrated square lattice made of Ising spins (not a spin glass). The interaction between spins along the edge of the square lattice (J_1) is ferromagnetic, but the interaction along the diagonal direction (J_2) is antiferromagnetic. Thus there is no obvious orientation for the left bottom spin.

The important concept here is that the essential physics of spin glasses is governed not by the microscopic details of their interactions but rather by the *competition* between quenched ferromagnetic and antiferromagnetic interactions. As simple as this Hamiltonian appears, not one spin configuration can simultaneously satisfy all spin couplings. Figure 3.2 illustrates how frustration can occur in a spin system. (Notice that this example is not a spin glass as there is no disorder involved here.) Therefore multiple pure and independent thermodynamic states can exist in spin glasses.

The Sherrington-Kirkpatrick (SK) model is an infinite-range version of the EA model [69]; that is, each spin is coupled randomly to every other spin (total N spins) rather than with just nearest neighbors. The corresponding Hamiltonian is:

$$H_{J,N} = -\frac{1}{\sqrt{N}} \sum_{1 \leq i < j \leq N} J_{ij} S_i S_j \quad (3.2)$$

The rescaling with $1/\sqrt{N}$ ensures a sensible thermodynamic limit for free energy per spin and other thermodynamic quantities. Although the SK model has had troubles describing spin glass behavior, especially in the low-temperature phase, it has served as a basis for many mean-field calculations including the Replica Symmetry Breaking (RSB) model by Parisi [70-72]. The RSB model's central idea is that the low-temperature spin glass state consists of "infinitely many pure thermodynamic states." A competing model to this is the "Droplet model" based on domain wall renormalization group concepts, introduced by Fisher and Huse [73-76]. In their model, there is only a single pair of spin-flip-reversed pure states at low temperature in any finite dimension. Which of these models accurately describes spin glasses is not clear in any dimension greater than one. Furthermore, it should be remembered that there are fundamental differences between the real, experimental spin glasses and the theoretical ones. For example, in a real spin glass, magnetic moments are randomly diluted within a material whereas in theoretical models, magnetic moments are often located at each lattice nodes (only the interaction is random). It is possible that such differences may be of great relevance in understanding the peculiarity of spin glasses [77]; *e.g.*, critical behavior, slow relaxation, aging and memory effects.

3.2 Experiments

3.2.1 Glass transition temperature: T_g

Cannella and Mydosh [78] observed a 'phase transition' in AuFe alloys via the low-field ac magnetic susceptibility exhibiting a cusp at a frequency-dependent temperature $T_f(\omega)$, which is now taken as a first indication of spin glass transition. Very similar frequency dependence is found in concentrated frozen ferrofluids (strongly interacting magnetic nanoparticles). An example of such effect is presented in Figure 3.3.

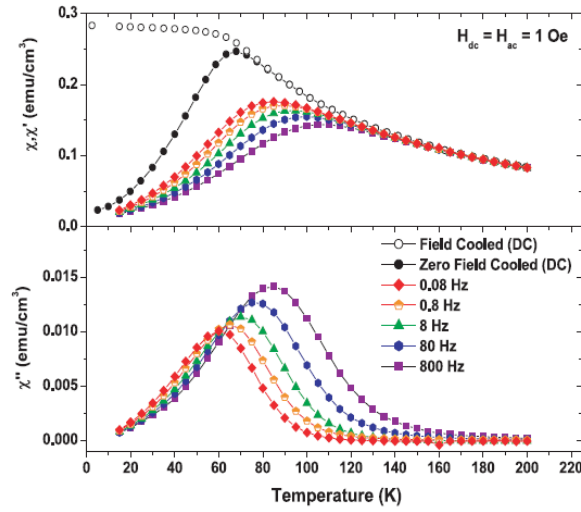


Figure 3.3: Real (top) and imaginary (bottom) parts of ac susceptibility as a function of temperature taken at various frequencies in a concentrated frozen ferrofluid sample (γ -Fe₂O₃ nanoparticles dispersed in glycerol at 15 vol.%). In the top panel, ZFC/FC curves from DC measurements (see next section for more explanation) are superimposed.

The precise frequency dependence of T_f varies from one spin glass type to another. In certain cases [79], the ac susceptibility has been found to resemble the superparamagnetic blocking behavior; *i.e.*, the Arrhenius law,

$$\frac{\omega}{\omega_0} = \exp\left[-\frac{E_a}{k_B T_f(\omega)}\right] \quad (3.3);$$

The Vogel-Fulcher law [47] has also been evoked [80]

$$\frac{\omega}{\omega_0} = \exp\left[-\frac{E_a}{k_B(T_f(\omega)-T_0)}\right] \quad (3.4).$$

This particular phenomenological model is widely used in many interacting systems; *e.g.*, in weakly interacting magnetic nanoparticles (as seen in the previous chapter) as well as in other glassy systems such as viscous fluids. However, the physical significance of the parameter T_0 is not clearly defined.

Overall, critical scaling appears to be most consistent with numerous experimental data and numerical simulations on the frequency dependent SG transition temperature.

$$\frac{\tau(T)}{\tau_0} = \left[\frac{T-T_g}{T_g}\right]^{-z\nu} \quad (3.5)$$

Here, $z\nu$ is the dynamic exponent and T_g is $T_f(\omega = 0)$. $z\nu$ is found to be 2 in the infinite range mean-field model [81] and about 7.2 in the simulation on short-ranged 3D Ising spin glasses. [82]. In real spin glasses, the critical exponents are scattered widely between 5 and 12 [83], with Heisenberg spin glasses generally showing greater values. Similar critical behavior in the frequency dependency of χ' peak is also observed in strongly interacting magnetic nanoparticle systems with a wide range of $z\nu$ values (between 5 and 10) [84].

3.2.2 Slow and out-of-equilibrium dynamics

Another important feature of the spin glass dynamics is the relaxation that takes place at all time-scales (from the microscopic (10^{-12} s) to possibly geological time scales). This occurs due to the disordered and frustrated nature of interactions that prohibits spins from quickly establishing a globally correlated spin configuration in a SG phase. Rather, spins form locally ‘correlated zones’ whose size grows steadily with time. Therefore, the slow and long-lasting magnetization relaxation can give access to how correlated spin zones grow in time. In general, the relaxation dynamics is induced by a small variation in applied magnetic field ΔH or temperature ΔT in the SG state and has been studied experimentally on various spin glass systems. The three most commonly used experimental methods are; a) dc magnetization, b) ac susceptibility and to a much lesser extent, c) spontaneous fluctuation (noise) measurements. The examples of experimental observations are described below.

3.2.2.1 DC measurements

To understand the DC magnetization relaxation phenomena in spin glasses, it is most instructive to start with the ZFC/FC measurement curves as illustrated in Figure 3.4.

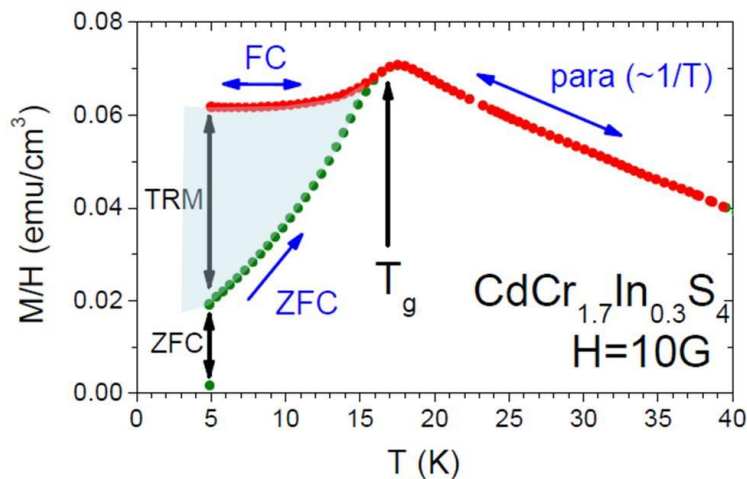


Figure 3.4: Zero-field cooled (ZFC) and field-cooled (FC) magnetization curves of $\text{CdCr}_{1.7}\text{In}_{0.3}\text{S}_4$ spin glass. Figure taken from [14]. The shaded area describes the *out-of-equilibrium* zone.

The FC curve corresponds to the magnetization measured after the sample is cooled in presence of a small measuring field H , while the ZFC curve is obtained after cooling in zero-field and applying H at the lowest temperature. In both cases, although not mandatory for the FC curve, the measurements are taken while gradually increasing the temperature. It should be noted that the separation between the ZFC and FC curves alone is not a signature of a low-temperature SG phase; rather, it simply indicates the existence of irreversibility. For example, non-interacting superparamagnetic nanoparticles also exhibit similar splitting between the ZFC and FC curves due to the blocking of individual magnetic moments (superspins) without having any collective phase. That being said, the apparent flatness, or a slight decrease in the FC curve below T_g is suggestive of a collective behavior and thus the ZFC/FC measurements have become a staple initial test when studying both spin glass and superspin glass samples.

If the sample is zero-field cooled quickly to a certain temperature $T < T_g$ and then a small magnetic field, H , is applied, the magnetization will first jump to the ZFC(T) value then slowly increase toward the equilibrium value; *ie.*, $FC(T)$. Alternatively, if the sample is field cooled in H to $T < T_g$ and subsequently, the field is turned off, the magnetization will decrease. The latter effect is called the “thermo-remanent” magnetization relaxation (TRM(t)). It has been demonstrated that $ZFC(T) + TRM(t, T) = FC(T)$. It is in this TRM(t) (shaded in blue in Figure 3.4 between the $FC(T)$ and $ZFC(T)$ curves) region where slow out-of-equilibrium behavior is observed in spin glasses and superspin glasses. One important aspect of the SG dynamics emerged from these DC magnetization relaxation measurements is the ‘ageing’ effect. The ‘age’ is defined by the time the sample has spent in a SG state prior to the application (or cutoff) of the magnetic field in ZFC (TRM) measurements, often denoted as t_w (waiting time) in relaxation experiments. The older the sample, the longer it takes for its magnetization to relax to the final value (See Figure 3.5). This apparent age-induced slowing of relaxation reflects the dynamic growth of the correlated spin zones. The detailed experimental protocol of field variation relaxation measurements as well as the phenomenological models used to extract characteristic length scales from experimental data will be presented later in the manuscript.

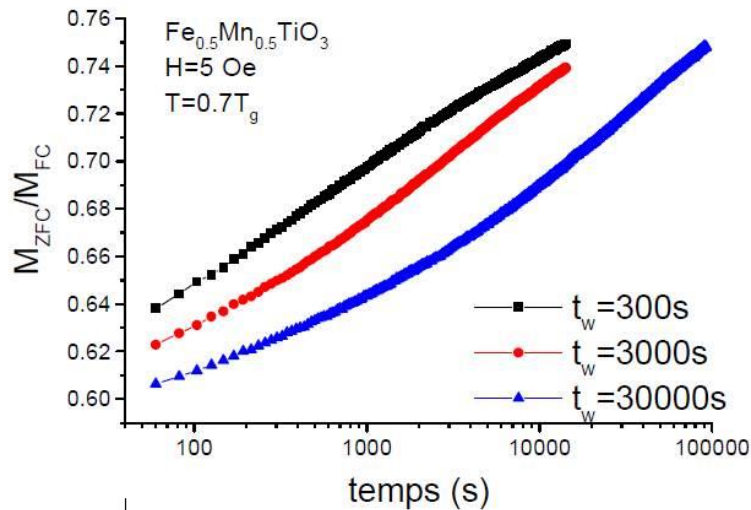


Figure 3.5: Zero-field cooled (ZFC) and field-cooled (FC) magnetization curves of $\text{CdCr}_{1.7}\text{In}_{0.3}\text{S}_4$ spin glass. Figure taken from [14]. The shaded area describes the *out-of-equilibrium* zone.

3.2.2.2 Ac measurements

Ageing and slow relaxation effects are also observed in the ac susceptibility measurements of spin glasses. However, the more spectacular dynamic phenomena revealed by the ac measurements are those of memory and rejuvenation effects. An excellent demonstration of these effects was reported by Dupuis *et al.* [85] via the “memory dip” experiment (see Figure 3.6 below). Here, the imaginary part of the ac susceptibility, χ'' , was measured on a $\text{CdCr}_{1.7}\text{In}_{0.3}\text{S}_4$ spin glass during a step-cooling through the transition temperature ($T_g = 16.7 \text{ K}$) to 5 K, with a holding period of about 30 minutes at each temperature step (see the inset in Figure 3.6). Once the lowest temperature is reached, the sample was heated back at a constant heating rate. During each isothermal cooling step, χ'' was found to relax downward (*ageing* effect). But once the cooling is restarted, the system appears to *rejuvenate* as χ'' increases back up abruptly. This rejuvenation process repeats at each temperature step down to the lowest temperature, although the effect is most pronounced between $0.5T_g$ and $0.9T_g$. During the subsequent continuous heating period, another remarkable feature manifests. That

is, χ'' shows defined ‘dips’ at temperatures where the sample had previously been let to age, indicating that the system has kept the ‘memory’ of previous cooling history. To understand the observed phenomena, the Trap Model and the Random Energy Model have been proposed [86, 87]. These models assume hierarchical organization of metastable states (of correlated spins) as a function of temperature. In real space, this can be understood once again in terms of dynamic correlation length growth [89]. The correlation length scale and how it grows in time depend strongly on temperature and thus by changing the temperature, one changes the length scale at which the system is observed; *i.e.*, in the example measurement presented here, the size of the correlated zones that respond to 0.1 Hz excitation at T is different from that of the zones responding to the same frequency at $T-\Delta T$. The mean field model with full Replica Symmetry Breaking can also reproduce rejuvenation and memory effects [90,91]. In the ‘domain growth like’ dynamics of the Droplet Model, these phenomena are explained by the introduction of ‘temperature chaos’ scenario [92, 93].

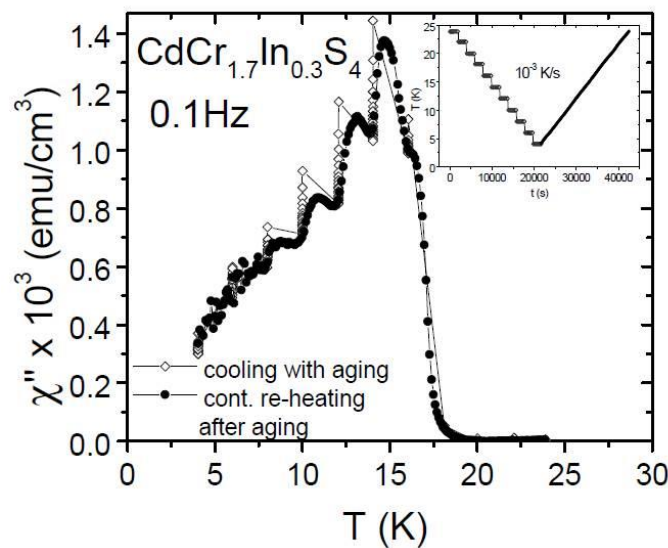


Figure 3.6: Memory-dip experiment performed on a $\text{CdCr}_{1.7}\text{In}_{0.3}\text{S}_4$ spin glass sample. The imaginary part of the ac susceptibility at 0.1 Hz was recorded during step cooling (cooling was halted for 30 minutes every 2K). The inset shows the temperature profile used during the cooling and the heating cycles. Figure taken from [85].

The exact nature microscopic arrangement of spins within the correlated zones (or droplets) and how they differ from one spin glass to another is not understood. However, the notion of *dynamic length scales* is a key ingredient in all theoretical models describing the ageing, rejuvenation and memory effects spin glasses.

3.2.2.3 Noise measurements

The fluctuation-dissipation theorem (FDT) states that in a given system, the linear response to an external perturbation can be expressed in terms of the response fluctuation in thermal equilibrium [94]. In its simplest form, FDT is described as:

$$S_x(\omega) = \frac{2k_B T}{\omega} \text{Im} \hat{\chi}(\omega) \quad (3.6)$$

where $S_x(\omega)$ is the power spectrum (noise) of the observable x as a function of frequency ω and $\chi(\omega)$ is the imaginary component of the susceptibility (response to a small perturbation) $\chi(\omega)$. This theorem is one of the most notable achievements of statistical thermodynamics and it has been

verified to hold in a plethora of real physical systems at thermodynamic equilibrium; *e.g.*, the thermal noise in a resistor and the Brownian motion of particles in a fluid. In out-of-equilibrium systems, such as liquid crystals, molecular glasses and colloids, the fluctuation-dissipation relation is expected to break down. Experimental findings have been rather conflicting; while some observe FDT violation in various glassy systems (*e.g.*, molecular glass [95], colloids [96], polymers [97], liquid crystal [98]), others report quite the opposite [99]. Thus, the systems and the conditions required for FDT violation observation are still an open question. On the theoretical side, attempts have been made to numerically investigate the fluctuation-dissipation relation to accommodate out-of-equilibrium states [100]. In the “weak ergodicity breaking” scenario [101], an effective temperature T_{eff} is introduced (to replace T of the system’s surrounding) in the FDT to represent the out-of-equilibrium state. The ratio T_{eff}/T indicates the degree of “out-of-equilibrium-ness” of the system. The larger the deviation from unity of this value, the further from equilibrium the system is.

Spin glasses are invariably out-of-equilibrium and therefore the FDT should be violated below the glass transition temperature. In order to demonstrate the FDT violation in spin glasses, it is necessary to measure the magnetization fluctuations at a given frequency and compare them to the corresponding imaginary part of the ac susceptibility during the “strongly ageing “ time regime; *i.e.*, during the TRM relaxation. Such experiments have proven quite difficult due to the extremely small magnetic noise amplitude with respect to the sample’s magnetization itself. Earlier attempts by Ocio *et al.* [102] did not observe FDT violation within their experimental limits. More recent measurements by Hérisson and Ocio succeeded in determining the effective temperature T_{eff} at three different temperatures below T_g that are all different from the bath temperatures as expected in non-ergodic systems, and follow the predictions by some Replica Symmetry Breaking models [103]. To this date, their work remains the only experimental example of FDT violation observed in spin glasses (via magnetization fluctuation measurements). In the SSG state of an interacting magnetic nanoparticle system, Jonsson *et al.*, did not observe FDT violation [104]. Recently, we have examined the validity of the FDT in a frozen ferrofluid via noise measurements using a micro-Hall sensor and showed that it violates FDT in its low temperature SSG phase ([105] more details on this study are given in Chapter 4), underlying once again the importance of experimental conditions required to observe this elusive effect.

3.3 Why Study Superspin Glasses?

Spin glasses are often considered as a model complex system by many, primarily for the following reasons. The theoretical models are conceptually simpler (compared to other complex systems with a higher number of degrees of freedom) and the out-of-equilibrium dynamic responses to small perturbations (applied field) are easier to control and access experimentally. Then why are there still so many open questions in spin glasses? Are there “infinitely many pure thermodynamic states” as predicted by the mean field theory, or are spin glasses closer to “disguised ferromagnets” with just two spin-flip reversed states as described by the Droplet model? Real spin glasses revealed a large collection of peculiar dynamic behaviors that cannot be explained by one universal model. One obstacle in comparing experimental results to numerical simulations (based on various theoretical models) is the large gap between the time scales explored by these two approaches. That is, the experimental time frame (10^{-3} to 10^5 s) [14, 106, 107] is many orders of magnitude larger than that generally explored by simulations [108-110]. Another difficulty is the small signal size of individual

spins that makes impossible to perform 'local' measurements to obtain microscopic information on one (or a few) correlated zones.

On both of these accounts, superspin glasses made of interacting magnetic nanoparticles present clear advantages. As outlined in the previous chapter, the microscopic flip-time, τ^* , of one superspin (in the order of 10^{-9} s at room temperature but can reach $10^{-6 \sim -3}$ s in the low temperature SSG phase) is much longer than an atomic spin flip time (in the order of 10^{-12} s). Therefore, with the same experimental time, t , one can explore a much *shorter* scaled time regime; *i.e.*, t/τ^* , than atomic spin glasses and approach the typical time frame explored by numerical simulations. Single domain magnetic nanoparticles possess a very large magnetic moment. For example, a γ - Fe_2O_3 nanoparticle with ~ 10 nm diameter has a permanent magnetic moment of $\sim 10^4 \mu_B$, to be compared to just a few μ_B of one atomic spin. Furthermore, the typical inter-spin distance increases by about two orders of magnitude going from an atomic spin glass material to a concentrated frozen ferrofluid sample. Combined together, a smaller number of correlated superspins should occupy a much larger volume and produce larger magnetic signals than in atomic spin glasses. Therefore the use of microprobes to measure local responses, *i.e.* magnetization fluctuations of a small number of correlated zones may also become possible. Another advantage of using magnetic nanoparticles, and concentrated frozen ferrofluids in particular, is the easy-access to key physical parameters that strongly influence the glassy dynamics, such as the interaction strength (through particle size and concentration control) and the anisotropy alignment (through high-field fluid texturing at high temperature). With these experimental advantages at hand, we have investigated the dynamic correlation length growth and the fluctuation-dissipation theorem violation in the SSG state of frozen ferrofluids. These results are presented in Chapter 4.

4. Superspin Glass: Experimental Investigations

In this chapter, two experimental investigations on the out-of-equilibrium dynamics in the superspin glass phase of concentrated ferrofluids are presented. These works were conducted at SPEC, CEA-Saclay since my arrival in 2005; “Dynamical Correlation Length Growth” and “The Violation of Fluctuation-Dissipation Theorem” in the SSG State of Frozen Ferrofluids.

4.1. Dynamic correlation length growth in superspin glasses

In Chapter 3 (section 3.2.2.1), the notion of the growing ‘correlation length’ and ‘correlated zones’ in the spin glass state was evoked. It is still a matter of debate how spins are arranged inside the correlated zones and how such zones evolve in real-space (the shape). Experimental ‘imaging’ of correlated zones will likely to put an end to these questions; however, microscopy techniques powerful enough to image such small correlated zones (both in physical size and in magnetic signal) are yet to be achieved. That being so, every spin-glass model predicts the existence of dynamic and nontrivial characteristic lengths ξ , in both Ising and Heisenberg spin glasses, and there are experimental means to access these values, albeit indirectly. In Ising spin glass, ξ is believed to grow as a power law $\xi(t, T) = A(t/\tau_0)^{z(T/T_g)}$ [108-111] and thus ξ taken at different temperatures and times can be scaled to a single curve using $[T/T_g \ln(t/\tau_0)]$ as a scaling parameter. Here, A is a constant, T_g the glass transition temperature, τ_0 the elementary time (*i.e.*, atomic spin-flip time constant $\approx 10^{-12}$ s) and z , the critical exponent [108]. In Heisenberg spin glasses, clear deviations from such a scaling occur [109] as illustrated in Figure 4.1. Due to the extremely small τ_0 value for atomic spins, the typical simulations stop at 10^{-6} s in the corresponding laboratory time, much too short to be compared directly to experimental data in real spin glasses. As mentioned earlier, the τ_0 values of magnetic nanoparticles (superspins) are considerably larger than that of the atomic spins; making SSG’s an attractive candidate for more direct comparison with the numerical simulation results.

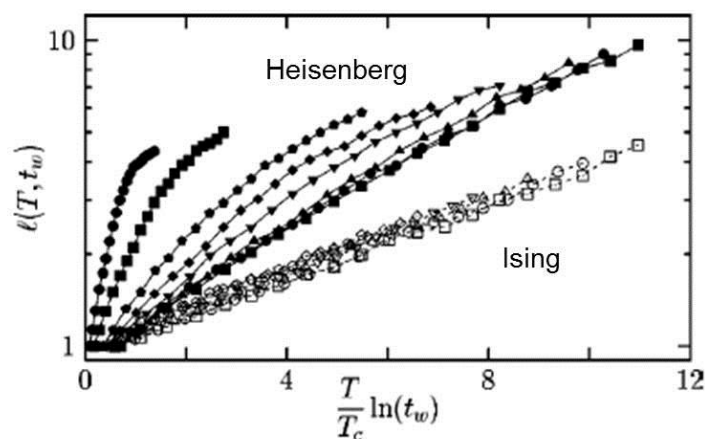


Figure 4.1: Correlation lengths growth simulation on Ising (open symbols) and Heisenberg (filled symbols) spin glasses by Berthier and Young [109] at various temperatures between 0.1 and 1.0 T_c . Here, l is in the units of average inter-spin distance ($l = \xi/\xi_0$). t_w corresponds to t/τ_0 and T_c to T_g in this manuscript. The image is reproduced from [109].

Using a simple commercial SQUID magnetometer, one can access the dynamical correlation length scales in both spin glasses and superspin glasses. In general, one measures the magnetization (or ac

susceptibility) relaxation following a small variation in applied magnetic field strength, in temperature or both. In the study presented here, we have used the field variation method; more specifically, the MZFC measurement protocol [106] to observe the dynamic correlation length growth in the SSG state of frozen ferrofluids. Here is how it works.

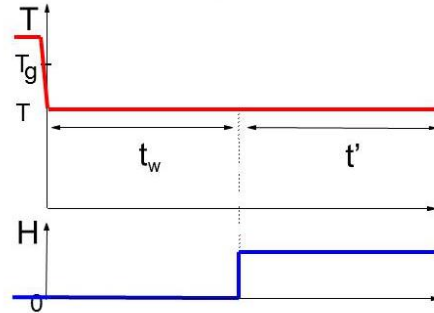


Figure 4.2: Temperature and field profile during the MZFC measurement protocol. See text below for explanation.

As depicted in Figure 4.2, first, a sample is cooled from a temperature well above the SG (or SSG) transition temperature, T_g to the measuring temperature, T_m (typically chosen between 0.7 and 0.9 T_g) in zero applied field. After a period of t_w (called ‘waiting time,’ ranging between 10^2 and 10^5 s) a small probing field H is applied at $t' = 0$. The magnetization relaxation towards a final value, $M_{FC}(T_m)$ (FC magnetization) is measured over a long period of time t' . The probing field must be sufficiently small not to perturb the system, and it is limited to about 10 Oe in SSG’s, but can be as large as a few hundred Oe in SG’s. Both the initial magnetization value at $t'= 0$ and the relaxation rate depend strongly on t_w (also known as ‘age’ of the sample). An example of such measurements performed at three t_w values (300, 3000 and 30000s) in an Ising spin glass [107] is given in Figure 4.3.

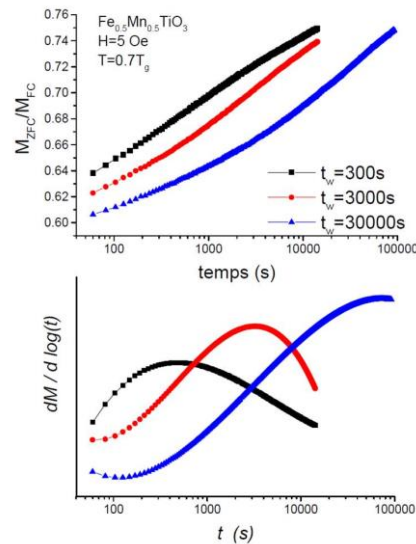


Figure 4.3: MZFC relaxation measurements on the $\text{Fe}_{0.5}\text{Mn}_{0.5}\text{TiO}_3$ spin glass [107]. (Top) Magnetization as a function of real measurement time. (Bottom) The logarithmic time derivative of magnetization as a function of time. See text for the physical meaning of this representation. The image reproduced from [14]

L. Lundgren *et al.* [112] proposed a phenomenological interpretation on the magnetization relaxation rate evolution $M(t', t_w)$, where it is argued that the magnetization relaxation can be represented by a

superposition of successive exponential decays, $\exp(-t/\tau_i)$, where τ_i corresponds to the decay time of the i^{th} correlated zone. Naturally, larger zones have longer τ values. As an SG state contains macroscopically large number of correlated zones of varying sizes, the logarithmic time derivative of $M(t')$; *i.e.*, $dM/d \log(t')$, plotted against $\log(t)$ is proportional to the density distribution of relaxation times and thus qualitatively equivalent to the size distribution of correlated spin zones. Therefore, the positions of the maxima appearing in the $dM/d \log(t')$ vs. $\log(t')$ curves presented in Figure 4.3 (bottom) represent the average size of the correlated zones created after each t_w . In the very low-field limit, the maximum appears approximately at $\tau = t_w$, indicating how the correlated zones grow with the waiting time. A conjecture from the observed t_w dependence is that $M(t')$ should scale with t'/t_w . The scaling is obtained when the ageing component of the relaxation curve is separated from the stationary contribution (which behaves as $\sim t'^{\alpha}$) and the subageing effect is properly taken in account [113]. Then the magnetization relaxation scales with a more complicated scaling time parameter;

$$\lambda/t_w^{\mu} = \{1/1-\mu\}\{t_w + t'\}^{1-\mu} - t_w^{1-\mu} \quad (4.1).$$

When $\mu < 1$ (and it almost always is) the system is said to have ‘subaged’; that is, the system had started to age before the experimentally defined $t_w = 0$, during the cooling process. The value of μ depends on the cooling rate in certain spin glasses [114] as well as on the spin anisotropy. In the case of SSG’s, an additional non-ageing term involving superparamagnetic relaxation contribution must further be subtracted [63].

More quantitative information on the size of correlated zones can be obtained by changing the applied field strength in the MZFC measurements. Beyond the very low-field limit, the magnetic field coupling to the magnetization of correlated zones, $M(N_s)$ containing N_s (super)spins. This coupling energy (the Zeeman energy) reduces the correlated zone barrier energy $E_B(N_s(t_w))$ that holds the N_s (super)spins together [115]. As a result, the relaxation time associated with a given correlated zone with $N_s(t_w)$ spins become faster; *i.e.*, the peak in $dM/d \log(t)$ appears at an earlier time, $\tau' < t_w$. By expressing the initial relaxation time and the new relaxation time with a larger applied field as $\tau \approx t_w$ and $\tau' \approx t_w^{\text{eff}}$, respectively, as

$$t_w = \tau_o^* \exp\left\{\frac{E_B(N_s(t_w))}{k_B T}\right\} \quad \text{and} \quad t_w^{\text{eff}} = \tau_o^* \exp\left\{\frac{E_B(N_s(t_w)) - E_z(N_s(t_w))}{k_B T}\right\} \quad (4.2),$$

one can obtain the following relationship between the acceleration in the relaxation time and the Zeeman energy, E_z :

$$\ln\left(\frac{t_w^{\text{eff}}}{t_w}\right) = -\left(\frac{E_z(H, N_s(t_w))}{k_B T}\right) \quad (4.3).$$

Recognizing that E_z is simply $\mathbf{H} \cdot \mathbf{M}(N_s)$, the number of correlated spins, $N_s(t_w)$ in an average sized correlated zone can be determined by applying different field strengths while keeping the t_w value constant and vice-versa. Berthier *et al.*, has numerically determined the fractal dimensionality of the “backbone spin structure” that relates N_s to the characteristic correlation length in spin glasses: $\xi/\xi_o = N_s^{1/(d-\alpha)}$, where $d = 3$ for a 3D system and $\alpha = 0.5$ and 1 for Ising and Heisenberg spin glasses, respectively.

We have performed a series of MZFC experiments on frozen concentrated ferrofluid samples and confirm all of the SG-like ageing phenomena in the SSG states. All measurements were performed on CRYOGENIC® SQUID magnetometer. The ferrofluid sample used in this study was composed of γ -

Fe_2O_3 nanoparticles ($d_{ave} \approx 8.6\text{nm}$) dispersed in glycerol at $\approx 15\%$ volume fraction. The sample was provided by E. Dubois from PECSA, UPMC and the technical information on the ferrofluid synthesis methods as well as their characteristics can be found in [116]. As expected, the larger τ_0 value of superspin moments have enabled near direct comparison of the dynamical correlation growth in the SSG to the existing numerical simulation results. The anisotropy effect on the SSG dynamics was also studied by measuring the magnetic behavior of a 'textured' frozen ferrofluid (the anisotropy-axis of all nanoparticles are aligned parallel in high magnetic field during the fluid freezing process) and comparing the results to those obtained from a non-textured (randomly oriented anisotropy-axis) sample. The two most representative (published) works are presented in the following sections 4.1.1 and 4.1.2.

4.1.1. Anisotropy axis orientation effect on the magnetization of $\gamma\text{-Fe}_2\text{O}_3$ frozen ferrofluid

Anisotropy-axis orientation effect on the magnetization of $\gamma\text{-Fe}_2\text{O}_3$ frozen ferrofluid

This article has been downloaded from IOPscience. Please scroll down to see the full text article.

2010 J. Phys. D: Appl. Phys. 43 474001

(<http://iopscience.iop.org/0022-3727/43/47/474001>)

View [the table of contents for this issue](#), or go to the [journal homepage](#) for more

Download details:

IP Address: 132.166.16.103

The article was downloaded on 22/11/2010 at 16:28

Please note that [terms and conditions apply](#).

Anisotropy-axis orientation effect on the magnetization of γ -Fe₂O₃ frozen ferrofluid

S Nakamae¹, C Crauste-Thibierge¹, K Komatsu¹, D L'Hôte¹, E Vincent¹, E Dubois², V Dupuis² and R Perzynski²

¹ Service de Physique de l'Etat Condensé (CNRS URA 2464) DSM/IRAMIS, CEA Saclay F-91191 Gif sur Yvette, France

² Physicochimie des Electrolytes, Colloïdes et Sciences Analytiques, UMR 7195, Université Pierre et Marie Curie, 4 Place Jussieu, 75252 Paris, France

E-mail: sawako.nakamae@cea.fr

Received 28 April 2010, in final form 30 April 2010

Published 11 November 2010

Online at stacks.iop.org/JPhysD/43/474001

Abstract

The effect of magnetic anisotropy-axis alignment on the superparamagnetic (SPM) and superspin glass (SSG) states in a frozen ferrofluid has been investigated. The ferrofluid studied here consists of maghemite nanoparticles (γ -Fe₂O₃, mean diameter = 8.6 nm) dispersed in glycerine at a volume fraction of ~15%. In the high temperature SPM state, the magnetization of aligned ferrofluid increased by a factor varying between 2 and 4 with respect to that in the randomly oriented state. The negative interaction energy obtained from the Curie–Weiss fit to the high temperature susceptibility in the SPM states as well as the SSG phase onset temperature determined from the linear magnetization curves were found to be rather insensitive to the anisotropy-axis alignment. The low temperature ageing behaviour, explored via ‘zero-field cooled magnetization’ relaxation measurements, however, shows a distinct difference in the ageing dynamics in the anisotropy-axis aligned and randomly oriented SSG states.

(Some figures in this article are in colour only in the electronic version)

1. Introduction

Ferrofluids are composed of nanometre-scale ferro- or ferrimagnetic particles such as maghemite and magnetite that are suspended in a fluid carrier. When diluted, these particles are small enough (diameter typically below 10 nm) to be dispersed uniformly within a carrier fluid and their thermal fluctuations contribute to the bulk superparamagnetic (SPM) response of the frozen fluid at high enough temperatures. Soon after the discovery of ferrofluids, it was recognized that the inter-particle dipole–dipole interactions and the polydispersity of nanoparticle sizes lead to equilibrium magnetization curves which cannot be approximated by an assembly of individual monodisperse superspins. Furthermore, when sufficiently concentrated, interparticle interactions were found to produce a collective state at low temperatures (usually well below the freezing point of the carrier fluid), showing

similarities with atomic spin glasses [1, 2]. Subsequently, experimental results in support of such disordered collective states, called superspin glass (SSG), have been obtained [3–7]. The SSG state is believed to be the product of the random distributions of positions, sizes and anisotropy-axis orientations of magnetic nanoparticles that interact with each other via dipolar interactions. The dipolar field falls off as r^{-3} and therefore, it is of a long range nature. Furthermore, the microscopic ‘flip time’ of one superspin (in the order of 10^{-9} s) is much longer than an atomic spin flip time (in the order of 10^{-12} s). These features differentiate the physics of SSG phase from that of atomic spin-glass phases. Nevertheless, theoretical models developed for atomic spin glass have so far succeeded in describing many aspects of SSG dynamics. The slow dynamics of SSGs is of particular interest because a much shorter time scale becomes experimentally accessible with SSGs. An example that can illustrate the advantage of such

a long flip time is the slow growth of a dynamical correlation length in spin-glass phases. Numerical simulations on the growth behaviour of correlation length exist [8–10]; however, a direct comparison between the experimental data and these predictions is difficult due to a large gap between the usual time scales explored by numerical simulations and that accessible in laboratory experiments on atomic spin glasses [11, 12]. With longer flip times one can hope to bridge the gap between experiments and theories [7].

Another advantage of using concentrated frozen ferrofluids is the easy-access to key physical parameters that strongly influence the SSG phase, such as the interaction energy, the individual superspin size and the anisotropy alignment. In magnetically aligned frozen ferrofluids, not only the positions of all particles are fixed in space but also their magnetic easy-axes are uniformly oriented parallel to the external bias field direction. Therefore, the distribution of anisotropy axes is no longer random. The effect of anisotropy-axis alignment on the physical properties of nanoparticle assemblies has been studied both theoretically and experimentally in their SPM state [13–19]. However, little is known about its influences at low temperatures in the presence of dipole–dipole interactions (i.e. high concentrations) [20–23]. Due to the loss of a disorder in the anisotropy orientation distribution, the SSG phase of a magnetically aligned frozen ferrofluid may well behave differently from that of randomly oriented nanoparticles.

In this study we have used a ferrofluid consisting of maghemite, γ -Fe₂O₃ nanoparticles dispersed in glycerine and aligned with the easy magnetization axis of individual nanoparticles by freezing glycerine in the presence of high magnetic fields ($H > 15$ kOe). After performing a series of magnetization measurements (dc magnetization, ac susceptibility and low temperature magnetization relaxation) the ferrofluid was warmed up to above the melting temperature of glycerine to destroy the anisotropy-axis alignment. Then the same series of experiments were repeated on the same ferrofluid, this time with the particles' anisotropy axis distributed randomly. As the anisotropy-axis alignment is the only difference between the two sets of measurements, the direct comparison between the two should elucidate exclusively its influence on their magnetic behaviour in both the SPM and the SSG states.

This paper is organized as follows. Section 2 is devoted to the sample description and the experimental methods used in our study. In section 3, phenomenological models used to analyse our experimental data are discussed. The experimental data analysis and the discussion are given in section 4. A brief summary of our findings is found in the last section.

2. γ -Fe₂O₃ ferrofluid sample and experimental methods

2.1. Ferrofluid sample and anisotropy-axis alignment

The ferrofluid used in this study is composed of maghemite, γ -Fe₂O₃, nanoparticles dispersed in glycerine at $\sim 15\%$ volume fraction. The distribution of the nanoparticles' diameters can be described by log-normal

distribution characteristics; i.e. mean diameter $d_0 = 8.6$ nm ($\ln(d_0) = \langle \ln(d) \rangle$) and dispersion $\sigma = 0.23$ [24]. Due to their small sizes, these nanoparticles are magnetic single-domains with an average permanent magnetic moment of $\sim 10^4 \mu_B$. Approximately, 1.5 μ L of ferrofluid was sealed hermetically inside a small glass capillary (1 mm inner diameter). The magnetization and the ac susceptibility measurements were performed using a commercial SQUID magnetometer (CRYOGENIC™ S600).

In order to physically rotate and align the nanoparticles' anisotropy axes, an external bias field H (15 and 30 kOe) was applied at 300 K for over 1 h. These values were chosen based on the birefringence measurements conducted on a concentrated ferrofluid similar to ours where an axis-alignment at $H > 5$ kOe at room temperature was observed [25]. The ferrofluid was cooled down to 150 K (< 190 K = freezing temperature of glycerine) before removing the strong bias field. Dc magnetization was then measured as a function of temperature with a 1 Oe applied field. The magnetization curves obtained from the sample aligned under 15 and 30 kOe were found to superimpose over one another within the experimental uncertainty, indicating that a uni-axial anisotropy orientation is achieved [22]. All data presented on the 'aligned' sample hereafter were taken on the ferrofluid aligned at 30 kOe. The frozen ferrofluid with randomly oriented nanoparticles is referred to as 'random' sample.

The comparison of 'aligned' and 'random' samples implies having the knowledge of the microscopic structure of the samples, especially under magnetic fields. This has been widely explored in several previous studies [25–27]. Coupled small angle scattering and magneto-optical measurements [25] proved that the properties of the magnetic nanoparticle dispersions are controlled by several parameters; the dipolar parameter γ/Φ , the osmotic pressure Π and the volume fraction Φ . These parameters define the location of the sample in the dispersion phase diagram, which mainly depends on the interparticle interactions. In these systems, the van der Waals attractions and the dipolar magnetic interactions (attractive on average) between the nanoparticles are counterbalanced by the electrostatic repulsion created by the surface charges; citrate molecules adsorbed on the nanoparticle surface. The pressure Π is essentially controlled by the electrostatic interaction, and the dipolar interaction can be quantified by $\gamma = \mu_0 \mu^2 / \bar{r}^3 k_B T$, the ratio between the magnetic dipolar energy and the thermal energy, $k_B T$ (μ : dipole moment of the particle, r : mean distance between particles). For the sample used here with $\Phi \sim 15\%$ and the salt concentration of 0.05M, γ/Φ equals 20 at 300 K and this value grows to 32 at 190 K and to 40 at 150 K. In glycerine as well as in water, no aggregates are formed under such conditions in similar nanoparticle dispersions, even in the presence of a strong magnetic field [25–27]. Therefore, the ferrofluid studied here is most likely to be an aggregation-free dispersion of individual particles even under a strong magnetic field and at low temperature. Note that under a strong field, the structure nevertheless becomes slightly anisotropic because the interparticle interactions become anisotropic due to the orientation of the magnetic dipoles. However, the mean distance between the nanoparticles is found to remain isotropic within the resolution of neutron scattering [26].

2.2. Magnetization measurements

In order to understand the effect of anisotropy-axis alignment on the high temperature SPM phase as well as on the low temperature SSG ageing dynamics of a frozen ferrofluid, we have carried out a series of measurements including low field dc magnetization (zero-field cooled (ZFC) and field cooled (FC)) versus temperature, ac magnetic susceptibility versus temperature (with an excitation field of 1 Oe oscillated at frequencies between 0.04 and 8 Hz) and the zero-field cooled magnetization (ZFCM) relaxation at temperatures below T_g . The experimental procedure for ZFCM relaxation measurements is as follows. First, the samples are cooled from a temperature (140 K) well above the SSG transition temperature, $T_g \sim 70$ K (for both SSG states), to the measuring temperature, $T_m = 49$ K ($\sim 0.7T_g$), in zero field. After waiting for a period of t_w (waiting time ranging between 3 and 24 ks), a small probing field ($0.15 \text{ Oe} \leq H \leq 8 \text{ Oe}$) is applied at $t = 0$. The magnetization relaxation towards a final value, M_{FC} (FC magnetization), is measured over a long period time, t , during which the relaxation rate also evolves, continuously changing the slope of the ZFCM response function. In the case of aligned SSG, measurements at 59.5 K ($\sim 0.84T_g$) were also performed.

3. Phenomenological models and data analysis methods

3.1. Magnetization relaxation scaling

Key physical phenomena of interest here related to the ageing in the SSG states are the time dependent magnetization relaxation and the associated relaxation rates. In atomic spin glasses, both the thermoremanent magnetization (TRM) and the ZFCM after a temperature quench in the spin-glass phase can be expressed as a sum of a stationary equilibrium term, $m_{eq}(t)$, and an ageing term, $m_{ag}(t, t_w)$.

$$\frac{M}{M_{FC}} = m_{eq}(t) + m_{ag}(t, t_w) = \pm A \left(\frac{\tau_0}{t} \right)^\alpha + f \left(\frac{\lambda}{t_w^\mu} \right), \quad (1)$$

where $\pm A$ is a prefactor which takes a positive value in the case of TRM and a negative value for ZFCM, τ_0 is a microscopic ‘spin-flip’ time, α and μ are scaling exponents. λ/t_w^μ with $\lambda = t_w[(1 + t/t_w)^{1-\mu} - 1]/[1 - \mu]$ is an effective time variable which takes in account the t_w dependent evolution of the magnetization relaxation [28, 29]. When fitting parameters (μ , α and A) are properly chosen, $m_{ag}(t, t_w)$ of spin-glass magnetization; i.e. $M/M_{FC} - m_{eq}$ at different t_w ’s all collapse onto a single master curve function of λ/t_w^μ . Values of $\mu \neq 1$ indicate by how much the ‘effective age’ of a spin glass deviates from its ‘nominal age’; that is, experimental waiting time, t_w .

In the magnetization relaxation of SSGs made of interacting fine magnetic nanoparticles, an additional non-ageing, time-logarithmic term has been identified [6, 30]. This relaxation term, $B \log(t/\tau_0)$, is believed to stem from SPM moments that do not participate in the SSG ageing dynamics and must be treated independently. The scaling of low temperature ZFCM curves would serve as an additional indication of a SSG phase in frozen ferrofluids with or without the anisotropy-axis alignment.

3.2. Magnetization relaxation rate, effective age of a (super)spin glass and dynamic spin correlations

In a spin glass, the magnetization relaxation rate (S) after an external field change is often expressed as a log-derivative of M/M_{FC} , i.e. $S = d(M/M_{FC})/d \log(t)$. $S(\log(t))$ contains a maximum reached at a characteristic time, t_w^{eff} , that corresponds to the time at which the relaxation rate becomes the fastest, S_{max} . The quantity $S(\log(t))$ is equivalent to the relaxation time distribution of dynamically correlated (super)spin zones [31], and thus t_w^{eff} is commonly referred to as the *effective age* of the system since the temperature quench time. A wide spread of $S(\log(t))$ is indicative of the slow and non-exponential relaxation of the response function in a (super)spin-glass state.

One can extract both qualitative and quantitative information on the dynamics of (super)spin correlations (number and length) in the glassy phase by studying the t_w^{eff} position shift in response to the changes in experimental control parameters, t_w and H via ZFCM measurements. This experimental approach relies on the assumption that the observed reduction in the effective age of the system upon the change in an external magnetic field is due to the Zeeman energy ($E_Z(H)$) coupling to many subsets of dynamically correlated (super)spins [11, 12, 32]. At $t = t_w$ after a temperature quench in zero field, a typical size of the correlated spins has grown to $N_s(t_w)$ with an associated free energy barrier of $E_B(t_w)$. The relaxing of $N_s(t_w)$ dynamically correlated (super)spins towards their final state requires a cooperative flip of all $N_s(t_w)$. Therefore, in response to a vanishingly small external field, such a cooperative flipping should equally require an amount of time $\sim t_w$:

$$t_w(H \sim 0) = \tau_0 \exp(E_B(t_w)/k_B T), \quad (2)$$

where τ_0 is, once again, a microscopic flipping time of a single (super)spin. Indeed in atomic spin glasses and in one randomly oriented SSG, S_{max} occurs at a characteristic time $t \sim t_w$ at very low fields. In the presence of a small but non-negligible H , however, $E_Z(H)$ acts to reduce the barrier energy to a new value, $E_B(t_w) - E_Z(t_w, H)$, by coupling to $N_s(t_w)$ correlated spins. Therefore, one expects a shift of the S_{max} position to shorter times $t_w^{\text{eff}}(H) < t_w$.

$$t_w^{\text{eff}}(H) = \tau_0 \exp\{(E_B(t_w) - E_Z(H, t_w))/k_B T\}. \quad (3)$$

By combining expressions (2) and (3), the relationship between the relative decrease in t_w^{eff} (effective age) with respect to t_w (nominal age) of the system and the Zeeman energy exerted onto the N_s correlated (super)spins can be written as

$$\ln \left(\frac{t_w^{\text{eff}}}{t_w} \right) = - \frac{E_Z(t_w, H)}{k_B T}. \quad (4)$$

$E_Z(H, t_w)$ depends on both the external field and the number of correlated spins, $N_s(t_w)$. Once $E_Z(H)$ is determined, N_s may be extracted knowing that $E_Z(H) = M(N_s)H$. The exact form of E_Z is not readily known and therefore it is often speculated from the experimental observations [11, 12]. In the case of Ising-type spin glasses $E_Z(H)$ was found to

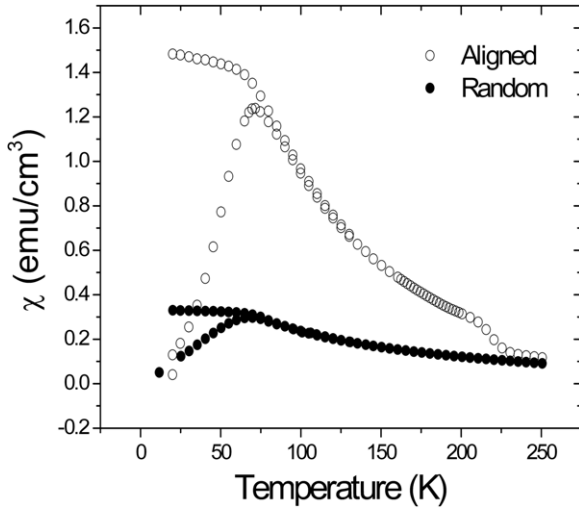


Figure 1. ZFC and FC DC magnetic susceptibility curves of γ - Fe_2O_3 ferrofluid in aligned and random states. An external field of 1 Oe was used in both measurements. Note that $M(T)$ at $T > 150$ K in the aligned sample were taken at the end of all other magnetization measurements presented in this study.

grow linearly with H , while in Heisenberg spin glasses, a quadratic dependence on H was reported. These experimental observations were interpreted to reflect $E_Z(H) = \sqrt{N_s}\mu H$ in Ising spin glasses (with relatively small values of N_s , see [11] for more details) and $E_Z = N_s\chi_{\text{FC}}H^2$ in the case of Heisenberg-like spins (with macroscopically large values of N_s) where μ is the magnetic moment of one spin and χ_{FC} is the FC susceptibility per (super)spin. The ZFCM method has been used successfully in atomic spin glasses [11, 12] and lately in a randomly oriented SSG by our group [7]. Our previous ZFCM experiments performed on a random SSG system exhibited closer to a quadratic dependence on H , and the N_s values were extracted based on the Heisenberg spin-glass model accordingly.

4. Results and discussion

4.1. Anisotropy-axis alignment effect on the SPM behaviour

In figure 1, the ZFC/FC dc susceptibility curves (M/H) of the frozen ferrofluid with and without anisotropy-axis alignment are presented. 1 Oe probing field was used in both measurements. Here, we have taken in account the demagnetization factor ~ 0.3 due to a short cylindrical shape of our sample [33]. Note that due to the melting of glycerine starting around 200 K and above, the $\chi(T)$ of the aligned sample approaches that of the random sample. Below 200 K where superspins are physically blocked, the χ of the aligned sample becomes considerably larger than that in the random state.

In the case of ‘non-interacting’ and monodisperse SPM particles, M_{\parallel} , magnetization in the direction of an external field of a randomly aligned ferrofluid at high T follows the Langevin function [34], $M_{\parallel}(\xi) = M_s[\coth(\xi) - 1/\xi]$ where M_s is the saturation magnetization of the magnetic material and $\xi = \mu H/k_B T$ ($\mu = V_p M_s$ is the magnetic moment of each particle

with V_p being the volume of one nanoparticle). In a weak field, high temperature limit $M_{\parallel}(\xi)$ becomes $N\mu^2 H/3Vk_B T$ (Curie Law). If all particles’ magnetic anisotropy axes are oriented parallel to an externally applied field, magnetization is no longer given by the Langevin law. In the extreme limit where anisotropy energy $E_a \rightarrow \infty$ and without interactions, $M_{\parallel} = M_s \tanh(\xi)$ which becomes $N\mu^2 H/Vk_B T$ in the weak field limit [35]. The anisotropy energy of our maghemite nanoparticles, $E_a/k_B = 2 \times 300$ K [36], is much greater than the magnetic energy $\xi T \sim 1$ K (for H in the order of 1 G).

In the presence of dipole–dipole interactions, each nanoparticle responds to its total local field, H_T , which is a sum of applied magnetic field and the dipolar fields exerted by the surrounding superspins near and far. Therefore for the total local field for a nanoparticle located at x_i , one has $H_T(x_i) = H_{\text{ext}} + H_{\text{dipole}}(x_i)$. Jönsson and Garcia-Palacios have calculated the linear equilibrium susceptibility χ in weakly interacting superparamagnets [4, 37]. In their work, χ is expressed in the form of an expansion with coefficients that depend on dipolar interactions as well as on anisotropy effects. The results indicated that (in the absence of an external bias field) all traces of anisotropy are erased in the linear susceptibility of a SPM system with randomly distributed anisotropy axes and the expression for isotropic spins ($N\mu^2/3Vk_B T$) is recovered. For systems with parallel aligned axes, the dipolar interactions were found to be stronger and the corresponding low temperature susceptibility approaches that of Ising spins; i.e. $N\mu^2/Vk_B T$. As seen in figure 1, the ratio between the $\chi(T)$ of the aligned frozen ferrofluid to that of the randomly oriented ferrofluid is approximately 2 at 200 K and this value grows to about 4 at the ZFC maximum temperature. The ratio between the two susceptibility values in the SPM regime that exceeds 3 may indicate that the dipole–dipole interactions in the present ferrofluid are beyond the weak interaction limit. The interparticle dipolar interactions are known to play an important role in concentrated magnetic nanoparticle systems and can lead to an increase >3 of the linear susceptibility from the Langevin value [38, 39]. Therefore, a change in dipolar interaction energy due to the anisotropy-axis alignment may explain the apparent increase in the linear χ observed here. However, the transition temperature, loosely defined here as the temperature at which the ZFC and FC curves separate, is found at ~ 70 K in both systems. As the T_g is known to depend strongly on the dipolar interactions (i.e. concentrations) the insensibility of T_g to the anisotropy alignment disproves a significant change in dipolar interaction energy speculated above.

To further elucidate the change in the interaction strength, we have plotted $1/\chi$ of the high temperature SPM phase as a function of temperature in order to extract the (negative) interaction energy appearing in the form of the Curie–Weiss law; $\chi(T) \propto (T - T_0)^{-1}$. The value of T_0 in the aligned ferrofluid = -15 K ± 10 is not very different from that found in the random state = -25 K ± 3 . Note that an arbitrary and temperature independent (diamagnetic) contribution needed to be subtracted from the raw data to perform these fits. Additionally, the upper bound of the experimentally accessible SPM temperature range is limited by

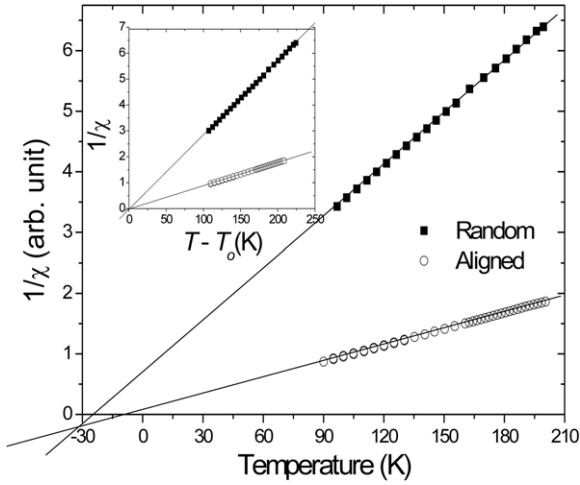


Figure 2. $1/\chi$ versus temperature in the high temperature SPM region. The x -axis intercepts indicate the values of T_0 . A diamagnetic and temperature independent contribution M_0 , presumably due to the sample holder (glass capillary) needed to be subtracted from the raw data for this analysis. The inset shows the same $1/\chi$ plotted against $T - T_0$ ($T_0 = -15$ and -25 K are used for the aligned and the random states, respectively).

the melting of glycerine near 200 K. These facts contributed to large uncertainties in T_0 . It is nevertheless interesting to consider the ratio between the susceptibilities in the aligned and random samples (~ 3.5 between 200 and 100 K, see figure 2). As a function of $(T - T_0)$ with their respective T_0 values (inset of figure 2), the ratio becomes 3.15, approaching the theoretical value of 3. In disordered systems such as ferrofluids studied here, the physical meaning of the negative interaction energy is not easily understood. It has been previously demonstrated by Chantrell *et al* [40] that the negative interaction energy (extracted from high temperature SPM simulation on interacting nanoparticle systems) depends strongly on the packing density of fine magnetic particles as well as on the system geometry; i.e. long-range interactions. Therefore, the lack of a discernible change in T_0 suggests that the dipolar interaction strength remains rather constant under the anisotropy alignment change.

4.2. Persistence of SSG state in an aligned ferrofluid at low temperature

In order to differentiate the SSG transition from the SPM blocking behaviour, frequency (ω) dependence of ac susceptibility was measured and the peak temperature $T_g(\omega)$ at which the real part of susceptibility reaches its maximum value was analysed. If the frozen ferrofluid in either form is an ensemble of independent superparamagnetic centres, $T_g(\omega)$ can be fitted to the Arrhenius law: $\omega^{-1} = \tau_0 \exp(E_a/k_B T_g(\omega))$, with a physically reasonable value of τ_0 (in the order of 10^{-9} – 10^{-10} s for the types of magnetic particles studied here). The fits to the Arrhenius law give unphysical values of $\tau_0 \sim 10^{-19}$ – 10^{-20} s in both cases indicating possible phase transitions taking place at $T_g(\omega)$. A second order phase transition (divergence of a correlation length) towards a disordered state exhibits a critical behaviour [41] that is

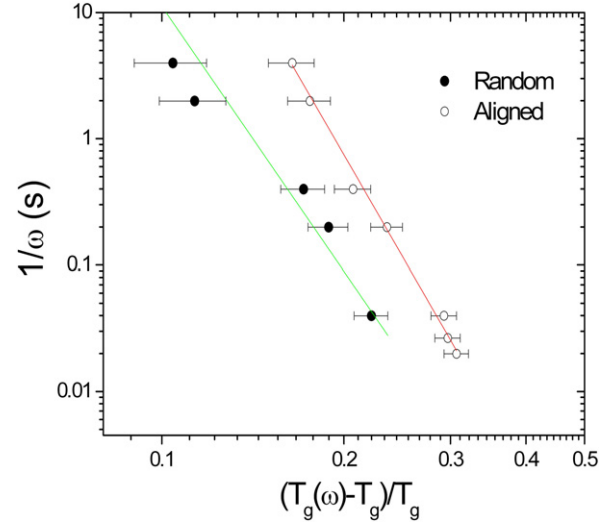


Figure 3. Displacement of transition temperature with frequency determined from in-phase ac susceptibility in a ferrofluid with and without anisotropy-axis alignment. The critical exponent, appearing as the slope on the log–log scale, is slightly larger in the aligned ferrofluid.

described by

$$\omega^{-1} = \tau_0^* \left[\frac{T_g(\omega) - T_g}{T_g} \right]^{-z\nu} \quad (5)$$

Our data can be fitted (figure 3) with plausible critical exponent values, $z\nu = 8.5 \pm 0.3$ and $\tau_0^* = 1 \pm 0.5 \mu\text{s}$ in the aligned ferrofluid and $z\nu \approx 7.5 \pm 0.3$ and $\tau_0^* \approx 1 \pm 0.5 \mu\text{s}$ in the random one. The large value of τ_0^* ($\sim 1 \mu\text{s}$) can be easily explained in terms of the Arrhenius–Néel law: $\tau_0^*(T) \sim \tau_0 \exp\{E_a/k_B T\}$. With $\tau_0 \sim 10^{-9}$ s and $E_a/k_B = 2 \times 300$ K, τ_0^* at $T_g = 70$ K reaches the order of microseconds. Thus, it appears that the SSG transition is not lost by the anisotropy-axis alignment of the ferrofluid but with the critical exponent that is slightly higher than its randomly oriented counterpart. Also, unlike the glass transition determined from static susceptibility, $T_g(\omega \neq 0)$ values are found to behave differently in the aligned and the randomly oriented states. It may be worth noting that in atomic spin glasses, the observed critical exponent ($z\nu$) is larger in Ising spin glasses than in Heisenberg-like spin glasses [8].

4.3. SSG ageing in the very low field limit

We now discuss the effect of anisotropy-axis alignment on the ageing behaviour in the low temperature SSG states. Let us start by comparing the relaxation rate distribution spectra $S(t) = dM/d \log(t)$ between the two systems. Examples of S spectra taken at $0.7T_g$ with $t_w = 3$ ks in both systems are presented in figure 4 (top panel). As can be seen from the graph, the peak (S_{max}) width of relaxation rate in the aligned SSG state is considerably narrower than that in the random SSG state. This may not come as a surprise considering that the anisotropy energy distribution of a uni-axial, single-domain nanoparticle system depends on the distribution of angles between the constituting particles' magnetization and the external field

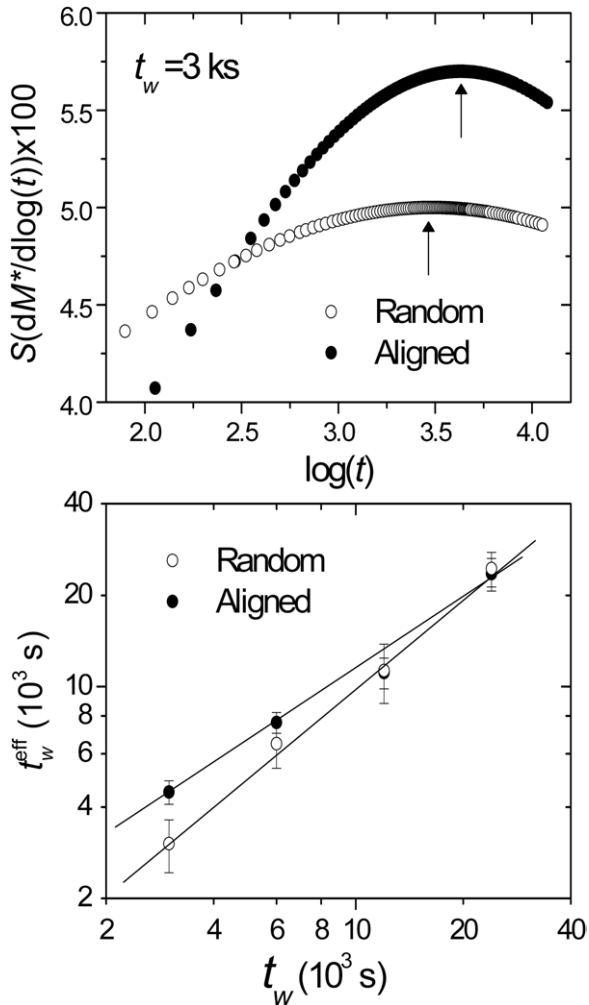


Figure 4. (Top) relaxation rate of ZFCM, S , versus $\log(t)$ in anisotropy-axis aligned and random SSG states with an external field of 0.5 Oe and the waiting time (t_w) of 3 ks. The arrows indicate the positions of S_{\max} . (Bottom) t_w^{eff} versus t_w found in the ZFCM relaxation curves at 0.5 Oe and with $t_w = 3, 6, 12$ and 24 ks on a log–log scale.

directions. Thus, the distribution of energy barriers of correlated superspin domains should be concentrated about a common value in the aligned SSG state.

In figure 4 (bottom panel), the $S_{\max}(t)$ locations, t_w^{eff} , obtained from the ZFCM relaxation rate curves are plotted against the experimental waiting time, t_w , on a log–log scale for both SSG states. These measurements were performed at $T_m = 49$ K ($\sim 0.7T_g$) with the excitation field $H = 0.5$ Oe and t_w was varied between 3 and 24 ks. As discussed in section 3.1, in the low field limit, one expects to obtain $\log(t_w^{\text{eff}}) = \log(t_w)$. As can be seen from the figure, t_w^{eff} is $\approx t_w$ in the random SSG state. On the other hand, the values of t_w^{eff} of the aligned SSG state are larger than the experimental t_w by approximately 1500 s. By adding an extra time, t_{ini} , to t_w ; $t_w \rightarrow t_w + t_{\text{ini}}$, with $t_{\text{ini}} \approx 1500$ s, the t_w^{eff} plot of the aligned SSG state coincides with that of the random state. The presence of t_{ini} may indicate that the *ageing* had started during the cooling, i.e. ~ 1500 s prior to the experimentally defined quench time, but only in the aligned SSG state despite the identical cooling rate used in both experiments.

Table 1. Fitting parameters used for the ZFCM scaling. Note that due to a multiple number of fitting parameters, slightly different solutions to A , B and α can equally produce reasonable scaling. However, μ is the most influential on the overall scaling quality and it must be close to the values indicated below.

	Random 49 K	Aligned 49 K	Aligned 59.5 K
A	0.26	0.26	0.25
α	0.22	0.07	0.09
B	0.001	0.005	0.015
μ	0.91	0.61	0.29
τ_o^*	200 μs	200 μs	26 μs

Similarly in atomic spin glasses, an enhanced sensitivity to cooling rates, also known as a ‘cumulative ageing’ effect; that is, a tendency for ageing to pile up from one temperature to another, has been observed in Ising systems [42, 43]. The effective age of an Ising spin glass *increased* after slower cooling, while Heisenberg spin glasses remained nearly insensitive to the same cooling-rate variations. This analogy is particularly appealing as the anisotropy-axis alignment should qualitatively drive the system towards an Ising-like magnetic state. Is is also consistent with the critical exponent analysis in the previous section where the critical exponent, $z\nu$, associated with the aligned SSG transition was found to be larger than in the random case.

4.4. Magnetization scaling

Next, we examine the ZFCM scaling of aligned and randomly oriented ferrofluids with t_w values ranging from 3 to 24 ks and under 0.5 Oe. As mentioned above, the subtraction of the SPM (m_{SPM}) and the equilibrium (m_{eq}) components is necessary in order to achieve a good scaling [6, 30]. These contributions follow the forms $B(\log(t/\tau_o^*))$ and $-A(t/\tau_o^*)^{-\alpha}$, respectively, where B and A are prefactors and α is a scaling exponent. The value of τ_o^* is fixed according to the Arrhenius–Néel law as described in section 4.2. The corresponding τ_o^* values at 49 K and 59.5 K are 200 μs and 26 μs , respectively. The fitting parameters used to scale the ZFCM curves are summarized in table 1 and the corresponding scaling curves are shown in figure 5.

The most remarkable difference between the two scaling curves at 49 K is the critical exponent ‘ μ ’ in the scaling variable λ/t_w^μ (see section 3.1). $\mu = 0.91$ found in the random SSG is close to the values found in atomic spin glasses [28] as well as the results obtained in more concentrated maghemite ferrofluids [6]. On the other hand, in the aligned SSG state μ has been shifted to a dramatically smaller value, 0.61. In atomic spin glasses, if $\mu = 1$ ($t_w^{\text{eff}} = t_w$) then the system is termed *fully ageing*, if $\mu = 0$ then there is no ageing (i.e. magnetization relaxation does not depend on t_w) and in-between values of μ reflect ‘subageing’ [44, 45]. Therefore, the μ value close to unity found in the randomly oriented SSG confirms the earlier observation $t_w^{\text{eff}} \propto t_w$. The results also agree with the smaller slope found in figure 4 (bottom panel) for the aligned SSG state and it may also reflect, partly, the cooling rate effect as discussed above.

We have also attempted to scale the ZFCM data obtained at 59.5 K (0.84 T_g) in the aligned SSG phase (figure 5, bottom

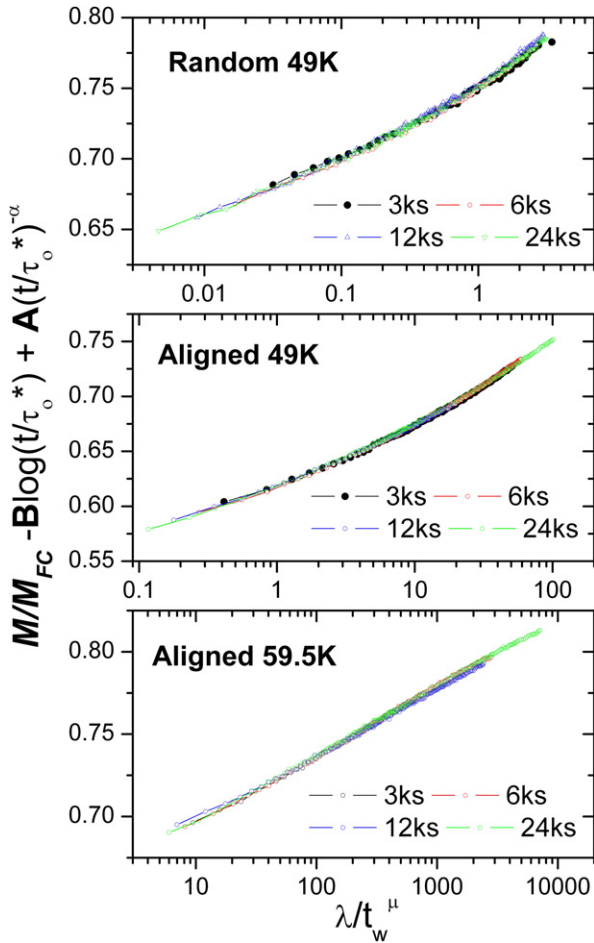


Figure 5. Scaling of ZFCM relaxation curves obtained at 49 K in random (top) and aligned (middle) SSG states and at 59.5 K in aligned SSG state (bottom) with $t_w = 3\text{--}24$ ks. A SPM contribution [$B \log(t/\tau_0^*)$] and an equilibrium contribution [$-A(t/\tau_0^*)^{-\alpha}$] are subtracted from the total ZFCM. See text for details.

panel). Due to the higher temperature towards T_g , a larger proportion of the total magnetization grew within the first few seconds immediately following the external field application, before we could perform our first measurement with our current experimental set-up. Consequently, the range of magnetization change became much smaller than those probed during the measurements at 49 K. Nevertheless, we were still able to achieve scaling using the same data treatment but with two marked differences. First, the B -term corresponding to the contribution from time-logarithmic SPM particles grew larger; $B(59.5\text{ K}) \sim 0.015$ as opposed to $B(49\text{ K}) \sim 0.005$. Second, the scaling exponent μ is further reduced to 0.29! In Heisenberg spin glasses, the value of $\mu(T)$ has a plateau like structure around $\mu \sim 0.9$ across a wide range of temperature between 0.5 and $0.9T_g$. $\mu(T)$ then falls off rapidly as the system approaches the critical region near the glass transition temperature; $T > 0.9T_g$ [46]. In an Ising spin glass, the cumulative ageing effect, which pushes μ towards smaller values in isothermal ageing experiments, was tentatively attributed to its more extended critical region compared with conventional Heisenberg spin glasses [42]. A similar phenomenology akin to the cumulative ageing is perhaps present in an aligned frozen ferrofluid system.

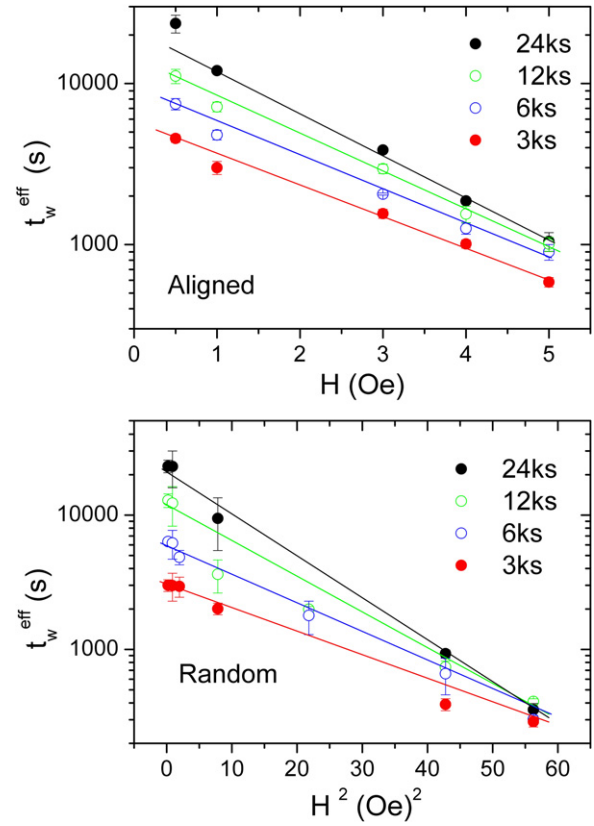


Figure 6. Effective age of the sample dependence on external magnetic field at 49 K. t_w^{eff} was found to depend linearly in the aligned SSG state (top) while in the random SSG state, it exhibited near H^2 dependence.

Additional magnetization relaxation measurements (ZFCM or TRM) are needed to test if the $\mu(T)$ drop-off occurs at a lower temperature (in T_g) in a frozen ferrofluid SSG phase.

4.5. Zeeman energy

Lastly, we focus our attention on the effective age (t_w^{eff}) change due to the application of H ; that is, the Zeeman energy coupled to dynamically correlated superspins. In figure 6, the effective times, t_w^{eff} , measured at different t_w values are plotted as functions of magnetic field. As $\ln(t_w^{\text{eff}}) \sim E_Z/k_B T$, a semi-log plot of t_w^{eff} versus H depicts equivalently the Zeeman energy dependence on H . The difference in the t_w^{eff} dependence on H between the two SSG states is very clear. For a randomly oriented ferrofluid, we confirm our previous observation that t_w^{eff} shows a near quadratic field dependence. In a stark contrast to this, t_w^{eff} of an aligned ferrofluid shows a close-to-linear dependence. Even at the 59.5 K where the relaxation was found to be much faster than at 49 K, the linear dependence of t_w^{eff} is still clear (see figure 7). Once again, the Zeeman energy dependence of H in a random and an aligned SSG states resembles that of Heisenberg (H^2) and Ising (H) spin glasses, respectively [11, 12].

In order to extract the typical number of dynamically correlated spins, $N_s(t_w)$, a more careful examination on the forms of E_Z and their interpretations is required. For example, although the t_w^{eff} versus H curves of the random SSG state on

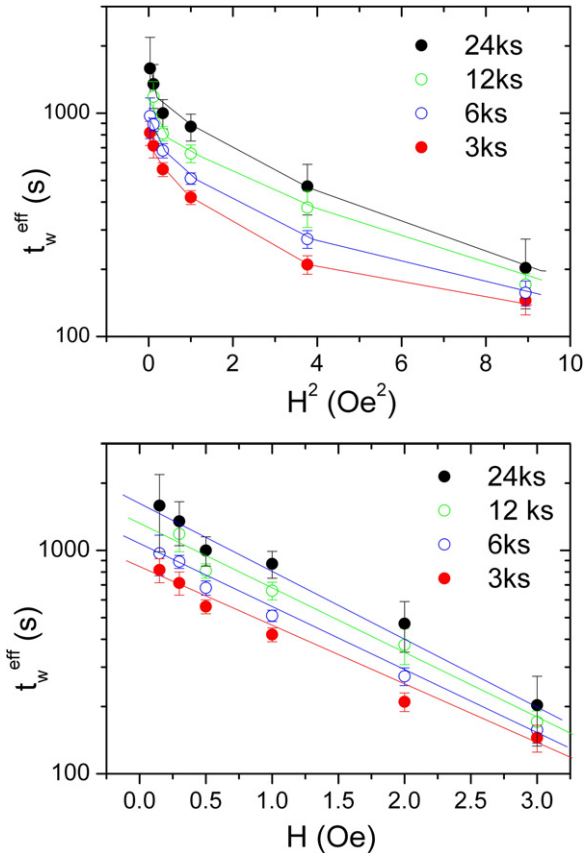


Figure 7. Effective age of the aligned sample versus H^2 and H at 59.5 K. Linear relationship between t_w^{eff} and H is clearly observed.

the log–log scale show near H^2 dependence, it is not purely so. In Heisenberg spin glasses, the quadratic dependence of E_Z has been phenomenologically associated with $N_s \chi_{\text{FC}} H^2$. While this interpretation may very well be valid in atomic spin glasses whose field range of investigation exceeds 1000 G [11], it may not be adequate for a SSG because the low field range (where the ZFCM approach is valid) is limited to $H < 10$ G due to a large magnetic moment of nanoparticles. The effective local field due to dipolar interactions, e.g., from nearby large nanoparticles that are too large to relax within a laboratory time scale, may significantly alter the N_s value to be determined. Furthermore, the possibility of another entirely different ageing mechanism specific to slowly interacting dipolar fine magnetic particles should also be considered [21, 22]. These analyses are currently underway to extract realistic N_s values.

5. Conclusion

We have investigated the effect of the magnetic anisotropy-axis alignment in the SPM and the SSG states of a frozen ferrofluid. The anisotropy-axis alignment was achieved by means of strong (>15 kOe) magnetic field applied to a ferrofluid in its liquid state. In the high temperature SPM state, the linear susceptibility of aligned ferrofluid increased by a factor of 2–4 with respect to that measured in the randomly oriented state. The SSG transition temperature extracted from the linear

magnetic susceptibility curves, $\chi(T)$, remained insensitive to the anisotropy-axis alignment. Additionally, $\chi(T)$ fit to the Curie–Weiss law in the high temperature SPM regime revealed the negative interaction energy to be similar in both states.

The low temperature SSG dynamics explored via ac susceptibility and ‘ZFCM’ relaxation measurements, however, shows distinct differences in the out-of-equilibrium dynamics of SSG phase due to the anisotropy-axis alignment. These changes are:

- Larger critical exponent in an aligned ferrofluid. $T_g(\omega)$ was also found to be larger in the aligned system for all ω values explored.
- Subageing-like behaviour in the aligned SSG state. The effect appeared only in the aligned sample as an initial age and as a smaller scaling exponent, μ (~ 0.9 in the random SSG state to ~ 0.6 in the aligned SSG state at $0.7 T_g$).
- Zeeman energy dependence on H . E_Z depends linearly in the aligned SSG state, while near-quadratic dependence was observed in the random SSG state.

Interestingly many of these above listed differences between the anisotropy-axis aligned and the randomly oriented SSG states resemble those found in Ising-like and Heisenberg spin glasses.

References

- Luo W, Nagel S R, Rosenbaum T F and Rpsenweig R E 1991 *Phys. Rev. Lett.* **67** 2721
- Vincent E, Yuan Y, Hurdequint H and Guevara F 1996 *J. Magn. Magn. Mater.* **161** 209
- Hansen M F, Jonsson P E, Nordblad P and Svedlindh P 2002 *J. Phys.: Condens. Matter* **14** 4901
- Jönsson P E 2004 *Adv. Chem. Phys.* **128** 191
- Sasaki M, Jönsson P E, Takayama H and Mamiya H 2005 *Phys. Rev. B* **71** 104405
- Parker D, Dupuis V, Ladiou F, Bouchaud J P, Dubois E, Perzynski R and Vincent E 2008 *Phys. Rev. B* **77** 104428
- Wandersman E, Dupuis V, Dubois E, Perzynski E, Nakamae S and Vincent E 2008 *Europhys. Lett.* **84** 37011
- Berthier L and Young A P 2004 *Phys. Rev. B* **69** 184423
- Berthier L and Bouchaud J-P 2002 *Phys. Rev. B* **66** 054404
- Belletti F *et al* 2008 *Phys. Rev. Lett.* **101** 157201
- Bert F, Dupuis V, Vincent E, Hamman J and Bouchaud J P 2004 *Phys. Rev. Lett.* **92** 167203
- Joh Y G, Orbach R, Wood G G, Hamman J and Vincent E 1995 *Phys. Rev. Lett.* **82** 438
- Dormann J L, Fiorani D and Tronc E 1996 *Adv. Chem. Phys.* **98** 283
- Hanson M, Johansson C and Mørup S 1993 *J. Phys.: Condens. Matter* **5** 725
- Bentivegna F *et al* 1998 *J. Appl. Phys.* **83** 7776
- Raikher Y L 1983 *J. Magn. Magn. Mater.* **39** 11
- Hrianca I 2008 *Physica B* **403** 1831
- Hasmonay E, Dubois E, Bacri J-C, Perzynski R, Raikher Y L and Stepanov V I 1998 *Eur. Phys. J. B* **5** 859
- Sollis P M, Bissell P R and Chantrell R W 1996 *J. Magn. Magn. Mater.* **155** 123
- Zhang H and Widom M 1995 *Phys. Rev. B* **51** 8951
- Russ S and Bunde A 2006 *Phys. Rev. B* **74** 024426
- Russ S and Bunde A 2007 *Phys. Rev. B* **75** 174445
- Nakamae S, Tahri Y, Thibierge C, L’Hôte L, Vincent E, Dupuis V, Dubois E and Perzynski E 2009 *J. Appl. Phys.* **105** 07E318

- Nakamae S *et al* 2010 *J. Appl. Phys.* **107** 09E135
- [24] Berkowski B (ed) 1996 *Magnetic Fluids and Application Handbook* (New York: Begell House)
- [25] Mériquet G *et al* 2006 *J. Phys.: Condens. Mater.* **18** 10119
- [26] Mériquet G, Cousin F, Dubois E, Boué F, Cebers A, Farago B and Perzynski R 2006 *J. Phys. Chem. B* **110** 4378
- [27] Wandersman E, Dubois E, Cousin F, Dupuis V, Mériquet G, Perzynski R and Cebers A 2009 *Eur. Phys. Lett.* **86** 10005
- [28] Vincent E 2007 *Lecture Notes Phys.* **716** 7
([arXiv:cond-mat/0603583](https://arxiv.org/abs/cond-mat/0603583))
- [29] Alba M, Ocio M and Hammann J 1986 *Europhys. Lett.* **2** 45
- [30] Parker D, Ladieu F, Vincent E, Mériquet G, Dubois E, Dupuis V and Perzynski R 2005 *J. Appl. Phys.* **97** 10A502
- [31] Lundgren L, Sveldindh P and Beckman O 1982 *Phys. Rev. B* **26** 3990
- [32] Vincent E, Bouchaud J-P, Dean D S and J Hammann 1995 *Phys. Rev. B* **52** 1050
- [33] Beleggia M, Vokoum D and De Graef M 2009 *J. Magn. Magn. Mater.* **321** 1306
- [34] Chantrell R W, Ayoub N Y and Popplewell J 1985 *J. Magn. Magn. Mater.* **53** 199
- [35] Cregg P J and Bessais L 1999 *J. Magn. Magn. Mater.* **202** 554 and references within
- [36] Gazeau F, Bacri J C, Gendron F, Perzynski R, Raikher Yu L, Stepanov V I and Dubois E 1998 *J. Magn. Magn. Mater.* **186** 175
- [37] Jönsson P E and Garcia-Palacios J L 2001
[arXiv:cond-mat/0101287v2](https://arxiv.org/abs/cond-mat/0101287v2)
- [38] Pshenichnikov A F 1995 *J. Magn. Magn. Mater.* **145** 319
- [39] Pshenichnikov A F and Mekhonoshin V V 2000 *J. Magn. Magn. Mater.* **213** 357
- [40] Chantrell R W, Walmsley N, Gore J and Maylin M 2000 *Phys. Rev. B* **63** 024410
- [41] Binder K and Young A P 1986 *Rev. Mod. Phys.* **58** 801
Djurberg C, Sveldindh P, Nordblad P, Hansen M F, Bødker F and Mørup S 1997 *Phys. Rev. Lett.* **79** 5154
- [42] Dupuis V, Vincent E, Bouchaud J P, Hammann J, Ito A and Aruga-Katori H 2001 *Phys. Rev. B* **64** 174204
- [43] Parker D, Ladieu F, Hammann J and Vincent E 2006 *Phys. Rev. B* **74** 184432
- [44] See Rodriguez G F, Kenning G G and Orbach R 2003 *Phys. Rev. Lett.* **91** 037203 and references within
- [45] Bouchaud J P, Vincent E and Hammann J 1994 *J. Phys. I France* **4** 139
- [46] Alba M, Hammann J, Ocio M, Refregier P and Bouchiat H 1987 *J. Appl. Phys.* **61** 3683

4.1.2. Dynamic correlation length growth in superspin glass; Bridging experiments and simulations

Dynamic correlation length growth in superspin glass: Bridging experiments and simulations

S. Nakamae, C. Crauste-Thibierge, D. L'Hôte, E. Vincent, E. Dubois et al.

Citation: *Appl. Phys. Lett.* **101**, 242409 (2012); doi: 10.1063/1.4769840

View online: <http://dx.doi.org/10.1063/1.4769840>

View Table of Contents: <http://apl.aip.org/resource/1/APPLAB/v101/i24>

Published by the [American Institute of Physics](http://www.aip.org).

Related Articles

Progress in the mathematical theory of quantum disordered systems

J. Math. Phys. **53**, 123307 (2012)

Universality in bipartite mean field spin glasses

J. Math. Phys. **53**, 123304 (2012)

Coexistence of reentrant-spin-glass and ferromagnetic martensitic phases in the $\text{Mn}_2\text{Ni}_{1.6}\text{Sn}_{0.4}$ Heusler alloy

Appl. Phys. Lett. **99**, 182507 (2011)

Surface spin glass and exchange bias effect in $\text{Sm}_{0.5}\text{Ca}_{0.5}\text{MnO}_3$ manganites nano particles

AIP Advances **1**, 032110 (2011)

Spin-glass magnetism of surface rich Au cluster film

Appl. Phys. Lett. **99**, 022503 (2011)

Additional information on *Appl. Phys. Lett.*

Journal Homepage: <http://apl.aip.org/>

Journal Information: http://apl.aip.org/about/about_the_journal

Top downloads: http://apl.aip.org/features/most_downloaded

Information for Authors: <http://apl.aip.org/authors>

ADVERTISEMENT

AIP | Applied Physics
Letters

SURFACES AND INTERFACES
Focusing on physical, chemical, biological, structural, optical, magnetic and electrical properties of surfaces and interfaces, and more...

ENERGY CONVERSION AND STORAGE
Focusing on all aspects of static and dynamic energy conversion, energy storage, photovoltaics, solar fuels, batteries, capacitors, thermoelectrics, and more...

EXPLORE WHAT'S NEW IN APL

SUBMIT YOUR PAPER NOW!

Dynamic correlation length growth in superspin glass: Bridging experiments and simulations

S. Nakamae,^{1,a)} C. Crauste-Thibierge,^{1,b)} D. L'Hôte,¹ E. Vincent,¹ E. Dubois,² V. Dupuis,² and R. Perzynski²

¹*Service de Physique de l'Etat Condensé (CNRS URA 2464) DSM/IRAMIS, CEA Saclay, 91191 Gif sur Yvette, France*

²*Physicochimie des Electrolytes, Colloïdes et Sciences Analytiques (CNRS UMR 7195), Université Pierre et Marie Curie, 4 Place Jussieu, 75252 Paris, France*

(Received 2 October 2012; accepted 19 November 2012; published online 12 December 2012)

Interacting magnetic nanoparticles display a wide variety of magnetic behaviors that are now being gathered in the emerging field of “supermagnetism.” We have investigated how the out-of-equilibrium dynamics in the disordered superspin glass (SSG) state of a frozen ferrofluid sample is affected by texturation. Via magnetization relaxation experiments at low temperatures, we were able to estimate superspin correlation lengths for both textured and non-textured samples. The comparison with simulations and experiments on atomic spin glasses shows that the dynamic correlations in SSG's appear to develop in a way reminiscent to those in atomic spin glasses at intermediate time/length scales. © 2012 American Institute of Physics.

[<http://dx.doi.org/10.1063/1.4769840>]

Interacting, single-domain ferro(ferri)magnetic nanoparticles (np) in solid media (e.g., frozen ferrofluid) are known to undergo a superparamagnetic (SPM)-to-superspin glass (SSG) transition at low temperature.^{1,2} The name “superspin” reflects the large magnetic moment associated with each nanoparticle. Superspines are generally ascribed a strong uni-axial anisotropy energy that results in a dramatic thermally activated increase of their individual flipping time (compared to atomic spins). These “slow” superspins are thus good candidates for revisiting some of the unsolved questions in the physics of spin glasses (SG) at intermediate time/length scales which were inaccessible by numerical simulations and experiments. Spin glasses, like all other glassy systems, are characterized by the out-of-equilibrium dynamics that fails to establish long-range ordered state due to frozen-in disorders. Instead, magnetic moments slowly establish microscopic local equilibrium whose domain size is defined by the correlation length. The question on how correlation length (ξ) grows in spin-glasses and how it compares to numerical simulations were never clearly answered. The main obstacles were (1) the experimentally accessible time scale (10^{-3} to 10^5 s) in atomic SG's³⁻⁵ is many orders of magnitude larger than what explored by simulations⁶⁻⁸ and (2) most numerical simulations were made on *Ising* SG's while a vast majority of experiments were performed on *Heisenberg-like* SG's.

It has been shown numerically by Berthier *et al.* that the correlation length dynamics of *Ising* and *Heisenberg* spin glasses follow different laws.^{6,7} A power law behavior, $\xi(t, T) = A(t/\tau_o)^{z(T/T_g)}$ and thus a scaling with $[T/T_g \ln(t_w/\tau_o)]$ can reasonably describe the simulation results in *Ising* SG's even at large times, whereas clear deviations from such a scaling

occur in *Heisenberg* SG's at $T < T_g$.⁷ Here, A is a constant of the order 1, t the lab time, τ_o the attempt time of a single spin, z the dynamics exponent, and t_w is the time the system has spent in the SG state. In experiments on real spin glasses, however, such a scaling behavior has only been found in *Heisenberg* SG's.³⁻⁵ To our knowledge there have been two recent studies that attempted to close the time scale gap between numerical simulations and experiments in spin glasses. On one hand, Belletti *et al.* have succeeded in conducting numerical simulation of ξ in *Ising* SG's over a time spanning 11 orders of magnitude.⁸ Their simulation yielded correlation lengths that are in the same order of magnitude as the experimentally determined values of *Heisenberg* spin glasses, rather than those of *Ising* SG's. On the other hand, Wood⁹ has examined $\xi(t, T)$ from various experimental results on thin-film (2D) and bulk (3D) spin glasses and compared these values to the simulation made by Kisker.¹⁰ When the correlation lengths in thin-film SG's were all fixed to 1.8 times the sample thickness, striking agreement was found between correlation lengths in thin film (susceptibility measurements) and bulk (thermoremanent magnetization measurements) *Heisenberg* spin glass samples and the simulation based on the *Ising* spin glass model.

Maghemite frozen ferrofluids have been found to exhibit *Heisenberg* SG-like behavior when anisotropy axes are randomly distributed.¹¹⁻¹³ Interestingly, once the anisotropy-axes are uniformly aligned, more *Ising* SG-like features were observed.¹⁴ Combined with the longer “flip-time” of individual superspins ($\sim 10^{-9}$ s at room temperature for ~ 10 nm np's compared to 10^{-12} s for atomic spins), concentrated ferrofluids (FF) may allow a more direct comparison between real three dimensional *Heisenberg-like* and *Ising-like* (super)spin glass systems to their corresponding numerical simulation results.

In this study, the number of correlated superspins N_s was extracted via zero-field-cooled-magnetization (ZFCM) relaxation measurements (see further below for experimental

^{a)} Author to whom correspondence should be addressed. Electronic mail: sawako.nakamae@cea.fr.

^{b)} Current address: Laboratoire de Physique de l'Ecole Normale Supérieure de Lyon, France.

protocol) in the SSG state of two types of frozen ferrofluids; namely, textured and non-textured FF's. In the non-textured FF, both the position and the anisotropy-axis orientation of nanoparticles were kept random, whereas in the textured FF, the particles' anisotropy axes were all aligned by application of a strong magnetic field (1.5 T) in the high temperature liquid state of the carrier fluid. Hereafter, these samples are called "random" and "aligned" samples. The corresponding values of $\zeta(t, T)$ were then deduced from N_s using the results from numerical simulations^{6,7} on the fractal growth of the correlation in the SSG state.

The glycerol based ferrofluid used in this study was made of maghemite, $\gamma\text{-Fe}_2\text{O}_3$, nanoparticles (~ 8.6 nm diameter) with a $\sim 15\%$ volume fraction. The nanoparticles are magnetically single-domain, possessing an average permanent magnetic moment of $\sim 10^4 \mu_B$ and the anisotropy energy of $E_a \sim 640$ K.¹⁵ The sample synthesis technique¹⁶ and the texturing procedure¹⁴ (anisotropy axis-alignment at high temperature, high field) are described elsewhere. All magnetization measurements were performed with a commercial SQUID magnetometer (Cryogenic S600). The existence of low temperature SSG state in these ferrofluids was verified via the critical slowing down behavior near the transition temperature, T_g (67–70 K for both) and the ZFCM scaling at $\sim 0.7 T_g$ (additional measurements were performed at $0.84 T_g$ in the aligned sample).^{12–14}

In the ZFCM protocol, samples are cooled from a temperature (140 K) well above the superspin glass transition temperature to the measuring temperature, $T_m < T_g$, and held for an experimentally fixed amount of time t_w (waiting time, or equivalently called, the system's "age") in zero applied field. During t_w , superspins form correlated zones of various sizes. At t_w , an average sized correlated zone contains $N_s(t_w)$ correlated (super)spins, with a corresponding free energy barrier $B(N_s(t_w))$;^{3,17} i.e.,

$$t_w = \tau_o^* e^{\left(\frac{B(t_w)}{k_B T}\right)}, \quad (1)$$

where τ_o^* is the temperature dependent microscopic flipping time of a (super)spin; i.e., $\tau_o^* = \tau_o \exp(E_a/k_B T)$ with $\tau_o = 10^{-9}$ s and $E_a = 640$ K. After a chosen waiting time t_w , a small magnetic field ($H = 0.15\text{--}8$ Oe) is applied, and the magnetization is recorded as a function of the probing time t , elapsed since the field change.

The values of N_s are extracted from the ZFCM data following an empirical model developed for atomic spin glasses.³ The magnetization relaxation toward the final value requires cooperative flipping of all (super)spins in a given correlated zone. Therefore, the magnetization relaxation rate spectrum, $S(\log(t)) (=d(M/M_{FC})/d \log(t))$ is a qualitative representation of the size distribution of such zones.^{17,18} As average sized zones possess the relaxation time $\sim t_w$, S becomes maximum near $t \sim t_w$ when $N_s(t_w)$ spins cooperatively flip, provided that the magnetic field is vanishingly small. When a larger magnetic field is applied, the Zeeman energy (magnetic field coupling to a group of correlated (super)spins) becomes non-negligible, and the barrier energy is reduced from $B(N_s(t_w))$ to $B(N_s(t_w)) - E_Z(H, N_s(t_w))$. Consequently, the relaxation rate reaches its maximum at $t = t_w^{\text{eff}} < t_w$. t_w^{eff} is called the *effective age* of the system and is described as

$$t_w^{\text{eff}} = \tau_o \exp\{B(t_w) - E_Z(H, N_s(t_w))/k_B T\}. \quad (2)$$

Combining Eqs. (1) and (2), one can deduce the relation between the observed *effective age* (t_w^{eff}) and $E_Z(H, N_s)$ of $N_s(t_w)$ correlated spins to

$$\ln(t_w^{\text{eff}}/t_w) = -(E_Z(H, N_s(t_w))/k_B T). \quad (3)$$

In atomic spin glasses, the form of $E_Z(H, N_s)$ was found to depend on the spin anisotropy nature. In one Ising-spin glass, $E_Z(H, N_s) \sim H$ was observed,⁵ while in several Heisenberg spin glasses, $E_Z(H, N_s) \sim H^2$ was reported.^{3–5} To account for these observations, the following empirical models were proposed:

$$E_Z(H) = \sqrt{N_s} \mu H; \text{ for Ising SG's, with relatively small } N_s \quad (4)$$

and

$$E_Z = N_s \chi_{FC} H^2; \text{ for Heisenberg SG' with macroscopically large } N_s, \quad (5)$$

where μ is the magnetic moment and χ_{FC} the field cooled susceptibility per spin. While the extraction of N_s from $E_Z(H)$ is rather straightforward, the calculation of the correlation length, ζ , from N_s is less palpable due to the fractal nature of the spatial correlations omnipresent in disordered systems such as spin glasses. To this end, Berthier *et al.* has determined numerically the fractal dimensionality of the "backbone spin structure," $d-\alpha$. In Ising and Heisenberg spin glasses these values correspond to $\approx d - 0.5$ and $d - 1$ ($d = 3$ for 3D systems), respectively.^{6,7} The simplest assumption is then to take $\zeta / \zeta_o = N_s^{1/(d-\alpha)}$ to deduce the correlation length from the experimentally determined values of N_s . ζ_o is the average distance between two neighboring (super)spins.

As depicted in Figure 1, SPM magnetization of the aligned (textured) sample was about 3 times that of the random sample. While the glass transition temperature ($T_g \sim 69$ K) was not affected by the anisotropy-axis alignment, there were appreciable changes in the SSG dynamics between the two systems. The notable differences between the two SSG's are as follows. (a) The critical exponent values were found to increase slightly from $z\nu \approx 7$ in the random sample to ≈ 8.5 in the aligned sample (inset of Figure 1). (b) Stronger cooling effect was observed in the aligned sample.¹⁴ (c) The field dependence of t_w^{eff} (see Figure 2) was nearly quadratic in the random SSG, whereas it became linear in the aligned SSG. These contrasts closely mimic the reported differences between Heisenberg (weak cooling rate effect and $t_w^{\text{eff}} \sim H^2$) and Ising (strong cooling effect, larger $z\nu$, and $t_w^{\text{eff}} \sim H$) atomic spin glasses. With this analogy in mind, we have used the above mentioned empirical model for atomic Ising spin glasses (Eq. (4)) to extract the number of correlated superspins in the aligned SSG sample.

The quadratic dependence of $E_Z(H)$ in the random SSG, however, is only true at higher field values. At lower fields, the growth appears to be slower than H^2 (bottom inset of Fig. 2). We can interpret this slope change in the following manner. Randomly oriented or aligned, the superspins

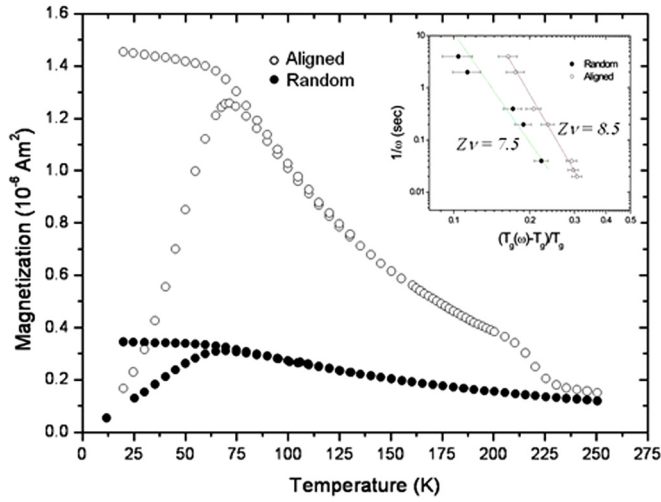


FIG. 1. ZFC/FC of aligned (textured) and random (non-textured) ferrofluids measured at $H = 1$ Oe. A sudden drop in the magnetization of aligned sample near 200 K indicates the onset of the melting of glycerol. Inset: determination of the critical exponents on both ferrofluids obtained from ac susceptibility measurements.

possess well defined anisotropy-axis. Therefore, for small values of N_s , the magnetization of randomly oriented super-spins must follow $M(N_s) = \sqrt{(N_s/3)}\mu$, which contributes a linear term in $E_z(H)$, observable only at low fields. With increasing field strength and N_s , the magnetization will crossover to a macroscopic and extensive form, $N_s\chi_{FC}H$, and thus the quadratic term, $N_s\chi_{FC}H^2$, dominates the total Zeeman energy. The corresponding total E_z in a random SSG is then expressed as

$$E_z(H) = \sqrt{(N_s/3)}\mu H + N_s\chi_{FC}H^2. \quad (6)$$

A quick verification reveals that for $N_s \sim 300$ (value previously reported in a maghemite frozen ferrofluid¹²) and the corresponding values of μ and χ_{FC} of the nanoparticles (same as those used in this study) the crossover from linear to quadratic dependence occurs at H as low as a few Gauss.¹⁹

In Figure 3, the extracted values of N_s of both aligned and random SSG's studied here along with the results from our previous report¹¹ are presented as a function of scaled time, $\ln(t_w/\tau_0)T/T_g$, and compared to the experimental results in atomic spin glasses from various groups.³⁻⁵ The scaling parameter is a direct consequence of the power law behavior of $\xi(t)$ as mentioned earlier. As can be seen from the figure, $N_s(t_w, T)$ data in two random SSG samples lie on the extension of data points collected from Heisenberg SG's. For the aligned SSG and the Ising spin glass data, a common growth curve may be drawn (dotted line) to accommodate both data sets; however, the agreement is less evident than in the Heisenberg counterpart.

We now attempt to estimate the correlation length ξ/ξ_0 from N_s in both aligned and random SSG's as well as in atomic spin glasses summarized in Figure 3. The fractal exponents used here are those introduced by Berthier and Young; namely, $d - \alpha \approx 2.5$ (Ising SG and aligned SSG) and 2 (Heisenberg SG and random SSG).^{6,7} One can see from Figure 4 that ξ/ξ_0 data of random SSG's position themselves nicely between the Heisenberg SG simulation curve and the experimental results within experimental error bars. It should be noted that in the simulation on Heisenberg SG's, a clear downward curvature was observed at low temperature and at large waiting times. Combined with the uncertainty associated with the fractal exponent values themselves, the qualitative agreement found between the experimentally extracted correlation lengths and the simulation results must be regarded with precaution. However, it should not be an overstatement to say that the Heisenberg simulation curves and the experimental results are in quantitative agreement.

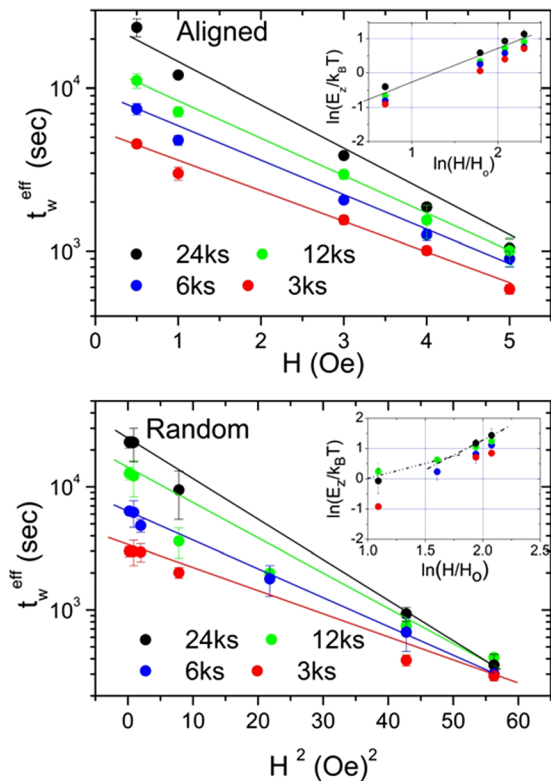


FIG. 2. The effective waiting times in ZFCM in aligned (top) and random (bottom) SSG samples at $T = 0.7 T_g$ as a function of H and H^2 , respectively. The insets show the log-log representation of Zeeman energy as a function of H/H_0 with $H_0 = 1$ Oe in the aligned SSG and $= 1.4$ Oe in the random SSG.

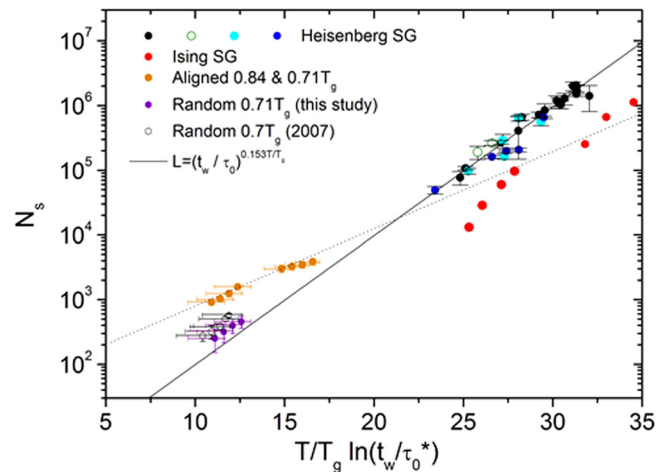


FIG. 3. $N_s(t_w, T)$ extracted using Eqs. (4) and (6), plotted against $T/T_g \ln(t_w/\tau_0^*)$ compared to the experimental results reported in atomic spin glasses.³⁻⁵ $N_s(t, T)$ in random SSG's (this and previous work¹²) coincide with the scaling curve found among Heisenberg atomic spin glasses within experimental uncertainties.

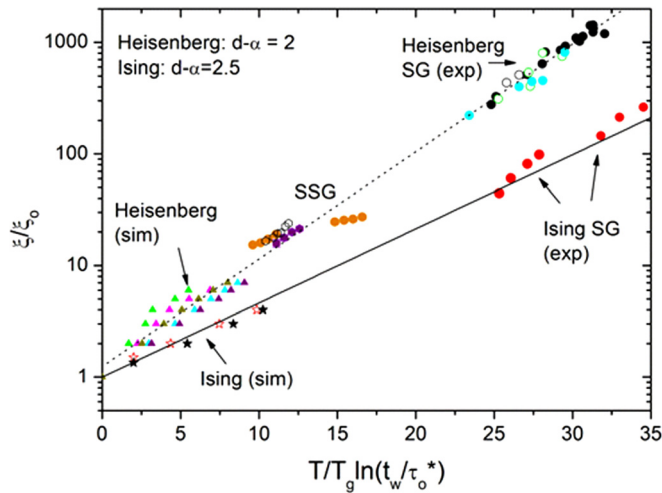


FIG. 4. Correlation lengths (ξ/ξ_0) calculated from N_s in aligned and random SSG's as well as in atomic SG's³⁻⁵ (experimental) using $\alpha = 0.5$ (Ising SG and aligned SSG) and 1.0 (Heisenberg SG and random SSG). The values are plotted as a function of scaled time (same symbols as in Fig. 3) and compared to the numerical simulations.^{6,7} Symbols: Stars—Ising SG (numerical) at $T = T_g$ and $0.5T_g$; solid triangles—from right to left, Heisenberg SG (numerical) at $T = T_g, 0.875T_g, 0.75T_g, 0.5T_g,$ and $0.25T_g$; solid circles—atomic SG's (experimental); octagons—SSG's (this work).

Further, the correlation length growths in randomly oriented SSG's appear to follow the same physical law as that of atomic spin glasses. The correlation length data in the Ising spin glass sample measured at two different temperatures⁵ fall upon the extension of the Ising simulation curves. The Ising simulation results all scale to a single master curve when plotted as a function of $\ln(t_w/\tau_0)T/T_g$ as it should if ξ grows as $(t_w)^{zT/T_g}$. In the aligned SSG, the correlation length appears to fall somewhere between the Heisenberg and Ising type dynamics. This may not be too surprising considering that magnetic nanoparticles do not possess infinite anisotropy energy, and therefore our aligned sample may still be far from a true Ising superspin glass system.

We have extracted the growing number of dynamically correlated superspins in the SSG state of textured (aligned) and non-textured (randomly oriented) frozen ferrofluids via ZFCM relaxation measurements. The number of correlated spins, N_s , in randomly oriented superspin glasses lies on the extension of the general curve found in Heisenberg spin glasses.³⁻⁵ The corresponding correlation lengths of random SSG and Heisenberg-like SG's estimated using the fractal exponent suggested by Berthier and Young are in a quantitative agreement with the numerical simulations on Heisenberg SG's by the same authors.^{6,7}

This work demonstrates the usefulness of interacting magnetic nanoparticle systems to revisit the physics of spin glass by virtue of their tunable physical parameters. With a right combination of particle size (tunes $\tau_0(T)$ and T_B) and concentration (tunes T_g) one can hope to fully bridge the gap between the experiments and the numerical simulations left behind by decades of research in atomic spin glasses.

S.N. and E.V. thank Professor S. Miyashita and Professor H. Yoshino for insightful discussions and suggestions.

- ¹S. Bedanta and W. Kleemann, *J. Phys. D: Appl. Phys.* **42**, 013001 (2009).
- ²For example, see also M. F. Hansen, P. E. Jönsson, P. Nordblad, and P. Svedlindh, *J. Phys.: Condens. Matter* **14**, 4901 (2002); P. E. Jonsson, *Adv. Chem. Phys.* **128**, 191 (2004); S. Sahoo, O. Petravic, Ch. Binek, W. Kleemann, J. B. Sousa, S. Cardoso, and P. P. Freitas, *Phys. Rev. B* **65**, 134406 (2002); K. Hiroi, K. Komatsu, and T. Sato, *ibid.* **83**, 224423 (2011).
- ³Y. G. Joh, R. Orbach, G. G. Wood, J. Hammann, and E. Vincent, *Phys. Rev. Lett.* **82**, 438 (1999); *J. Phys. Soc. Jpn.* **69**(Suppl. A), 215 (2000).
- ⁴E. Vincent, *Lect. Notes Phys.* **716**, 7 (2007); e-print [arXiv:cond-mat/0603583](https://arxiv.org/abs/cond-mat/0603583) and references therein.
- ⁵F. Bert, V. Dupuis, E. Vincent, J. Hammann, and J.-P. Bouchaud, *Phys. Rev. Lett.* **92**, 167203 (2004).
- ⁶L. Berthier and J.-P. Bouchaud, *Phys. Rev. B* **66**, 054404 (2002).
- ⁷L. Berthier and A. P. Young, *Phys. Rev. B* **69**, 184423 (2004).
- ⁸F. Belletti, M. Cotallo, A. Cruz, L. A. Fernandez, A. Gordillo-Guerrero, M. Guidetti, A. Maiorano, F. Mantovani, E. Marinari, V. Martin-Mayor, A. M. Sudupe, D. Navarro, G. Parisi, S. Perez-Gaviro, J. J. Ruiz-Lorenzo, S. F. Schifano, D. Sciretti, A. Tarancon, R. Tripiccion, J. L. Velasco, and D. Yllanes, *Phys. Rev. Lett.* **101**, 157201 (2008).
- ⁹G. G. Wood, *J. Magn. Magn. Mater.* **322**, 1775 (2010).
- ¹⁰J. Kisker, L. Santen, M. Schreckenberg, and H. Rieger, *Phys. Rev. B* **53**, 6418 (1996).
- ¹¹D. Parker, V. Dupuis, F. Ladieu, J.-P. Bouchaud, E. Dubois, R. Perzynski, and E. Vincent, *Phys. Rev. B* **77**, 104428 (2008).
- ¹²E. Wandersman, V. Dupuis, E. Dubois, R. Perzynski, S. Nakamae, and E. Vincent, *Europhys. Lett.* **84**, 37011 (2008).
- ¹³S. Nakamae, Y. Tahri, C. Thibierge, D. L'Hôte, E. Vincent, V. Dupuis, E. Dubois, and R. Perzynski, *J. Appl. Phys.* **105**, 07E318 (2009).
- ¹⁴S. Nakamae, C. Crauste-Thibierge, K. Komatsu, D. L'Hôte, E. Vincent, E. Dubois, V. Dupuis, and R. Perzynski, *J. Phys. D: Appl. Phys.* **43**, 474001 (2010).
- ¹⁵The E_a value was extracted from AC susceptibility measurements data following the method introduced by J. L. Dormann, L. Bessais, and D. Fiorani, *J. Phys. C: Solid State Phys.* **21**, 2015 (1988) with τ_0 fixed to 10^{-9} s. This is slightly higher than the value reported on the same maghemite nanoparticles; however, the modification does not alter our conclusions reached in our previous works (Refs. 11–13).
- ¹⁶*Magnetic Fluids and Application Handbook*, edited by B. Berkowski (Begell House, New York, 1996).
- ¹⁷J. P. Bouchaud, *J. Phys. I* **2**, 1705 (1992); E. Vincent, J. P. Bouchaud, D. S. Dean, and J. Hammann, *Phys. Rev. B* **52**, 1050 (1995).
- ¹⁸L. Lundgren, P. Svedlindh, and O. Beckman, *Phys. Rev. B* **26**, 3990 (1982).
- ¹⁹We suspect that the crossover from linear to quadratic regimes in these samples had gone undetected in the ZFCM experiments on Heisenberg spin glasses because of high magnetic fields (extending to a few thousand G's) used and the large N_s values (in the order of 10^5 – 10^6).

4.2. Violation of the Fluctuation-Dissipation Theorem in a Superspin Glass

4.2.1. Background

The Fluctuation Dissipation Theorem (FDT) relates the internal spontaneous fluctuations of a system at thermal equilibrium to its response to the perturbation from an external constraint. Therefore FDT should hold only in ergodic systems. In its fundamental form, it relates two time-dependent quantities; the response function $\chi(t)$ and the thermodynamic time autocorrelation function $C(t)$:

$$\chi(t) = -\frac{1}{k_B T} \frac{d}{dt} C(t) \quad (4.4)$$

Equivalently, the above expression can be written for a magnetic system as [104]:

$$\langle \delta M(\omega)^2 \rangle = \frac{2k_B T}{\pi V} \left(\frac{\chi''(\omega)}{\mu_0 \omega} \right) \quad (4.5)$$

$\langle \delta M(\omega)^2 \rangle$ is the ensemble average of the power spectrum of the magnetization fluctuations (noise), $\chi''(\omega)$ the imaginary component of the ac susceptibility and V the sample volume. In out-of-equilibrium systems where $C(\infty) \neq 0$, this relation is no longer valid. The ageing effects must appear in the noise at frequencies smaller than the inverse of the age, while at higher frequencies the spectra remain stationary. The violation of FDT has been studied in different types of complex systems, and in the case of short-range spin glasses, it has been analyzed in the framework of mean field theory (with full RSB) [117]. The departure from equilibrium can be expressed in terms of the effective temperature T_{eff} , that provides a generalized form of FDT extending to out-of-equilibrium systems [101]; *i.e.*,

$$\langle \delta M(\omega, t_w)^2 \rangle = \frac{2k_B T_{eff}}{\pi V} \left(\frac{\chi''(\omega, t_w)}{\mu_0 \omega} \right) \quad (4.6)$$

T_{eff} is larger than T for frequencies larger than the inverse of t_w , but otherwise should equal to T . The experimental evidence in an insulating spin glass by Hérisson and Ocio [103] attests to this effect, although this is a singular demonstration of its kind in spin glasses, and to the best of my knowledge no other experimental reports have been published to confirm, or contradict their results.

The lack of experimental evidence can easily be explained by the technical challenges involved in measuring the magnetization fluctuations. In the noise measurements by Hérisson and Ocio [105], a large quantity of $\text{CdCr}_{2x}\text{In}_{2-2x}\text{S}_4$ powder-grease mixture was required (a 40 mm long, 5 mm diameter cylindrical sample holder) in order to simultaneously record the bulk magnetic susceptibility (response) and the noise (temporal correlation) signals. The measured thermodynamic fluctuations in their experiment were equivalent of only 10^{-7} G. To this end, superspin glasses are of particular interest because going from atomic spin glasses to superspin-glasses, the typical inter-spin distance increases by about two orders of magnitude, with individual superspins having dipolar magnetic moments of 10^4 - $10^5 \mu_B$ each. Typical number of correlated spins N_s (as seen in the previous section) in the SSG state of frozen ferrofluids can reach 10^3 after a waiting time of $\approx 10^4$ s. In a concentrated system, this corresponds to about $(0.1 \mu\text{m})^3$ to be occupied by an average-sized correlated zone. Consequently, with micro-meter sized probes with a high enough signal resolution one should be able to perform local measurements to detect the fluctuations from a small number of correlated zones.

4.2.2. Noise Measurements Using Micro-Hall probes

Encouraged by this prospect, we have developed an experimental setup based on micro-Hall probes that is capable of detecting small fluctuations in the local magnetic field. The Hall probes are magnetic field sensors based on the Hall effect (named after E. Hall) is the production of a transverse voltage difference (known as the Hall voltage) across an electrical conductor when a magnetic field is applied perpendicularly to the electric current. The Hall voltage is proportional to the strength of the applied field and thus it is a direct measure of magnetic induction B , rather than magnetic flux. For our study we have used a particular kind of Hall probes, Quantum Well Hall Sensors (QWHS). QWHS's make use of 2D electron gas confined in a quantum well that is formed in a thin semiconductor material (GaAs, for example) sandwiched between two layers of another type of semiconductor with a wider bandgap (see Fig. 4.4). These structures are most often grown by molecular beam epitaxy and the width of a QWHS cross can be made very small, to less than $1 \mu\text{m}$. For the magnetization noise measurements, we have used a microHall probe with a nominal Hall cross area of $2 \times 2 \mu\text{m}^2$. The effective area size, however, is estimated to be less than $1 \mu\text{m}^2$ due to the lateral etching and the depletion zone appearing at each edge (see Figure 4.4).

For the fluctuation-dissipation study, the most important advantage of using a microHall sensor is the sensor-to-sample proximity ($< 1 \mu\text{m}$). At this distance, the local field fluctuations (due to collective superspin fluctuations) are expected to reach 10^{-3}G . Much effort and time were invested in reducing the system noise at various frequencies; *e.g.*, anti-vibration and anti-RF measures and the 'spinning current' measurement technique; until the system signal noise became smaller than the expected values of induced local magnetic field ($B_z \approx 0.6 \text{G}$ (at 50K , and $H_{\text{app}} = 1 \text{G}$) and of magnetic noise ($\langle \delta B_z \rangle > \approx 12.5 \text{mG/Hz}^{0.5}$) from a ferrofluid sample of $1 \mu\text{m}^3$. The $\langle \delta B_z \rangle$ value was estimated from the FD relation with available experimental data from the bulk magnetic susceptibility measurements.

As before, a ferrofluid made of maghemite $\gamma\text{-Fe}_2\text{O}_3$ nanoparticles with 8.6nm diameter and 15% volume fraction was used. A thin gold wire ($17 \mu\text{m}$ diameter) was dipped in ferrofluid and was then used to deposit a small volume (1-10 pico-liter) of the ferrofluid sample directly onto the Hall sensor surface (Figure 4.4 left). Once the sample is in place, we quickly cooled down the sample + sensor to temperature below the freezing temperature of glycerol (190K) in the helium atmosphere to avoid the fluid evaporation. During the subsequent noise measurements that lasted over 6 months, the sample was never brought to temperature above 140K .

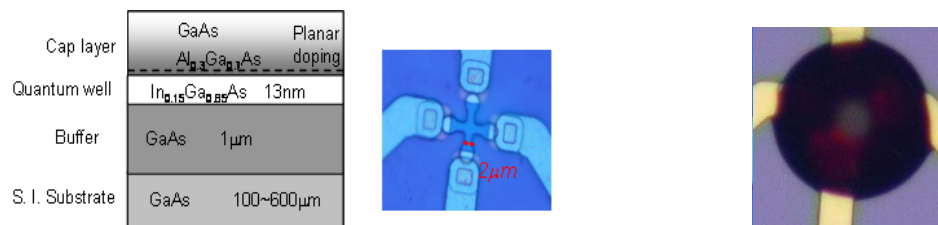


Figure 4.4: (left/middle) Pseudomorphic heterostructure of Hall-sensor. The epilayer sequence incorporates a $1 \mu\text{m}$ thick GaAs buffer, followed by a 13nm thick $\text{In}_{0.15}\text{Ga}_{0.85}\text{As}$ quantum well, $\text{Al}_{0.3}\text{Ga}_{0.7}\text{As}$ barrier layer with graded aluminum concentration and $5\text{-}10 \text{nm}$ GaAs capping layer. All layers, apart from the quantum well, are fully depleted of charge carriers. (right) The same microHall probe with a small drop of $\gamma\text{-Fe}_2\text{O}_3$ ferrofluid deposited directly on top.

The more detailed accounts on the spinning current technique (see also [118]) used to improve the signal resolution and the calculation methods for $\langle \delta B_z \rangle$ are found in the articles presented in Section 4.2.3. In Section 4.2.4, our published work on the experimental investigation on the FDT violation using a microHall probe is presented. As described in the article, the FD relation was found to break down below the glass transition temperature T_g . The effective temperature extracted $T < T_g$ was found to grow with decreasing temperature. While the T_{eff} values found here are in the same order as those reported by Hérisson and Ocio in an insulating spin glass, its temperature dependence is opposite. The discrepancy may not be surprising considering the difference in two systems as well as the methods for extracting T_{eff} values. Since this publication, we have performed over 100 temperature quench measured with raw magnetic signals recorded for 10^4 s (at every 0.1 s). These data will be analyzed for different values t_w which may bring correction to these findings.

4.2.3. A local noise measurement device for magnetic physical systems

This article was published in *Journal of Statistical Mechanics: Theory and Experiment* **2009** p01027.

A local noise measurement device for magnetic physical systems

D L'Hôte¹, S Nakamae¹, F. Ladiou¹, V Mosser², A Kerlain² and M. Konczykowski³

¹Service de Physique de l'Etat Condensé (CNRS/MIPPU/URA 2464),
DSM/IRAMIS/SPEC, CEA Saclay, F-91191 Gif/Yvette Cedex, France

²ITRON SAS, 76 avenue Pierre Brossolette, F-92240 Malakoff, France

³Laboratoire des Solides Irradiés, Ecole Polytechnique, F-91128 Palaiseau, France

Abstract. We present an experimental setup developed to measure locally the fluctuations of the magnetization of physical systems such as spin and superspin glasses, etc. It is based on micronic and submicronic Hall probes. We present the noise reduction at ambient temperature owing to the use of the spinning current technique. Finally, we show why, with such probes, the noise measured on a macroscopic sample probes only a microscopic volume of the sample.

Pacs. 07.55.-w, 85.30.Fg, 75.30.Kz, 75.50.Lk, 75.30.Mb

1. Introduction

Many open problems in the physics of complex systems require local and microscopic measurements of the physical observables. This is particularly true in what concerns the time fluctuations of these observables, which are directly related to the correlations due to the interactions among the elementary components of the system. The correlation between the fluctuations of a physical quantity considered at two points of the system can be characterized by its size in space and time. A local microscopic probe of size W and bandwidth $[0, f]$ will enable measurements of correlations having space-time size larger than $W \times 1/f$, that are experimentally unreachable in the bulk measurements involving macroscopic sizes. An example of local noise measurements that shows the interest of such experiments is the direct observation of molecular cooperativity near the glass transition in a polymer [1].

2. Physics goals

We intend to measure the local magnetic fluctuations of spin or superspin glasses [2-6], and more generally 2 and 3D assemblies of magnetic (or superconducting) interacting nano-objects with various disorder levels. We are also interested in the non-equilibrium properties of aging ferromagnetic systems under an external field, etc [7]. Below a critical temperature, those systems are highly out of equilibrium, thus the fluctuation-dissipation theorem is no longer verified [8-11], and the fluctuations harbor a physical information which is not contained in the linear response functions. In addition, close to the transition, the fluctuations should exhibit a critical behavior [12]. Finally, the fluctuations are related to the correlations among the elementary magnetic moments, thus their measurement will provide an information on the correlation lengths and lifetimes [1].

Our experiment is based on high resolution submicron Hall probes. With such devices, the measurable space-time correlation sizes should be larger than $\sim 300 \text{ nm} \times \sim 1 \text{ ms}$. The physical system of interest can be macroscopic or microscopic and even smaller than the probe itself.

3. Experimental setup

To measure the magnetization of physical systems at a microscopic level, we developed an experimental setup based on micronic and sub-micronic magnetic sensors working at temperatures $4 \text{ K} < T < 300 \text{ K}$. Aiming at achieving high resolution measurements, several techniques minimizing parasitic noise contributions have been used: Antivibration devices, complete anti-RF shieldings from

the sample up to the first amplification stage, use of very low noise preamplifiers (NF-LI75A[®]), eventual use of the coincidence between two amplifiers to suppress their voltage noise contribution, etc.

We use micro-Hall sensors made from a two-dimensional electron gas (2DEG) in AlGaAs/InGaAs/GaAs heterostructures [13-16]. Hall probes are widely used as magnetic sensors because of their versatility and simplicity of use [17,18]. Contrary to micro-SQUIDs (Superconducting Quantum Interference Device) and to GMR sensors (Giant Magnetoresistance), their dynamics on the measured magnetic field is unlimited. A GMR sensor is able to measure small field variations around a given field value, while Hall probes can measure any field up to 10 T and higher. Such an advantage can become a decisive factor because in many experiments the sum of the applied field (which is usually varied) and the response of the sample needs to be measured. In addition, our micro-Hall probes [13-16] have the advantage in comparison with micro-SQUIDs to be functional in large temperature (and frequency) intervals : From a few mK to above 300K, another decisive advantage for most application. A niobium micro-SQUID for instance works only at temperatures below 7K. We should also mention the possibility to move the probe « scanning Hall probe microscopy [19-23] » in front of the sample.

Most Hall sensors are realized from semiconducting materials which offer the low carrier densities allowing a high sensitivity. Confining the carriers in a quantum well such as our AlGaAs/InGaAs/GaAs heterostructures [13-16,24,25] do, leads to a temperature independent carrier density. The low density of the electron gas results in a large Hall coefficient of $820 \Omega \cdot T^{-1}$ for $4K < T < 350K$. We plan to use simple Hall crosses, as well as linear arrays of Hall crosses that will allow spatial correlation measurements (see figure 1). Note that in addition to the Hall sensors themselves, it is possible to pattern additional circuits such as thermometers, coils, front-end electronics, grids etc. At present, our Hall probe sizes range from 1×1 to $5 \times 5 \mu m^2$, and are patterned by photolithography at Thales Research Technology. Reaching submicronic sizes either by electron beam lithography, or by focussed ion beam passivation is also envisaged in our project.

In a standard experiment, the sample is deposited on the Hall probe wafer. The sample can be meso or nanoscopic. We succeeded in depositing a microdrop of 20 pl of a ferrofluid on the Hall probe surface (see figure 1(a)), a first step towards submicronic samples. On the other hand, if the physical system of interest is macroscopic, it can be shown that the volume which is probed in the sample is microscopic provided that the probe and the distance between the sample surface and the 2DEG are small enough (see section 5).

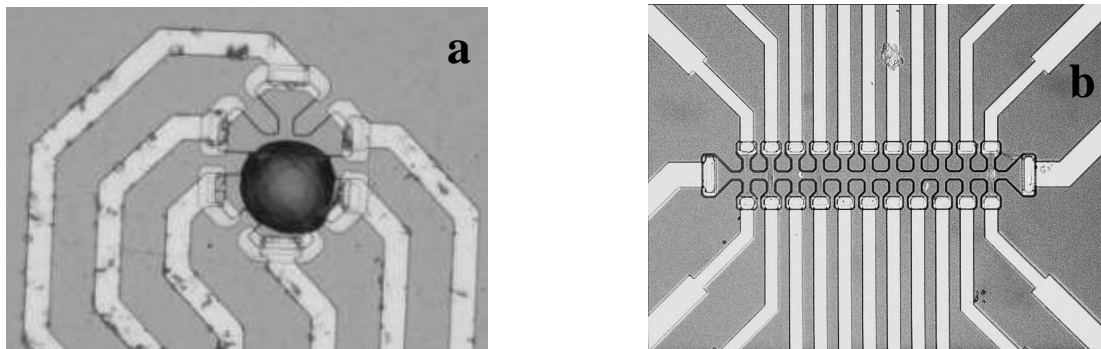


Figure 1 (a): A Hall bar made of two Hall crosses in series, on which the 20 pl drop of ferrofluid ($\sim 25 \mu m$ in diameter) has been deposited. (b): An array of 11 Hall crosses which allows the correlation measurements between two crosses, thus providing an information on the size and location of a volume that generates the magnetic field measured in the two crosses.

4. Improvement of the resolution by using the spinning current method

With a simple Hall voltage measurement, the resolution we obtained ranges from 5 to 15×10^{-7} T (FWHM) for temperatures below 80 K and measurement rates of 0.1 – 10 Hz. The main limitation to the resolution comes from excess noise, with $1/f^\alpha$ ($0.3 < \alpha < 2$) or Lorentzian spectra, and a power

proportional to the squared bias current squared (see figure 2).

However, we started to use the “spinning current” method - which has been developed first to cancel the Hall voltage offset, see figure 3(b) - in order to improve the resolution [15,26-31]. Figure 3(a) shows a spectrum obtained with this method at ambient temperature. The striking result is that the excess noise has been suppressed and the noise is almost independent of the bias current, close to the Johnson-Nyquist level. The resolution improvement expected at low temperature is thus larger than one order of magnitude.

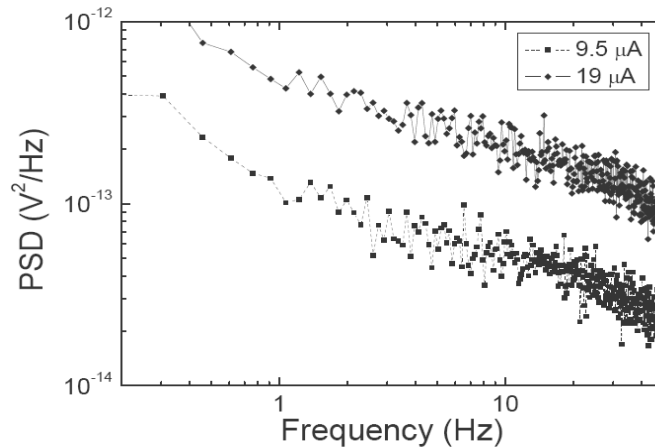


Figure 2. An example of Hall voltage power noise spectra obtained at 296 K, for bias currents of 9.5 and 19 μA .

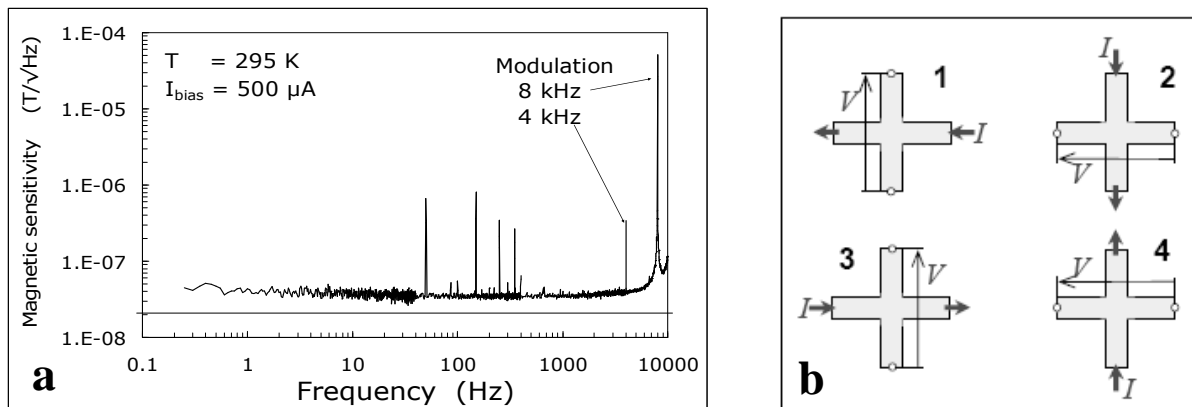


Figure 3. (a): Power noise spectra of the Hall voltage at ambient temperature obtained on a Hall cross by using the spinning current method. The horizontal line is the Johnson-Nyquist noise of the arm of the cross along which the voltage is measured. (b): The spinning current technique: at each step (1 to 4), the directions in which the current I is injected and the Hall voltage V is measured are rotated by 90° . V is then low-pass filtered at a frequency lower than the rotation/modulation frequency and larger than the typical frequencies of the fluctuations to be measured.

5. Locality of the noise measurement

If the physical system of interest is macroscopic, the geometry of an experiment will consist in placing a local probe on the surface of the sample. Thus an important question is that of the fractional volume within the sample that will contribute to the measured signal. A simple calculation gives a first answer

to this question. Assuming that the magnetic probe is at the distance d from the surface of the sample, with its three dimensions supposedly much larger than d and the probe size, it is possible to calculate the average value $\langle B_z \rangle$ of the magnetic field along the z -direction perpendicular to the surface, as well as the variance $\langle \delta B_z^2 \rangle$ of its fluctuations. Note that in practice d is usually larger than a few hundreds of nanometers because the layer probing the magnetic field (i.e. the 2D carrier gas) is located below the surface of the Hall probe. The geometry assumed for the calculation is shown on figure 4 (a): The field \mathbf{B} is calculated at point O located at the distance d from the sample surface which occupies an infinite volume delimited by a plane. We assume that the field is due to independent magnetic moments \mathbf{m}_0 fluctuating isotropically. From the equation giving \mathbf{B} ,

$$\mathbf{B} = \int \frac{d^3 r}{v_0} \frac{\mu_0}{4\pi} \left[3 \frac{\mathbf{m}_0(\mathbf{r}) \cdot \mathbf{r}}{r^5} \mathbf{r} - \frac{\mathbf{m}_0(\mathbf{r})}{r^3} \right], \quad (1)$$

where \mathbf{r} is the position ($r^2 = r^2$) of the magnetic moment, $\mathbf{m}_0(\mathbf{r})$ and v_0 the volume associated to \mathbf{m}_0 (typically, the volume occupied by an elementary magnetic moment of an atom, a nanoparticle, etc.), it is possible to calculate the variances of the fluctuations of \mathbf{B} , $\delta \mathbf{B}$:

$$\langle \delta B_i \delta B_j \rangle = \int \frac{d^3 r}{v_0} \left(\frac{\mu_0}{4\pi} \right)^2 \left\langle \left[3 \frac{\delta \mathbf{m}_0(\mathbf{r}) \cdot \mathbf{r}}{r^5} r_i - \frac{\delta m_{0i}(\mathbf{r})}{r^3} \right] \left[3 \frac{\delta \mathbf{m}_0(\mathbf{r}) \cdot \mathbf{r}}{r^5} r_j - \frac{\delta m_{0j}(\mathbf{r})}{r^3} \right] \right\rangle, \quad (2)$$

where the subscripts i, j correspond to the coordinates x, y and z , $\delta \mathbf{m}_0$ is the fluctuations of \mathbf{m}_0 and $\langle \rangle$ stand for an average on the fluctuations. Assuming that the variances of \mathbf{m} are uniformly distributed in space, the variances of all three components of \mathbf{B} fluctuations are

$$\langle \delta B_i \delta B_i \rangle = \left(\frac{\mu_0}{4\pi} \right)^2 \frac{\sigma_{0i}^2}{v_0} \int \left(\frac{1}{r^6} + 3 \frac{r_i^2}{r^8} \right) r^2 \sin \theta dr d\theta d\varphi, \quad (3)$$

with σ_{0i} the standard deviation of δm_{0i} and r, θ, φ the spherical coordinates corresponding to \mathbf{r} . The contribution of the magnetic moments located at a distance r to the variances of $\delta \mathbf{B}$ can be calculated by integrating with respect to θ and φ in Eq. (3) and by looking at the r dependence of the remaining term in the integral. The result is shown on figure 4(b) where the calculated spatial distribution of the magnetic moments contributing to the measured variance of the B_z component of the field is given as a function of their distance r to the probe (continuous thick line). This distribution is peaked for $r \approx 1.2 d$, and approaches zero as r^{-4} when r increases. As a consequence, only the moments located at a distance to the surface of the order of d contribute to the fluctuations of the measured magnetic field. Thus, when the probe is used to measure fluctuations, it is truly 'local' provided that d is sufficiently small. This is due to the fact that the variance $\langle \delta B_z^2 \rangle$ is the sum of squares (the contributions of the elementary moments which are proportional to r^{-6}) weighted by a geometrical jacobian $\propto r^2$.

On the contrary, the measured magnetic field $\langle B_z \rangle$ (when the sample magnetization is finite) is not that 'local' in the sense that the distribution of the magnetic moments contribution as a function of r varies as r^{-1} for large r : This results from the r^{-3} dependence of the field magnitude of a magnetic moment and the r^2 dependence of the volume element $d^3 r = r^2 \sin \theta dr d\theta d\varphi$ (see Eq. (1)). In fact the situation is a bit more subtle as shown on figure 4: If the sample is assumed to occupy the whole space on one side of a plane located at the distance d of the Hall probe (hatched area on figure 4(a)), the r distribution of the contribution to $\langle B_z \rangle$ is peaked at $1.4 d$ and decreases as r^{-2} when r increases (dashed thick line on figure 4(b)). However this results from the difference of two distributions. The first one (dot-dashed thin line on figure 4(b)) corresponds to the contribution of the magnetic moments located at an angle $\theta > \theta_L$ (see figure 4(a)), which give a positive contribution to $\langle B_z \rangle$ if $m_{0z} > 0$. The second one (dotted thin line on figure 4(b)) corresponds to the moments located at an angle $\theta < \theta_L$, giving a negative contribution to $\langle B_z \rangle$ again if $m_{0z} > 0$. Those two contributions decrease only as r^{-1} when r increases. As a result, the contribution from the moments located at distances $r \gg d$ may be non negligible, depending on the geometry and homogeneity of the sample.

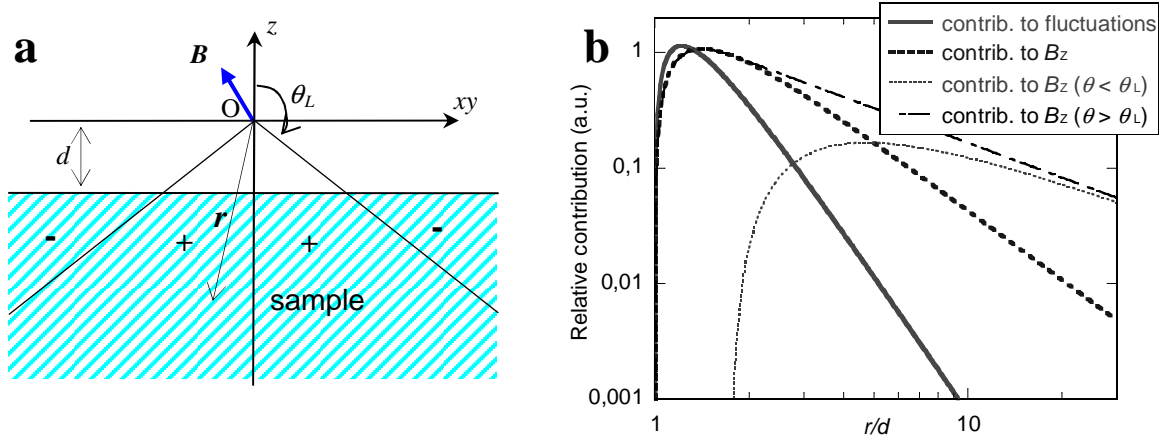


Figure 4. Calculated spatial distributions of the contributions to the average magnetic field $\langle B_z \rangle$, and to its fluctuations variance $\langle \delta B_z^2 \rangle$ measured at a distance d of the surface of the magnetic sample. (a): The geometry assumed for the calculation: the Hall probe is located at point O where \mathbf{B} is calculated, and the sample (hatched area) contains magnetic moments uniformly distributed in the whole volume $z < -d$. (b): The distributions are presented as a function of r/d , r being the distance from the probe center O to a microscopic volume element in the sample. The r/d distribution of the contribution to $\langle \delta B_z^2 \rangle$ is given (continuous thick red line) together with the distribution of the contribution to $\langle B_z \rangle$ (dashed thick blue line), which is the sum of the (positive) contribution of the volume $\theta > \theta_L$ (dot-dashed thin line) and the (negative) contribution of the volume $\theta < \theta_L$ (dotted thin line giving the absolute value).

6. Conclusion

We have presented a device developed to measure locally the fluctuations of the magnetization of disordered and/or frustrated systems such as spin glasses, assemblies of magnetic (or superconducting) interacting nano-objects with various disorder levels, aging ferromagnetic systems, etc. At low temperature those systems cannot reach equilibrium within the experimental time scale, and the fluctuation-dissipation theorem (FDT) is violated [8-11]. Their microscopic description remains an open problem. It has been proposed that aging should be associated with the growing of a typical lengthscale [5-7,11,32-35] in a given system at a given time. Large lengthscales subsystems would be frozen while small ones could evolve towards equilibrium. This is why local noise measurements are of fundamental interest: The out-of-equilibrium situation is expected to be heterogeneous. As an example, a Monte-Carlo simulation of an Ising spin glass predicts that the FDT violation and the resulting effective temperature exhibit strong spatial fluctuations [34,35]. It should be mentioned that as for bulk properties, local properties of spin glasses can be considered as a reference to analyze more complex systems such as structural glasses. Recently, the heterogeneous dynamics of structural glasses has been experimentally investigated by using local noise measurements [36,37].

Another interest of local noise measurements (however related to FDT violation) is the fact that the fluctuations depend on the correlations among the elementary components of the system: correlated fluctuations add in a way that leads to a noise with a magnitude and a time structure different from those induced by independent fluctuators. Local noise measurements should thus give information on correlation lengths and lifetimes that will serve as the main keys for understanding disordered and out of equilibrium systems.

Acknowledgements

We thank Roland Tourbot for the realization the improved experimental setup with the anti-parasitic noise devices evoked in the text. This work is supported by the RTRA-Triangle de la Physique (MicroHall).

References

- [1] Vidal Russell E and Israeloff N E 2000 *Nature* **408** 695
- [2] Parker D, Dupuis V, Ladiou F, Bouchaud J-P, Dubois E, Perzynski R and Vincent E 2008 *Phys. Rev. B* **77** 104428
- [3] Jonsson T, Mattsson J, Djurberg C, Khan FA, Nordblad P and Svedlindh P 1995 *Phys. Rev. Lett.* **75** 4138
- [4] Binder K and Young A P 1986 *Rev. Mod. Phys.* **58** 801
- [5] Dupuis V, Bert F, Bouchaud JP, Hammann J, Ladiou F, Parker D and Vincent E 2005 *Proc. of Stat Phys 22 (Bangalore, India), Pramana Journal of Physics* **64** p 1109 (Preprint arXiv:cond-mat/0406721)
- [6] Mydosh JA 1993 *Spin glasses: an experimental introduction* (London: Taylor & Francis)
- [7] Biroli G 2005 *J. Stat. Mech.* P05014
- [8] Hérisson D and Ocio M 2002 *Phys. Rev. Lett.* **88**, 257202
- [9] Hérisson D and Ocio M 2004 *European Physical Journal B* **40**, 283
- [10] Cugliandolo L F and Kurchan J 1994 *J. Phys. A.* **27** 5749
- [11] Cugliandolo L F and Kurchan J 1997 *Phys. Rev. E.* **55** 3898
- [12] Joubaud S, Petrosyan A, Ciliberto S and Garnier N B 2008 *Phys. Rev. Lett.* **100** 180601
- [13] Mosser V, Kobbi F, Contreras S, Mercy JM, Callen O, Robert JL, Aboulhoda S, Chevrier J and Adam D 1997 *Proc. 9th Int. Conf. on Solid-State Sensors and Actuators June 1997 (Chicago, USA)*
- [14] Mosser V, Jung G, Przybytek J, Ocio M and Haddab Y 2003 *SPIE Fluctuations and Noise Symposium, Santa Fe (NM), 1-4 June 2003, Proc. SPIE Vol 5115*, p 183
- [15] Kerlain A and Mosser V 2008 *Sensors & Actuators A* **142**, 528
- [16] Mosser V, Contreras S, Aboulhoda S, Lorenzini P, Kobbi F, Robert JL and Zekentes K 1994 *Sensors and Actuators A* **43** 135
- [17] Boero G, Demierre M, Besse PA and Popovic RS 2003 *Sensors and Actuators A* **106** 314
- [18] Popovic RS 2004 *Hall Effect Devices* (Bristol Philadelphia: IOP Publishing, 2nd Edition)
- [19] Oral A, Barnard JC, Bending SJ, Kaya II, Ooi S, Tamegai T and Henini M 1998 *Phys. Rev. Lett.* **80** 3610
- [20] Oral A, Bending SJ and Henini M 1996 *Appl. Phys. Lett.* **69** 1324
- [21] Marchevsky M, Higgins MJ and Battacharia S 2001 *Nature* **409** 591
- [22] Chang AM, Hallen HD, Harriott L, Hess HF, Kao HL, Kwo J, Miller RE, Wolfe R, Van der Ziel J and Chang TY 1992 *Appl. Phys. Lett.* **61** 1974
- [23] Pross A, Crisan A, Bending SJ, Mosser V and Konczykowski M 2005 *J. Appl. Phys.* **97** 096105
- [24] Haned H and Missous M 2003 *Sensors and Actuators A* **102**, 216
- [25] Kunets VP, Pomraenke R, Dobbert J, Kissel H, Muller U, Kostial H, Wiebicke E, Tarasov GG, Mazur YI and Masselink WT, 2005 *IEEE Sensors J.* **5** 883
- [26] Kammerer JB, Hébrard L, Frick V, Poure P and Braun F 2006 *Eur. Phys. J. Appl. Phys.* **36** 49
- [27] Popovic RS, Flanagan JA, Besse PA 1996 *Sensors and Actuators A* **56** 39
- [28] Munter PJA 1991 *Sensors and Actuators A* **21-23** 743
- [29] Steiner R, Maier C, Häberli A, Steiner F-P and Baltes H 1998, *Sensors and Actuators A* **66** 167
- [30] Bilotti A 1997 *IEEE J. Sol. State Circuits* **32** 829

- [31] Müller-Schwanneke C, Jost F, Marx K, Lindenkreuz S, Von Klitzing K 2000 *Sensors and Actuators* **81** 18
- [32] Bouchaud J-P, Dupuis V, Hammann J and Vincent E 2001 *Phys. Rev.* **B65** 024439
- [33] Dupuis V, Vincent E, Bouchaud J-P, Hammann J., Ito A, Katori H A, 2001 *Phys. Rev.* **B64** 174204
- [34] Castillo H E, Chamon C, Cugliandolo L F, Iguain J L and Kennett M P 2002 *Phys. Rev. Lett.* **88** 237201
- [35] Castillo H E, Chamon C, Cugliandolo L F and Kennett M P 2002 *Phys. Rev.* **B68** 134442
- [36] Sinnathamby K S, Oukris H and Israeloff N E 2005 *Phys. Rev. Lett.* **95** 067205
- [37] Israeloff N E, Oukris H and Crider P S 2006 *J. Non-Cryst. Sol.* **352** 4915

4.2.4. Experimental Evidence for Violation of the Fluctuation-Dissipation Theorem in a Superspin Glass

Experimental Evidence for Violation of the Fluctuation-Dissipation Theorem in a Superspin Glass

Katsuyoshi Komatsu,^{1,*} Denis L'Hôte,^{1,†} Sawako Nakamae,¹ Vincent Mosser,² Marcin Konczykowski,³
Emmanuelle Dubois,⁴ Vincent Dupuis,⁴ and Regine Perzynski⁴

¹*Service de Physique de l'Etat Condensé (CNRS/URA 2464), DSM/IRAMIS/SPEC, CEA Saclay, F-91191 Gif/Yvette Cedex, France*

²*ITRON/Issy Technology Center, 52 rue Camille Desmoulins, F-92130 Issy-les-Moulineaux, France*

³*Laboratoire des Solides Irradiés, UMR7642 CNRS, Ecole Polytechnique, F-91128 Palaiseau, France*

⁴*Laboratoire PECSA, UMR 7195 CNRS, Université Pierre et Marie Curie, 4 place Jussieu, Boîte 51, 75252 Paris Cedex 05, France*
(Received 14 October 2010; revised manuscript received 14 March 2011; published 14 April 2011)

We present the experimental observation of the fluctuation-dissipation theorem violation in an assembly of interacting magnetic nanoparticles in the low temperature superspin-glass phase. The magnetic noise is measured with a two-dimension electron gas Hall probe and compared to the out of phase ac susceptibility of the same ferrofluid. For “intermediate” aging times of the order of 1 h, the ratio of the effective temperature T_{eff} to the bath temperature T grows from 1 to 6.5 when T is lowered from T_g to $0.3 T_g$, regardless of the noise frequency. These values are comparable to those measured in an atomic spin glass as well as those calculated for a Heisenberg spin glass.

DOI: 10.1103/PhysRevLett.106.150603

PACS numbers: 05.70.Ln, 75.10.Nr, 75.50.Lk

During the last two decades, the extension of the fluctuation-dissipation theorem (FDT) to the out-of-equilibrium regime has been the subject of many theoretical and experimental investigations [1–21]. In the “weak ergodicity breaking” scenario [1,3], it has been shown that the concept of an effective temperature (T_{eff}) [3] that differs from the bath temperature (T) enables the extension of the FDT to the out-of-equilibrium regime. The FDT violation has been investigated in several numerical simulations [1,2,5–7,22,23], while experimental studies are rather scarce: they concern one molecular glass [8], colloids [9,12,15–17,20], polymers [13,14,21], one liquid crystal [18], and one spin glass (SG) [10,11]. On the other hand, the absence of FDT violation is reported in colloids [17,19] and in a magnetic nanoparticle system [24,25]. Thus, the systems and the conditions in which the FDT is violated still represent an open question.

Here, we investigate the FDT violation in an out-of-equilibrium superspin-glass (SSG) system. The magnetic nanoparticles suspended in fluid (glycerol) have a single-domain magnetic structure. Therefore, their magnetic moment of $\sim 10^4 \mu_B$ behaves as one large spin, and is called a “superspin.” Once the carrier matrix is frozen, the positions as well as the anisotropy axis orientations of the particles are fixed, and the only remaining degree of freedom is the superspin rotation. The randomness and disorder found in the nanoparticle positions, orientations, and sizes lead to magnetically glassy behaviors at low temperatures, including slow dynamics and aging effects, similar to those of atomic SGs; hence these systems are called “superspin glasses” [24,26–31]. Because of the large magnetic moment, slow correlation length growth, etc., the observation of magnetic noise within experimental frequency or time range becomes more feasible in a SSG system.

Furthermore, the much slower microscopic time scale in SSG than that in SG can help to fill the large time scale gap between the computer simulations and experiments.

The FDT describes the relation between the power spectrum of fluctuations of an observable, $\delta M(\omega)$ (here M is the magnetization) and the imaginary component of the ac susceptibility $\chi''(\omega)$ to the conjugate field [32]:

$$\langle \delta M(\omega)^2 \rangle = \frac{2k_B T}{\pi V} \left(\frac{\chi''(\omega)}{\mu_0 \omega} \right) (\text{SI units}). \quad (1)$$

Here, $\langle \dots \rangle$ denotes the ensemble average per frequency unit, k_B is the Boltzmann constant, T the temperature, and $\omega = 2\pi f$ (f is the measurement frequency). The departure from equilibrium can be estimated through the fluctuation-dissipation ratio $X(\omega, t_w) = 2k_B T \chi''(\omega) / (\mu_0 \omega \langle \delta M(\omega)^2 \rangle \pi V)$, or the effective temperature $T_{\text{eff}} = T/X(\omega, t_w)$. X (and T_{eff}) depend on t_w , the waiting time (or the “age”) at T after a temperature quench from above the glass transition temperature of the system. At equilibrium, the FDT gives $X = 1$ and thus $T_{\text{eff}} = T$ while in the aging regime, $X < 1$ and equivalently, $T_{\text{eff}} > T$. The effective temperature provides a generalized form of FDT in out-of-equilibrium cases as

$$\langle \delta M(\omega, t_w)^2 \rangle = \frac{2k_B T_{\text{eff}}}{\pi V} \left(\frac{\chi''(\omega, t_w)}{\mu_0 \omega} \right), \quad (2)$$

where T_{eff} rather than T acts as the system temperature, e.g., “weak ergodicity breaking” system. Note that in the $1/\omega \ll t_w$ limit, the quasiequilibrium regime is reached [3]; that is, the FDT relation is recovered and $X = 1$.

In this Letter, we report the experimental observation of the FDT violation in a frozen ferrofluid in the SSG state via magnetic noise measurements coupled with ac-susceptibility measurements. The ferrofluid used here is made of maghemite $\gamma\text{Fe}_2\text{O}_3$ nanoparticles of average

diameter 8.6 nm, dispersed in glycerol with a volume fraction $\phi \sim 15\%$ in which the SSG state is observed [29,30,33,34], in agreement with Refs. [26,27] where the ϕ dependent SSG transition is tested with ϵ -Fe₃N ferrofluids. Indeed the dipolar interaction energy over anisotropy energy $\sim \mu_0 m_s^2 V_{np} \phi / E_a$ (m_s , V_{np} particle magnetization and volume) is here close to that of SSG sample with $\phi \sim 2\%$ in Ref. [26]. Particle uniaxial anisotropy energy $E_a \sim 10^{-20}$ J (as in Ref. [26]), is obtained from the superparamagnetic relaxation time of a diluted sample, $\tau = \bar{\tau}_0 \exp(E_a/k_B T)$ with $\bar{\tau}_0 = 10^{-9}$ s [28], compatible with direct anisotropy field measurements [35]. To measure the magnetic noise, a small drop of ferrofluid was deposited directly onto a Hall probe [36,37] (see inset in Fig. 1). All measurements were made well below 190 K, the freezing temperature of glycerol. In a frozen sample, the magnetic moments (superspins) interact with one another through dipolar interactions leading to a static superspin-glass transition at $T_g \sim 67$ K [29]. The ac susceptibility of the bulk ferrofluid sample (approximately 5 μ l) was measured with a commercial SQUID magnetometer. The magnetic noise was measured with a two-dimension electron gas (2DEG) quantum well Hall sensor (QWHS) based on pseudomorphic AlGaAs/InGaAs/GaAs heterostructure with a high mobility and a large Hall coefficient R_H (~ 800 Ω /T). The QWHS has a nominal sensitive area of $\sim 2 \times 2$ μm^2 , located at $d \sim 0.7$ μm beneath the probe surface (see inset in Fig. 1). The ferrofluid drop of about 7 pl has a diameter ~ 30 μm , much larger than the probe sensitive area.

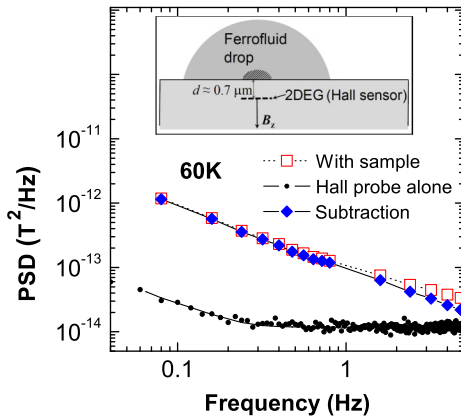


FIG. 1 (color online). Noise power spectrum $S(f)$ of the magnetic field due to the frozen ferrofluid (filled diamonds), obtained by subtracting the Hall probe only spectrum (dots) from the total power spectral density (PSD) (open squares) as a function of frequency f , at 60 K in zero applied field. The power spectral density of the magnetic noise due to the sample was larger than that of the bare Hall sensor by factors of about 25 and 2 at 0.1 and 4 Hz, respectively. Inset: Schematic picture of the magnetic noise measurement setup. The magnetic noise measured in the probe comes mainly from that part of the drop located in front of the 2DEG [36], indicated by the dark shaded region (see text).

We have made use of the spinning current technique which effectively suppresses both the offset and the low frequency background noise of the Hall probe simultaneously [38]. In this method, the directions of the current injection and the Hall voltage detection in Hall cross are continuously switched at a spinning frequency f_{spin} which is larger than the largest noise frequency of interest. Low frequency background noise ($f < 10$ Hz) suppression is of great importance because the typical time scales involved in the fluctuation dynamics of a SSG system are much larger than 1 s. With $f_{\text{spin}} = 1$ kHz, we achieved a field sensitivity of 2×10^{-7} T/ $\sqrt{\text{Hz}}$ (for $f \sim 0.1$ Hz) for the temperature range between 20 and 85 K, a tenfold improvement with respect to the sensor sensitivity obtained without this technique. The noise power spectra $S(f)$ of the magnetic field were measured in two distinct frequency regions: from 0.08 to 0.7 Hz and from 0.8 to 8 Hz. All magnetic noise data of the ferrofluid (except at 85 K) were taken following a temperature quench from 85 K ($= 1.27 T_g$) to the measurement temperatures and a waiting time of 10 min for temperature stabilization. Figure 1 shows an example of such a spectrum, taken at 60 K. $S(f)$ is calculated via $S(f) = \langle [\delta B_z(f)]^2 \rangle = (IR_H)^{-2} \langle (\delta V_H)^2 \rangle$, where δV_H is the fluctuation of the measured Hall voltage, δB_z is the corresponding fluctuation of the (uniform) field B_z perpendicular to the Hall probe and I the injection current. Here the symbol $\langle \dots \rangle$ indicates an averaging over a large data set. Each spectrum was obtained from averaging over 300 and 3000 spectra in the low and high frequency regions, respectively. The aging time t_w of the system is thus this averaging time, here of the order of a few 10^3 s. This is an “intermediate” waiting time used in typical aging experiments on bulk ferrofluid SSG samples where t_w 's range from a few 10^2 s to several 10^4 s [29].

Figure 2 shows the imaginary part of the ac magnetic susceptibility $\chi''(f, T)$ of a bulk sample as a function of

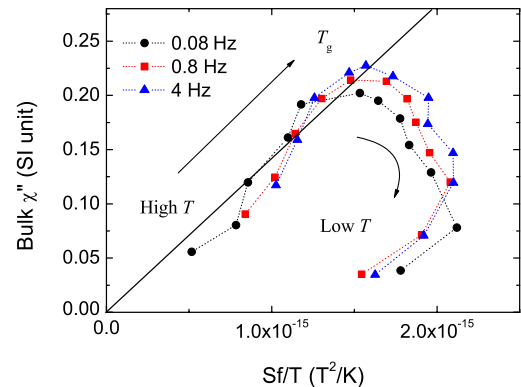


FIG. 2 (color online). $\chi''(f, T)$ of bulk sample as a function of $S(f, T)f/T$ for frequencies, 0.08, 0.8, and 4 Hz. Each data point corresponds to χ'' and S measurements at a given bath temperature T and frequency f . The solid straight line indicates the linear relation in the high temperature region above T_g .

Sf/T at $f = 0.08, 0.8, 4$ Hz. $\chi''(f, T)$ at each temperature was measured with the aging time t_w of 1 h after the temperature quench from 85 K. We found that all data points collected above $T_g = 67$ K are aligned along a common straight line; i.e., $\chi'' \propto Sf/T$. The solid straight line in Fig. 2 is the best fit to these data points for $T = T_g$ for all three frequencies. This linear relationship is independent of f , indicating that the FDT holds between the two quantities in this T range according to Eq. (1). The data points deviate from the straight line starting from the maximum value of χ'' occurring near $T = T_g$ and downwards in temperature. Figure 3 shows the temperature dependencies of χ'' and Sf/T (same data as in Fig. 2). The relative normalization of the two vertical scales, χ'' and Sf/T , is given by the slope of the straight line found in Fig. 2. As can be seen from the figure, χ'' and Sf/T superpose in the high temperature region above T_g , while they separate below T_g . The deviation from the linear relation and the separation of the normalized χ'' and Sf/T below T_g indicate a clear departure from FDT. The slope value, $\chi''/(Sf/T) = (1.4 \pm 0.2) \times 10^{14}$ [K/T²] in the high temperature region (see Fig. 2) is determined by the effective volume V_{eff} of ferrofluid that contributes to the magnetic noise measurement [36] and by the magnitude of the magnetic field induced by the ferrofluid in the Hall probe. Because of the sample geometry and of the $1/r^4$ [36] dependence of the dipolar field variance $\langle(\delta\bar{B}_z)^2\rangle$, where \bar{B}_z is the average of B_z induced by the sample over the probe sensitive area, V_{eff} is confined within a volume close to the sensor surface (see inset of Fig. 1). To check the quantitative consistency of the above analysis, we have estimated the slope value independently. In depth investigations of the response of a Hall cross to an inhomogeneous perpendicular field B_z have revealed that this response is proportional to the average of B_z over the effective area a_{eff} of the probe which is about twice the

junction area, i.e., $a_{\text{eff}} = 2w^2$ (w being the width of the cross arms) [39]. We evaluated numerically the variance $\langle(\delta\bar{B}_z)^2\rangle$ with B_z being the sum of contributions from elementary volumes d^3r of the sample, each having a magnetic moment variance given by FDT, that is $(2k_B T \chi'' / \pi \mu_0 \omega) d^3r$. The calculated slope is $(0.7 \pm 0.25) \times 10^{14}$ [K/T²]. The uncertainty comes mainly from that of the response function of the probe, which is partly due to the uncertainty in the true value of w ($1 \mu\text{m} < w < 2 \mu\text{m}$) caused by the edge depletion effect. Another source of uncertainty comes from the fact that the effect of averaging B_z over the probe area has been evaluated using a Monte Carlo simulation to which some simplifying assumptions were made, i.e., independent superspins, square probe area, etc. Despite these elements taken into account, the measured and calculated slope values are close to each other, lending credibility to our results.

Below the SSG transition temperature T_g , where the system is in an out-of-equilibrium state, we have witnessed a departure from the equilibrium FDT relation. We now estimate the effective temperature T_{eff} as evoked above from the FDT ratio of χ'' to Sf/T [see Eq. (2)]. The inset in Fig. 3 shows the temperature dependence of T_{eff}/T obtained at 0.08, 0.8, and 4 Hz. T_{eff}/T increases monotonically when T decreases, starting from 1 around T_g , to 6.5 at $0.3T_g$ ($= 20$ K) regardless of the frequency. The values of T_{eff}/T are of the same order as those reported in the experimental study of an atomic SG, $T_{\text{eff}}/T = 2.8 - 5.3$ [11] and in a Monte Carlo simulation on a Heisenberg SG, $T_{\text{eff}}/T = 2 - 10$ [7].

The observation of $T_{\text{eff}} > T$ suggests that the system is in the aging regime, i.e., not in the so-called quasiequilibrium regime [3] where observation times $t_{\text{obs}} = 2\pi/\omega$ are much smaller than the aging time t_w . Here, $t_{\text{obs}} \sim 1$ s is rather short compared to $t_w \sim 10^3$ s, corresponding to $t_{\text{obs}}/t_w \sim 10^{-3}$. Violations of FDT have been observed experimentally for very low values of t_{obs}/t_w : $10^{-7} - 10^{-4}$ in a molecular glass [8], $10^{-5} - 10^{-3}$ in polymer glasses [13,14], and $10^{-7} - 10^{-4}$ in colloidal glasses [9,12,20]. Furthermore, in those experimental systems, T_{eff} does not rapidly approach the bath temperature T with waiting time t_w . Through numerical simulations on domain growth systems [5], the breaching of the quasiequilibrium state depends on the system itself and on the two time scales (t_{obs} and t_w) separately rather than on t_{obs}/t_w [40]. Similar conclusions were drawn in SG simulations [22,23]. In an interacting magnetic nanoparticle SSG system similar to ours, the FDT remained valid for $t_{\text{obs}}/t_w < 10^{-5}$ [25]. Thus, it is tempting to conjecture that the limit between the two regimes lie somewhere between $t_{\text{obs}}/t_w = 10^{-5}$ and 10^{-3} . However, one must be careful because the differences between the two systems (particle sizes, concentrations, etc.) and their experimental conditions (measurement techniques, temperature quench protocol, etc.) do not allow direct comparison between the two studies.

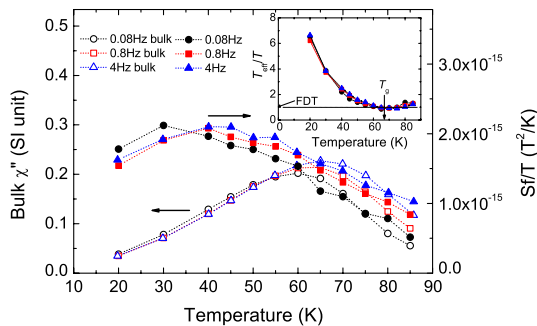


FIG. 3 (color online). Temperature dependent χ'' of bulk sample (open symbols) and Sf/T (filled symbols) at frequencies 0.08, 0.8, and 4 Hz. The relative normalization of the two vertical scales corresponding to χ'' and Sf/T is given by the slope of the straight line in Fig. 2. Inset: The temperature dependence of T_{eff}/T at $f = 0.08, 0.8,$ and 4 Hz. The horizontal line corresponds to the FDT relation, i.e., $T_{\text{eff}}/T = 1$.

Comparing the SSG and SG systems, we note that the interaction between superspins is of the long range dipolar type whereas between atomic spins, it is of the short range exchange type [10,11,23]. Thus far, a large scale dynamical simulation on nanoparticle systems with random anisotropy has not been investigated in terms of the FDT relation. Comparisons of experimental data to such simulation result will be very interesting.

In conclusion, we have presented experimental evidence of FDT violation in the out-of-equilibrium, aging SSG state of a frozen ferrofluid through magnetic noise measurements. For an aging time of about 1 h, the extracted effective temperature (normalized to the bath temperature), increases by a factor of 6.5 when T decreases from T_g to $0.3 T_g$. Such values are of the order of those found in an atomic SG [11] and in a numerical simulation of a Heisenberg SG [7]. More investigations are needed to elucidate aging time dependence of T_{eff} as well as the particle system dependence with different interaction strengths and anisotropy energies.

We thank R. Tourbot for precious technical help and L. Cugliandolo, J. Kurchan, F. Ladieu, S. Franz, A. Barrat, and E. Vincent for illuminating discussions. This work was supported by Triangle de la Physique (contracts MicroHall and DynMag).

*katsuyoshi.komatsu@cea.fr

†denis.lhote@cea.fr

- [1] J. P. Bouchaud, *J. Phys. I (France)* **2**, 1705 (1992).
- [2] G. Parisi, *Phys. Rev. Lett.* **79**, 3660 (1997).
- [3] L. F. Cugliandolo, J. Kurchan, and L. Peliti, *Phys. Rev. E* **55**, 3898 (1997).
- [4] E. Marinari, G. Parisi, F. Ricci-Tersenghi, and J. Ruiz-Lorenzo, *J. Phys. A* **31**, 2611 (1998).
- [5] A. Barrat, *Phys. Rev. E* **57**, 3629 (1998).
- [6] F. Sciortino and P. Tartaglia, *Phys. Rev. Lett.* **86**, 107 (2001).
- [7] H. Kawamura, *Phys. Rev. Lett.* **90**, 237201 (2003).
- [8] T. S. Grigera and N. E. Israeloff, *Phys. Rev. Lett.* **83**, 5038 (1999).
- [9] L. Bellon, S. Ciliberto, and C. Laroche, *Europhys. Lett.* **53**, 511 (2001).
- [10] D. Hérisson and M. Ocio, *Phys. Rev. Lett.* **88**, 257202 (2002).
- [11] D. Hérisson and M. Ocio, *Eur. Phys. J. B* **40**, 283 (2004).
- [12] B. Abou and F. Gallet, *Phys. Rev. Lett.* **93**, 160603 (2004).
- [13] Buisson and S. Ciliberto, *Physica (Amsterdam)* **204D**, 1 (2005).
- [14] M. Lucchesi, A. Dminjon, S. Capaccioli, D. Prevosto, and P. A. Rolla, *J. Non-Cryst. Solids* **352**, 4920 (2006).
- [15] N. Greinert, T. Wood, and P. Bartlett, *Phys. Rev. Lett.* **97**, 265702 (2006).
- [16] D. R. Strachan, G. C. Kalur, and S. R. Raghavan, *Phys. Rev. E* **73**, 041509 (2006).
- [17] S. Jabbari-Farouji, D. Mizuno, M. Atakhorrami, F. C. MacKintosh, C. F. Schmidt, E. Eiser, G. H. Wegdam, and D. Bonn, *Phys. Rev. Lett.* **98**, 108302 (2007).
- [18] S. Joubaud, B. Percier, A. Petrosyan, and S. Ciliberto, *Phys. Rev. Lett.* **102**, 130601 (2009).
- [19] P. Jop, J. R. Gomez-Solano, A. Petrosyan, and S. Ciliberto, *J. Stat. Mech.* (2009) P04012.
- [20] C. Maggi, R. DiLeonardo, J. C. Dyre, and G. Ruocco, *Phys. Rev. B* **81**, 104201 (2010).
- [21] H. Oucris and N. E. Israeloff, *Nature Phys.* **6**, 135 (2009).
- [22] J. O. Andersson, J. Mattsson, and P. Svedlindh, *Phys. Rev. B* **46**, 8297 (1992).
- [23] S. Franz and H. Rieger, *J. Stat. Phys.* **79**, 749 (1995).
- [24] T. Jonsson, J. Mattsson, C. Djurberg, F. A. Khan, P. Nordblad, and P. Svedlindh, *Phys. Rev. Lett.* **75**, 4138 (1995).
- [25] T. Jonsson, P. Nordblad, and P. Svedlindh, *Phys. Rev. B* **57**, 497 (1998).
- [26] H. Mamiya, I. Nakatani, and T. Furubayashi, *Phys. Rev. Lett.* **80**, 177 (1998).
- [27] H. Mamiya, I. Nakatani, and T. Furubayashi, *Phys. Rev. Lett.* **82**, 4332 (1999).
- [28] D. Parker, V. Dupuis, F. Ladieu, J. P. Bouchaud, E. Dubois, R. Perzynski, and E. Vincent, *Phys. Rev. B* **77**, 104428 (2008).
- [29] E. Wandersman, V. Dupuis, E. Dubois, R. Perzynski, S. Nakamae, and E. Vincent, *Europhys. Lett.* **84**, 37011 (2008).
- [30] S. Nakamae, Y. Tahri, C. Thibierge, D. L'Hôte, E. Vincent, V. Dupuis, E. Dubois, and R. Perzynski, *J. Appl. Phys.* **105**, 07E318 (2009).
- [31] Y. Sun, M. B. Salamon, K. Garnier, and R. S. Averback, *Phys. Rev. Lett.* **91**, 167206 (2003).
- [32] M. Alba, J. Hammann, M. Ocio, P. Refregier, and H. Bouchiat, *J. Appl. Phys.* **61**, 3683 (1987).
- [33] D. Parker, F. Ladieu, E. Vincent, G. Meriguet, E. Dubois, V. Dupuis, and R. Perzynski, *J. Appl. Phys.* **97**, 10A502 (2005).
- [34] E. Wandersman, E. Dubois, F. Cousin, V. Dupuis, G. Meriguet, R. Perzynski, and A. Cebers, *Europhys. Lett.* **86**, 10005 (2009).
- [35] F. Gazeau, J.-C. Bacri, F. Gendron, R. Perzynski, Y. Raikher, V. Stepanov, and E. Dubois, *J. Magn. Mater.* **186**, 175 (1998).
- [36] D. L'Hôte, S. Nakamae, F. Ladieu, V. Mosser, A. Kerlain, and M. Konczykowski, *J. Stat. Mech.* (2009) P01027.
- [37] K. Komatsu, D. L'Hôte, S. Nakamae, V. Mosser, A. Kerlain, M. Konczykowski, E. Dubois, V. Dupuis, and R. Perzynski, *J. Appl. Phys.* **107**, 09E140 (2010).
- [38] A. Kerlain and V. Mosser, *Sens. Actuators A, Phys.* **142**, 528 (2008).
- [39] S. J. Bending and A. Oral, *J. Appl. Phys.* **81**, 3721 (1997); I. S. Ibrahim, V. A. Schweigert, and F. M. Peeters, *Phys. Rev. B* **57**, 15416 (1998).
- [40] L. F. Cugliandolo, arXiv:cond-mat/0210312 v2.

5. Perspectives

My future research will continue to focus on different aspects of ‘magnetic nanoparticles.’ These subjects can be broadly classified into two fields of research; 1) Emerging supermagnetic phenomena and the development of new measurement techniques, and 2) Applications of magnetic *np*'s in energy science. In both fields, new experimental projects have been initiated in the last 3 years. Current state of these projects, their future directions and goals are presented in this chapter.

5.1. The Quest for Superferromagnetism

Collaborators (as of July 2013):

- I. Lisiecki LM2N, UPMC: supracrystal synthesis and structural characterizations
- P.A. Albouy LPS, Univ. Paris Sud: GISAXS measurements
- J. J. Weiss LPS, Univ. Paris Sud and J. Richardi LM2N, UPMC: numerical simulations

As outlined in Chapter 2, *Supermagnetism* groups three magnetic states created by assemblies of magnetic nanoparticles (superspins): *superparamagnetism* (SPM), *superspin glass* (SSG) and *superferromagnetism* (SFM). Upon decreasing the inter-particle distance, the interaction energy among them becomes stronger to produce a ‘collective state’ below a finite transition temperature (T_g or T_c). If the superspins are randomly oriented, or other types of randomness are present in the system (particle size polydispersity, positions, etc.) then the collective state below T_g behaves almost always as an SSG. If superspins in correlated zones are aligned all parallel, on the other hand, the ordered state below T_c is said to be in SFM [5]. Just as SSG is characterized by the out-of-equilibrium dynamics, the SFM domains are also believed to reach equilibrium only after a long time and its relaxation dynamics is non-trivial, reminiscent of many complex systems [119].

5.1.1. Superferromagnetism: Dipolar Ferromagnetism of Superspins?

Superferromagnetism, as originally introduced by Mørup *et al.*, considers dipolar interactions between magnetic moments of nanoparticles as the prevailing source of interaction [120]. Therefore, it is a type of dipolar ferromagnetism (DFM). Dipolar ferromagnetism occurs when the *polarization force* from distant parts of the sample overcomes the *depolarization force* from relatively nearby spins. Consequently, DFM is strongly sample-shape dependent and presents a *soft* ordered state. [121-123]. As Luttinger and Tisza stated “... *dipole ferromagnetism -if it exists- has a character essentially different from exchange ferromagnetism*” [121]. The existence of DFM states has been tested numerically on various sample dimensions and shapes, with and without disorders (*e.g.*, spin positions and orientations) [121-127]. In 3D systems, ellipsoidal samples with dipole moments on regular FCC and BCC lattices favor a ferromagnetic ground state. Disordered assemblies, on the other hand, show a spin-glass like phase [123]. The relative orientations of dipole moments are also believed to influence the DFM formation [126]. In dilute ‘atomic’ spin systems, where magnetic ions are too far apart to result in exchange interactions, the DFM transition has been found occur at very low temperatures ($T < 1$ K) and the onset is strongly frequency dependent. [79]

Early hints of SFM in magnetic nanoparticle (*np*) assemblies were found in Mössbauer experiments [66, 128]. As the dominant interaction energy source in most magnetic *np* system is that of dipole-dipole, such “collective magnetic excitations” was analyzed in terms of dipolar ferromagnetism.

However, the samples studied did not satisfy aforementioned structural conditions, thus the applicability of dipolar SFM is debatable. In fact, to the best of my knowledge, structurally ideal macroscopic 3D magnetic *np* assemblies are yet to be produced, therefore it is not surprising that there has been no confirmation of 3D *dipolar* SFM in such systems. A rare example of a 3D-SFM-like state in CoFe nanoparticles ($\text{Co}_{80}\text{Fe}_{20}/\text{Al}_2\text{O}_3$ multilayers) reported by Chen, Bedanta, Kleeman *et al.*, attributes the observed phenomena to “*tunneling superexchange through atomically disperse ultra-small particles*” [119, 129, 130]. In 2D monolayers, there are multiple reports on the SFM-like domain formations. The electrographic images (taken by X-PEEM [131], electron holography [132, 133]) show uniformly magnetized domain structure. In the case of Fe_3O_4 *np* monolayer [133], the domains were found to be stable over 1 hour at 108 K. Magnetic property measured using Kerr magnetometry [134] in the monolayer nanostripes of Fe also shows an SFM-like transition.

As in the DFM case, the dipolar SFM of interacting magnetic nanoparticles depends strongly on the sample dimensions and disorder. Numerical simulations predict metastable antiferromagnetic columnar order in a simple cubic lattice sample (3D) [135] and very short-ranged FM (AFM) order in hexagonal (square) lattice (2D) [138]. Furthermore, the finite anisotropy energy of nanoparticles complicates the nature of low temperature ordered state. The recent calculation suggests that the “interaction-to-anisotropy” energy ratio should be larger than ~ 0.1 in FCC arranged nanoparticle arrays [139]. Therefore, with the exception of Fe monolayer nanostripes [134], the observed SFM-like domains require *other* interaction mechanisms such as multipolar and exchange interactions (for review, see [5]).

It is rather straightforward to see that in order to observe a dipolar SFM phase, one needs to prepare well-ordered, monodisperse magnetic nanoparticles in a FCC or BCC lattice structure as suggested by Bouchaud and Zerah 20 years ago [123]. Mørup and Christiansen have shown that the easy-axis alignment of nanoparticles can enhance the dipolar ordering temperature of interacting magnetic *np* systems [120].

To this end, we have been investigating the magnetic property of supracrystals made of Co nanoparticles. Supracrystals are three-dimensional *thick* superlattices of regularly stacked nanoparticles. I. Lisiecki and her co-workers have pioneered a novel technique to produce highly organized, large 3D supracrystals of monodisperse cobalt nanoparticles on FCC lattices [140]. The precise annealing protocols to improve the *supracrystalline* order (from a disordered 3D assembly to an FCC long-range ordered assembly) as well as the *nanocrystalline* order of individual particles (from a polycrystalline FCC structure to a pure HCP single crystal) have been established. These supracrystals can also be synthesized into a long rod-like shape. The existence of superspin glass-like state in supracrystals made of similar Co nanoparticles has already been reported previously, including the critical slowing down near the superspin freezing temperature and the memory effect [139, 140]. Currently, we are focusing on the nanocrystallinity effect of individual Co nanoparticles on the collective magnetism of supracrystals to assess the possibility to create dipolar-superferromagnetism in these systems.

What is the degree of anisotropy axis alignment needed to produce SFM rather than SSG? Can SFM domain wall relaxation dynamics be described by the same model used in superspin glasses, or do they belong to different universality classes of complex systems? These are some of the questions we intend to address.

5.1.2. Magnetism of Supracrystals and Nanocrystallinity Effect

5.1.2.1. Cobalt Nanoparticles and Supracrystals

Cobalt nanoparticles are synthesized using the reverse micelle techniques under a N_2 atmosphere [138]. At the end of the synthesis, 7.4 nm cobalt nanoparticles coated with dodecanoic acid and characterized by 9.4 % as the size distribution are produced. As synthesized Co nanoparticles possess highly disordered polycrystalline structure, with individual crystalline domains (typical size 1 nm or less) showing fcc organization. Subsequently, a Highly Oriented Pyrolytic Graphite (HOPG) substrate (10 mm x 5 mm) is immersed horizontally in the colloidal solution of Co nanoparticles dispersed in hexane. The solvent is then slowly evaporated at room temperature under N_2 . The end product is superlattices composed of a few hundred layers of Co nanoparticles, called *supracrystals* (SC) as shown in Figure 5.1. It should be noted that the HOPG surface coverage by SC's is not homogeneous, but rather concentrated at the border (~ 1 mm) of the substrate. At a higher magnification, a cracked topology is clearly seen (see Figure 5.1 right) with a broad SC domain size distribution. The supracrystals are characterized by long-range FCC mesoscopic order with the following structural parameters: the (111) stacking periodicity = 8.49 nm, the centre-to-centre interparticle distance (D_{c-c}) = 10.4 nm and the edge-to-edge interparticle distance (D_{i-p}) = 3 nm.

To control the *nanocrystallinity* of individual Co particles, 3D supracrystals are placed in a closed quartz capsule with a N_2 atmosphere and annealed in a furnace at various temperatures (220, 250 and 350 °C) for 15 min. Up to 220 °C, the annealing performed does not affect the supracrystalline or nanocrystalline organisations. Conversely, the heat treatments at temperatures 250 °C and higher induce significant improvement in both the nano- and supra-crystallinity. After annealing at 250 °C, the diffraction pattern shows the coexistence of the FCC and HCP phase. At 350 °C, SC's with a vast majority of Co nanoparticles in the HCP-single-crystalline phase are created. For all annealing temperatures, no oxidation was detected and the GISAXS patterns show that the FCC supracrystalline order remains intact without coalescence, although the interparticle distance, and consequently the (111) stacking periodicity decreases at higher annealing temperatures (See Table 5.1). It should be noted that up to 350 °C, the SC's remain highly stable against coalescence because of the high thermal stability of the dodecanoic acid molecules surrounding the *np*'s. Above this temperature, Co nanoparticles will start to coalesce giving rise to a drastic increase in the particle size polydispersity and then to a loss of the FCC supracrystalline order.

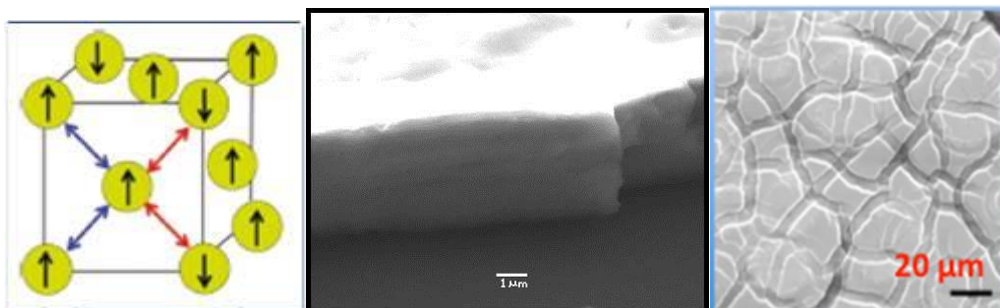


Figure 5.1: Supracrystals made of magnetic nanoparticles. (Left) A schematic view of FCC-supracrystal and how particle moments may interact. (Center) SEM image of a supracrystal sample. (Right) SEM image taken at a higher magnification. (Images courtesy of I. Lisiecki)

Table 5.1 : Supercrystal structural parameters

	Native	220 °C	250 °C	350 °C
(111) Stacking periodicity (nm)	8.49	8.49	8.32	8.00
Center-to-Center dist. D_{c-c} (nm)	10.4	10.4	10.2	9.8
Inter-particle distance, D_{i-p} (nm)	3	3	2.8	2.4

5.1.2.2. Nanocrystallinity effect on the magnetic behavior of Co-supracrystals

The nanocrystallinity effect was clearly seen in the magnetic behavior of supracrystals. As depicted in Figure 5.2, the transition temperature, as defined as the position of zero-field-cooled (ZFC) magnetization peak, increases from 110 K (Native sample) to 290 K (350°C sample) passing through a minimum value of 102 K (220 °C sample). The ac susceptibility as a function of temperature and frequency showed usual ‘critical slowing down’ behavior signaling ‘collective states’ below T_c in all samples. Using the Vogel-Fulcher model for weakly-interacting systems (See Chap. 2, Equation 2.7), the particle anisotropy energy E_a and the effective temperature T_o are extracted. The anisotropy energy was found to increase from about 1360 to 1700 K, again exhibiting an anomalous behavior for the 220 °C sample (see Figure 5.3).

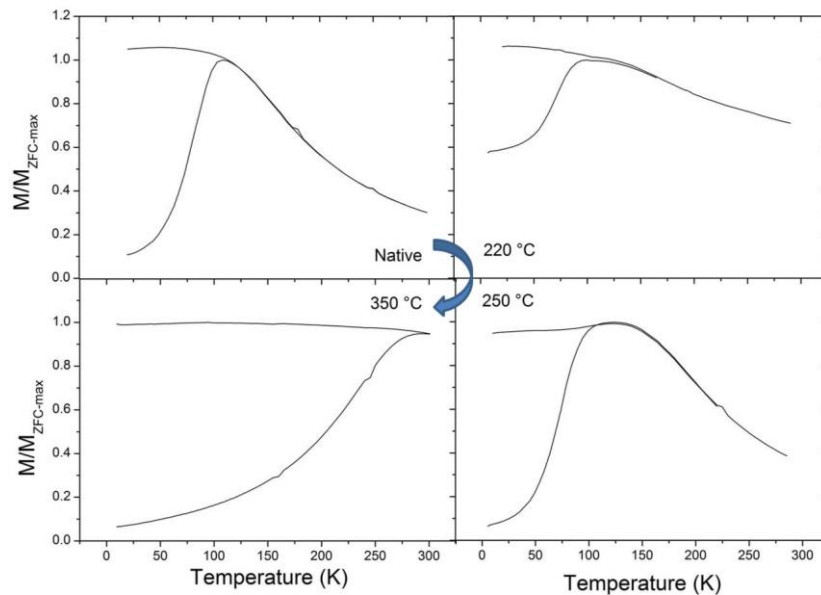


Figure 5.2: ZFC/FC magnetization (normalized) measurements of Native, 220 °C, 250 °C and 350°C samples, presented clockwise from top left. All measurements were taken under an applied magnetic field of 10 Oe.

It has previously been suggested at low annealing temperatures, at which the re-crystallization is barely initiated, nanocrystalline structure become very heterogeneous among nanoparticles. The anomalous behavior as well as the broad ZFC-peak and a relatively high ZFC magnetization at the lowest temperature observed in the 220 °C sample here are most likely due to such structural inhomogeneity. We also remark that the value of T_o , related to the interaction energy, grows much

faster than the anisotropy energy; *i.e.*, E_a grows by mere 25% from Native to 350°C annealed sample, whereas a near 400% gain was observed in T_o values between the two samples. Thus the abovementioned ‘interaction-to-anisotropy’ energy ratio becomes larger with improved nanocrystallinity, a condition favorable for the formation of an SFM state. The salient features (superspin freezing temperature T_c , anisotropy energy E_a and interaction energy T_o) are summarized in Table 5.2.

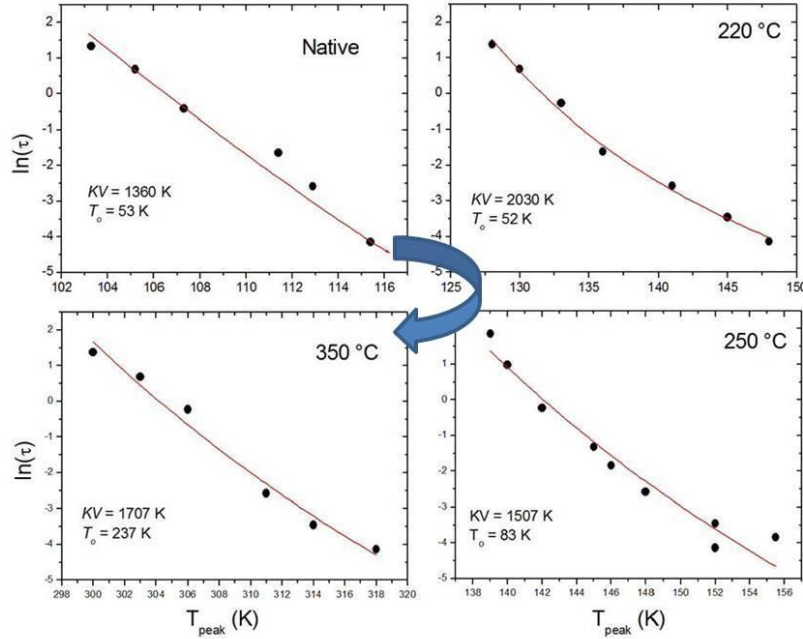


Figure 5.3: Evolution of frequency dependent transition (or collective blocking) temperature of all four samples. τ is the inverse of applied ac field frequency f ($\tau = 1/2\pi f$) and T_{peak} is the temperature at which in-phase ac-susceptibility attains the maximum value at a given frequency. Solid lines are fits to the V-F law.

Table 5.2: critical temperature, anisotropy energy and interaction energy evolution

	Native	220 °C	250 °C	350 °C
T_c (K)	110 (5)	102(10)	220 (5)	290(5)
E_a (K)	1360	2030	1507	1707
T_o (K)	53	52	83	237

5.1.3. Superferromagnetism in Co-Supracrystals

Any further improvement of the sample quality in favor of increasing the dipolar interaction energy (e.g., anisotropy-axis alignment) and/or anisotropy energies (e.g., larger nanoparticles) will cause the transition temperature to exceed the room temperature. Thus a magnetometer that can operate at $T > 300$ K is required. For this purpose, we have recently acquired financial supports (from two regional funding sources) to purchase an add-on furnace insert to the existing CRYOGENIC SQUID magnetometer (see Figure 5.4) at SPEC, CEA-Saclay. The furnace, comprised of a top-loading sample holder and a small resistive heater oven, will enable continuous magnetization measurements in the

temperature range between 77 and 500 K with a maximum applied field DC of 5.5 T. It is also capable of heating the sample space up to 700 K for a short period of time (also in field). With this new high temperature feature, in-field annealing will be possible to align the anisotropy axis of magnetic nanoparticles.

The transition temperature from SPM to SFM (or SSG) state in an anisotropy-axis aligned supracrystal is also an unknown quantity. According to Bouchaud and Zerah [123], in a three-dimensional systems of dipolar moments (particles) on FCC lattices, the intrinsic dipolar FM transition temperature can be defined the dimensionless ratio of $\rho\mu^2/k_B T_c = 2.316 \pm 0.015$ where ρ is the density of dipoles each possessing a magnetic moment μ , and T_c is the SFM transition temperature. Using the values of ρ for an FCC supracrystal (~7 nm diameter nanoparticles and 2.5 nm inter-particle distance) and of μ for an HCP Co nanoparticle (3400 – 4000 μ_B , [141]), one can estimate T_c to be in the order of 300-340 K [142]. This value is not too different from the SSG transition temperature observed in the non-axis-aligned SC sample annealed at 350 °C (~300 K).



Figure 5.4: Future small furnace insert that can be seen in behind the SQUID magnetometer against the wall. (photo, courtesy of CRYOGENIC ®).

5.1.3.1. In-situ magnetic property measurements using SQUID magnetometer

To produce anisotropy-aligned supracrystals, the sample will be annealed (at 350 °C) inside the SQUID magnetometer under the presence of applied magnetic field. *In-situ* measurements of the magnetic properties will follow immediately. The anisotropy-axis alignment is expected to occur during the slow cooling (under magnetic field). The exact field strength required to induce the magnetic anisotropy axis alignment is not yet known; however, previous attempts indicate the field values higher than 1 T is required (unpublished results). The FCC supracrystalline structure of magnetic nanoparticles was not affected during these in-field annealing attempts due to the inter-digitation between the surfactant molecules surrounding the *np*'s that remains intact, holding the nanoparticles within the 3D network.

In the SPM state ($T > T_c$), the magnitude of the low-field magnetization can reveal the degree of axis alignment to a large extent. Between the randomly distributed and the fully aligned anisotropy axis configurations, one expects to find approximately a three-fold difference [143, 144]. Magnetic property measurements that may be used to detect the presence of SFM ordered domains include:

magnetization hysteresis loop $M(H)$ (isothermal magnetization vs. applied field), temperature dependent thermoremanent magnetization $M_{TRM}(T)$, frequency dependence of T_c (ac susceptibility) and ageing effect in the thermoremanent magnetization relaxation, $M_{TRM}(t)$. The ageing experiments will be most interesting in terms of studying the complex nature of the SFM domain growth. Chen *et al.*, has reported an ageing effect in the SFM state of a granular multilayer $\text{Co}_{80}\text{Fe}_{20}/\text{Al}_2\text{O}_3$, where a double relaxation mechanism in $M_{TRM}(t)$ curves were observed, quite different from those found in superspin glasses [119]. Our previous observation in the aligned superspin glasses (cf. Section 4.1), the dynamics of correlated zone growth in an anisotropy axis aligned SSG system deviates from a scaling law common to Heisenberg atomic spin glasses *and* superspin glasses with random anisotropy axis distribution. Therefore measurements on the ageing effects in dipolar SFM state may reveal a slow dynamics belonging to an independent universality class. It should be noted, however, that the bulk samples will always contain supracrystalline domains of various sizes and certain degrees of structural defects are inevitable. Therefore we do not expect to see a clear-cut SFM signature using our SQUID magnetometer that detects only a macroscopic bulk magnetization from the entire sample. To observe a clear SFM transition, if it exists, a more local approach is necessary.

5.1.3.2. Magnetization Measurements of Supracrystalline Nano-Rods Using microHall Probes

Lisiecki *et al.* has also succeeded in growing FCC supracrystals in a columnar, rod-like shape (See figure 5.5). These nano-rods are made of monodisperse Co *np*'s stacked in a FCC supracrystalline structure. The long cylindrical shape and the SC ordering should favor the formation of a superferromagnetic state below T_c .

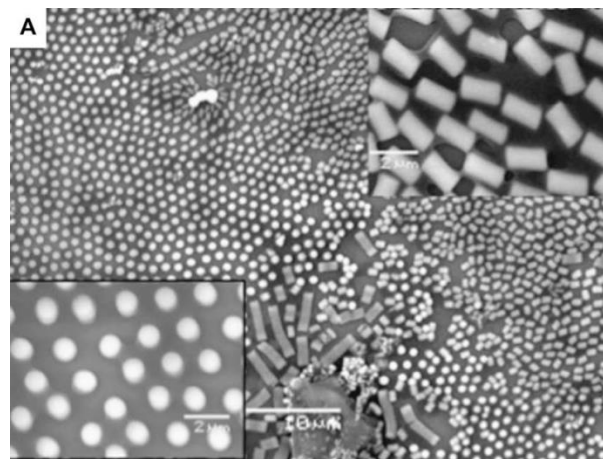


Figure 5.5: SEM image of rod-shaped Co-supracrystals. In each rod, monodisperse 5.7nm Co nanoparticles are arranged in a FCC supracrystalline structure. The average rod-diameter is about 1 μm and the height can reach several microns. (Image taken from [145]).

We will take advantage of the microHall probe technique previously developed for the magnetic noise measurements (cf. Section 4.2). If a spontaneous magnetization due to the SFM (dipolar or not) transition does exist, the microHall probes should be able to detect the corresponding change in the local magnetic field. To perform such experiments, one or several nano-rods must be positioned onto the probe surface with a ~ 100 nm spatial precision. We are currently contacting research groups capable of such feat, and simultaneously, studying the possibility to grow nano-rods directly on the probe surface. Our future microHall measurement sample holder is shown in Figure 5.6., developed

specifically to be used in the lab's new pulsed-tube cryo-cooler cryostat. A similar sample holder will be built for the high temperature measurements.

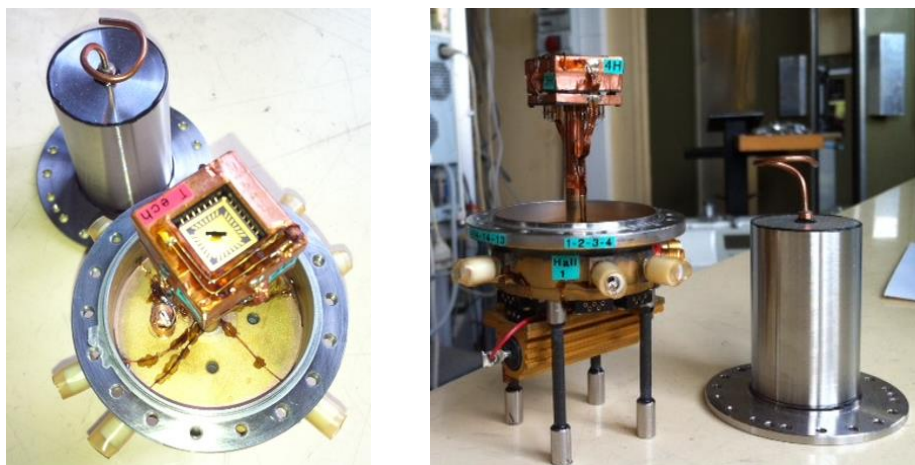


Figure 5.6: MicroHall probe sample holder adapted for pulsed-tube cryocooler. (Left) A microHall probe, visible as a black speck at the center of a clip-on sample holder with 28 electrical connection pins (gold colored). (right) The side view of the sample holder with a cover. A Cu-coil magnet will be placed around the cover to generate magnetic field (200G max).

5.1.4. Beyond Superferromagnetism

From my personal standpoint as a researcher, any new 'class' or 'state' of matter is worth exploring. Of course, some classes of materials are more important than others; meaning that they have greater use in technological applications, they give rise to new theoretical ideas and/or they can be used to confirm existing theories/models. The unique properties of magnetic nanoparticles and their interactions with their environment offer innovative experimental possibilities both inside and outside the field of conventional magnetism. In Chapter 4, I have given one example of their use for investigating the strongly interacting magnetic nanoparticle ensembles to be compared to certain spin glass models. Our understanding of superspin glass dynamics is far from advanced. In this regard, I will further develop local magnetization measurement techniques and protocols based on micro-Hall probes to tackle some of the unanswered questions in (super)spin glasses. The experimental investigation of the step-wise magnetization increase in the SSG state of ferrofluids (predicted to occur at mesoscopic scales when a group of correlated (super)spins become collectively magnetized [146]), for example, will certainly be beneficial for our understanding of (super)spin glasses.

Magnetic nanoparticles can also be used to study 'non-magnetic' property of the surrounding medium. At SPEC, we have developed an experimental approach to investigate the structural glass transition in glycerol via rotational dynamics of magnetic np 's suspended within. By monitoring the nanoparticles' frequency dependent magnetic susceptibility and their slow magnetization relaxations, one can uncover the translational dynamics of the surrounding glycerol molecules. This experiment illustrates a novel use of magnetic np 's as a probe in the physics of "complex systems" which is a unifying research theme of our laboratory, SPHYNX/SPEC.

The vast majority of current technological applications (biomedical, data storage, etc.) of magnetic nanoparticles exploit the *single particle* magnetism; *i.e.*, interactions are not welcome. Therefore, it is

not clear what sort of practical applications can be born out of strongly-interacting magnetic nanoparticle systems. One possibility may be found in the magnetic refrigeration, also known as adiabatic demagnetization. The adiabatic demagnetization is a well-known cooling technique at very low temperatures, often used in research laboratories. It is based on the magnetocaloric effect (MCE); *i.e.*, the adiabatic temperature variation in a magnetic material induced by a change in the external magnetic field [147]. The cooling effect becomes the strongest near the transition temperature where $M(T)$ varies rapidly. By virtue of their high transition temperatures, the use of superparamagnetic materials for magnetic refrigeration has been considered for many years [66, 148] and recently been demonstrated [149, 150]. According to [123] the specific heat “*seems to*” diverge at dipolar ferromagnetic transition temperature; therefore, the FCC structured supracrystals may be a promising candidate for magnetic refrigeration applications. As a long-term goal, and in-line with my second research theme “Magnetic Nanoparticles for Energy Science,” the investigation of the magnetocaloric effect near the SFM/SPM transition in supracrystals is also within the scope of my future research.

5.2. Magnetic Nanoparticles for Energy Science: Magnetothermoelectric Effect in Ferrofluids

The second axis of my future research is in the field of Energy Science. Ever rising energy costs and the need to reduce CO₂ gas emissions prompt wider research efforts in the field of energy science and technology. One possible solution is found in recycling waste heat energy from various sources such as industrial plants, geothermal and solar heating and automobile exhaust systems. Heat is a naturally occurring by-product in all energy conversion processes; from primary fuels to work or to another form of energy, and from energy to work. It is said that between 20 to 50 % of the industrial energy input is lost in some forms of heat (gases, hot equipment surfaces, etc.).

Existing large-scale waste heat recovery systems rely on the heat-pump or the heat-pipe (exchanger) technologies; while on smaller scales, thermoelectric (TE) power generators are also available. The TE generators make use of materials’ intrinsic property to convert thermal energy (temperature gradient across the material) to electric energy (thermoelectric voltage). This property is widely known as the Seebeck effect, named after T. Seebeck who discovered the effect nearly 200 years ago. Conventional TE devices are based mainly on low-gap solid-state semiconductors, and have been commercially available since the mid-20th century. However, due to their limited efficiency, TE generators have never entered the main stream energy market. In recent years, a considerable improvement in the thermoelectric efficiency has been achieved in nanostructured TE materials, although fabrication of such devices remains laborious and costly, and the devices often contain environmentally harmful or scarce elements such as Pb, Te, Sb and Se.

At SPEC, we are engaged in an on-going research activity to explore the thermoelectric effect in conducting liquids, as alternative TE materials. As an extension to our group’s current research effort, I intend to study the magneto-thermoelectricity in ferrofluids. This is a hitherto unexplored property of ferrofluids and consequently, many fundamental aspects must be first resolved. Below, I will outline the theoretical basis that has led us to believe that such an effect exists in ferrofluids and that the outcome will be useful for waste-heat recovery applications.

5.2.1. Background

The unique properties of magnetic nanoparticles and their interactions with their environment have given rise to innovative experimental possibilities outside the field of conventional magnetism. One such example is in the field of energy science, and in particular, thermal engineering. In this respect, research on refrigeration technology based on the magnetoconvection property of ferrofluids (FF) has attracted attention in the past decades [151-153].

On the other hand, the thermoelectric property (or more commonly known as ‘thermopower’) of ferrofluids has so far remained unexplored. In the simplest terms, thermopower describes the material’s property where an electric voltage ΔV , is induced by the application of a temperature difference ΔT across its body:

$$\Delta V = -S_e \Delta T \quad (5.1).$$

S_e is called the Seebeck coefficient. Conversely in the Peltier effect, ΔV application results in a temperature gradient, and it is widely exploited in the solid-state refrigeration and heating device technologies.

The Seebeck effect also occurs in conducting ionic fluids (electrolytes, ionic liquids, liquid metals, etc.). It is coupled to the movement of anions and cations and is closely related to the ‘‘Soret effect’’ which describes their concentration gradients Δn_i , induced by a thermal gradient ΔT ,

$$\left(\frac{\Delta n_i}{n_i} \right) = -\alpha_i \Delta T \quad (5.2)$$

where α_i is called the Soret coefficient. For positive α values, the ions move toward the cold region, while for negative values they accumulate in the hot region. While the Soret effect or ‘‘thermophoresis’’ has been extensively studied during the last decades (see for example [154-156]), the corresponding thermoelectric effects have attracted much less attention. In a simple 1M aqueous solution of HCl, the Seebeck coefficient is approximately 0.2mV/K, comparable to the values reached in TE semiconductors. As TE effects are generally proportional to the entropy transported by the heat/charge carriers, one can expect large Seebeck coefficients in electrolytes containing larger carriers that possess higher degrees of freedom; *e.g.*, macroions, charged copolymers and charged magnetic nanoparticles. However, the coupling between the Seebeck and Soret effects of colloidal dispersion is far from simple. Recently, Majee and Würger have conducted extensive study on the TE effects in charged colloidal dispersions in electrolytes, occurring in multiple steps [157]. Put simply, in the initial step the ions (counter ions) of the electrolyte solution migrate under a temperature gradient. Because the velocity of one ionic species is different from another, a charge separation occurs and a macroscopic electric field is established. The resulting thermoelectric field acts upon the charged colloidal particles in the solution causing them to migrate further. Once the steady-state is reached, the bulk thermoelectric field of the fluid has a complicated form:

$$-S_e = \frac{2(1+\phi)\alpha_+ - 2\alpha_- - \phi T \mu_T / D}{2 + \phi + \phi \xi} \frac{k_B}{e} \quad (5.3).$$

Here α_{\pm} , is the reduced Soret coefficients of positive and negative ions, μ_T the colloidal thermophoretic mobility coefficient and D the diffusion coefficient. ϕ is the ratio of the colloidal charge density to the salinity and ξ the ratio of the colloidal electrophoretic mobility coefficient μ and colloidal diffusion coefficient D ; *i.e.*,

$$\phi = \frac{Z\bar{n}}{n_o} \quad (5.4),$$

$$\xi = \frac{k_B T |\mu|}{e D} \quad (5.5),$$

where $Z\bar{n}$ is the charge density of colloids and $n_o = \frac{1}{2} \sum_i n_i$ the salinity.

A large value of S_e can be expected when ϕ and ξ are small, and $T\mu_T/D$ is large. ϕ can be reduced rather easily by reducing the colloidal particle concentration and/or the effective charge number on colloidal surfaces. It is not at all straightforward; however, to reduce ξ and increase $T\mu_T/D$ simultaneously, as the two mobility coefficients μ and μ_T both depend on the colloidal surface potential ζ , the solvent permittivity ϵ and viscosity η as; $\mu_T \propto \epsilon\zeta^2/\eta T$ and $\mu = \epsilon\zeta/\eta$. In a typical dilute colloidal suspension with about 10 nm sized nanoparticles, $\phi \approx 0.1$, $T\mu_T/D \approx 10$, and $\xi \approx 10$, the expected Seebeck coefficient will amount to a few hundred $\mu\text{V/K}$ at 300 K, about the same order of magnitude as the values found in TE semiconductor materials. However, the pre-factor in the thermophoretic mobility coefficient μ_T (related to the Soret coefficient) is known to be both size and material dependent. And this is where ferrofluids may have an advantage over other colloidal suspensions.

Ferrofluid (*FF*) is a magnetic colloidal dispersion consisting of magnetic nanoparticles (*np*) suspended in a carrier liquid. A typical *np* size is about 10 nm in diameter and the particle surface is either charged (electrostatic repulsion) or coated with a surfactant (steric repulsion) for stabilization against particle aggregation. It has been experimentally demonstrated that the magnitude and the sign of the Soret coefficient of ferrofluids is strongly material dependent (both fluid and nanoparticle). In a dilute ferrofluid with $\gamma\text{-Fe}_2\text{O}_3$ nanoparticles (*i.e.*, magnetic *np* volume fraction at 5 - 6 % or less) $\alpha \approx 0.1/\text{K}$ has been reported [158, 159] and with MnFe_2O_4 nanoparticles, α as high as 1 K^{-1} was obtained at 0.02% dilution [160]. These values are one to two orders of magnitude higher than those found in typical colloidal suspensions. Noting that the surface potential of $\gamma\text{-Fe}_2\text{O}_3$ is in the order of 30 mV, comparable to common colloids, one would expect S_e values in the 1 mV/K range. It should be mentioned here that the number of electrical charges on the nanoparticle surface is quite high (typically, 1-2 charge/nm²); however in stable, aggregate-free ferrofluids the particle surface charges are compensated either by counter ions dispersed in the solution or by polar heads of the surfactants, greatly reducing the effective number of electrical charges per particle to just a few. Lastly, in ferrofluids one can also rely on the effect of external magnetic field to anisotropically control the diffusion of magnetic particles [161], which opens an additional path to influence the thermoelectric voltage generated by the system. To the best of our knowledge, such experimental attempts to verify the connection between (magneto)thermodiffusion of magnetic nanoparticles and the thermoelectric power of ferrofluid have never been reported.

5.2.2. Current and Future Research on Liquid Thermoelectric Materials

Since 2009, I am actively involved in a research project on the thermoelectric property of liquid electrolytes. So far non-aqueous liquids with large ions such as quaternary ammonium cations dissolved in alcohol and binary mixtures of ionic liquid and organic solvent have been investigated. We have recently been granted financial support from regional and national research agencies (Iles de France (Greater Paris region), Campus Saclay and ANR-PROGELEC) to continue our research

efforts, a large part of which will be dedicated to studying the ‘Soret’ and the ‘Seebeck’ effects in ferrofluids and the link between the two.

Collaborators (as of July 2013):

- M. Bonetti and M. Roger, V. Zinovyeva (post-doc 2011-2012) SPEC: Seebeck coefficient and electrical and thermal conductivity measurements, numerical modeling
- R. Perzynski, E. Dubois, V. Peyre, G. Mériquet, G. Demouchy, PECSA UPMC: Ferrofluid synthesis and thermodiffusion (Soret coefficient) measurements

5.2.2.1. Thermoelectric Effects in Nonaqueous Electrolytes and Ionic Liquids (current research)

The possibility of producing an electrical current through two electrodes maintained at different temperatures in a “*thermogalvanic cell*” has been known for a quite some time [162,163]. Unlike the thermoelectric field produced by the Seebeck effect described above, thermogalvanic cells rely solely on the large reaction entropy occurring at the electrodes maintained at two different temperatures. One of the most studied thermocells uses aqueous potassium ferro/ferricyanide redox solutions [162, 164-166]. The proof-of-concept cycled thermogalvanic energy storage through reversible lithium intercalation in Li_xTiS_2 and $\text{Li}_x\text{V}_2\text{O}_5$ electrodes in a cell containing LiPF_6 /alkyl-carbonate as electrolyte was also provided recently [167]. In these systems, the thermoelectric voltage due to the Seebeck effect was considered negligible. In colloidal suspensions and electrolytes containing macroions, however, the thermogalvanic and the Seebeck voltages can be comparable in size. They can either add to produce a larger effect, or cancel each other if the two components carry opposing signs.

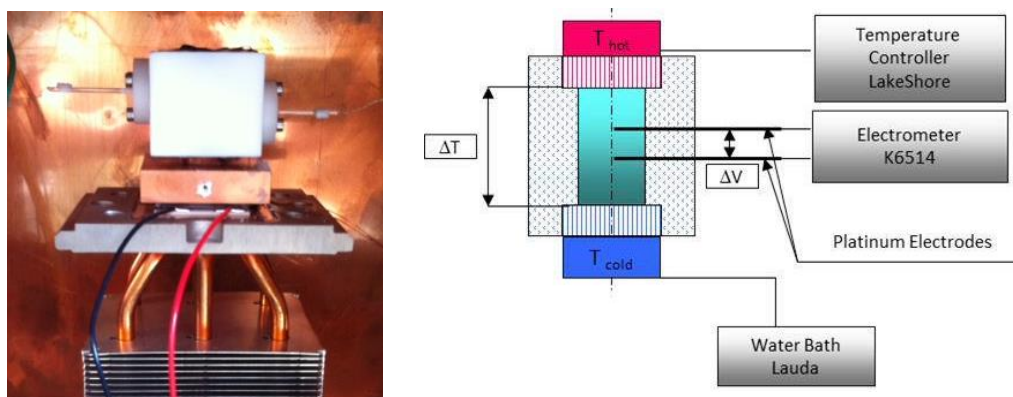


Figure 5.7: Thermopower measurement cell made out of Teflon with two Pt electrodes (left) and the measurement schematics (right). See text for more explanation.

Experimental apparatus for thermopower, thermal conductivity and electrical conductivity measurements have been developed since the start of this project in 2009 [168, 169]. Figure 5.7 shows the Seebeck coefficient measurement cell and its schematic view. The fluid sample is contained in a hollow Teflon cylinder 15 mm high and 10 mm diameter. The two ends of the cylinder are closed by two horizontal thick sapphire windows. The cell is positioned vertically and heated from the top by means of a thin film resistance glued onto the upper window, while the lower window is maintained at a constant temperature, *e.g.*, 30°C. The open-circuit potential is measured by two

home-made electrodes made from polished platinum wires located 6 mm apart from each other with their tips positioned along the vertical cell axis. The open circuit potential difference ΔV is read by an electrometer with large input impedance ($2 \times 10^{14} \Omega$). In 2011, we achieved a high Seebeck coefficient of 7 mV/K in the tetrabutylammoniumnitrate (TBAN) dissolved in 1-dodecanol [169]. However, the corresponding electrical conductivity is poor, lowering the TE efficiency of the liquid.

Low conductivity of electrolytes can be improved by the use of ionic-liquids (ILs). IL's are molten salts whose melting point is usually around room temperature. Pure ILs have relatively good conductivities among conducting liquids ($10\text{-}20 \text{ mS cm}^{-1}$) at 300 K, and it can be enhanced by a factor of ~ 5 at low dilution in an organic polar solvent [170, 171]. There are additional advantages to using ionic liquids for waste-heat recovery applications. For example, in aqueous or common organic media the temperature of the hot electrode is limited to $\sim 100^\circ\text{C}$. This limit can be extended by using IL's, many of which are stable above 200°C . Furthermore, they present a large electrochemical window and are now widely used as electrolytes in lithium batteries and supercapacitors [172, 173]. Abraham *et al.* [174] have recently measured the thermoelectric power in various ionic liquids (IL) with the redox couple I^-/I_3^- and reported a drastic influence of the nature of IL on the entropy change in the redox reaction. But the Seebeck was once again considered negligible.

In our most recent study, we have investigated binary mixtures of an ionic liquid (1-ethyl-3-methylimidazolium tetrafluoroborate $\text{EMIM}^+\text{BF}_4^-$) in an organic solvent (acetonitrile). Both the thermogalvanic and the thermodiffusion contributions (the Seebeck effect) to the overall TE voltage were measured as a function of IL concentration. The thermogalvanic voltage was produced by the reduction/oxidation (redox) reactions of a thiolate/disulfide organic redox couple (McMT/BMT) at the two electrodes. The role of the redox couple is two-fold. First, it produces and fixes the thermogalvanic potential at two electrodes. Second, the redox couple renders the extraction of electrical current from a thermoelectric cell possible via (quasi)reversible reactions. Thermogalvanic potential is established almost immediately once the temperature difference, ΔT is stabilized, whereas the Seebeck potential, due to the diffusion of larger molecules is a slow process that can take several hours. Owing to the characteristic time difference between the two processes, we were able to separate the thermogalvanic voltage and the Seebeck voltage (slow process). Although the measured values $S_{tot} \sim -0.6 \text{ mV/K}$ is much smaller than the value obtained in the previous example, this work demonstrates the possibility to exploit the combination of thermogalvanic and thermodiffusion effects to tailor the thermoelectric power of ionic liquids [175].

5.2.2.2. Thermoelectric and Magnetothermoelectric effects in ferrofluids

The next step in our liquid thermoelectric materials research is to examine systems with even larger charge/heat carriers; *i.e.* colloidal solutions, including ferrofluids. Ferrofluid samples are synthesized by our project partner at PECSA, University of Pierre & Marie Curie (E. Dubois and V. Peyre). The Seebeck coefficient measurement cell is similar to the one used in our previous experiments (see Figure 5.4) but with a smaller liquid volume. In tandem, the Soret coefficient in FF's will be examined also by PECSA, UPMC (R. Perzynski's, G. Demouchy and G. Mériquet) using the Forced Rayleigh scattering technique. Both coefficients will be studied as functions of the nanoparticle concentration and size, as well as the counterion and the redox couple types. As a starting material, we are currently using DMSO (dimethyl sulfoxide) based ferrofluids with $\gamma\text{-Fe}_2\text{O}_3$ nanoparticles and HClO_4^- counterions. A redox couple, ferro/ferricyanide, has been identified to be suitable; that is, reversible

reactions at the electrodes are verified via cyclic voltammetry measurements and the ferrofluid stability is maintained. The initial choice to use DMSO as a carrier fluid is based on its negligibly small thermoelectric power, which will facilitate the observation of the TE effect due to the diffusion of nanoparticles.

In electrolytes, the electrical conductivity and the Seebeck coefficient are manipulated by introducing different ionic species. In ferrofluids, one can also rely on the effect of external magnetic field to control the diffusion of magnetic particles, and consequently, to influence the thermoelectric power of the fluid. The application of transverse magnetic fields (to the temperature gradient) is known to produce both positive and negative effects the Soret coefficient in ferrofluids. For our experiments, the magnetic field will be provided either by a split magnet or a Halbach array magnet. Both magnets can produce 5000 Gauss DC (transverse) field, sufficiently large to saturate the Soret coefficient in dilute ferrofluids saturate.

It needs to be mentioned that DMSO is a very poor electric conductor and thus we do not expect to obtain a highly efficient thermo-electric material as the end product of the current series of experiments. However, the proven, experimental observation of the TE effect stemming from the thermodiffusion of nanoparticles will give rise to a wealth of possibilities to be explored, both fundamentally and technologically. For future applications, it will be far more interesting to use conducting fluids such as ionic liquids. The ionic liquid EAN (Ethylammonium nitrate) or EAN/solvent mixtures will be first tested. Although the ionic conductivity of EAN is not the highest among IL's, ferrofluids in EAN and in some EAN/solvent mixtures have been obtained and are currently under investigation at PECSA (*Understanding colloidal stabilization in ionic liquids*, PhD thesis). Therefore, ample electrochemical and structural data exist on these ferrofluids, which will serve as a model IL based ferrofluid system to conduct the Seebeck and Soret effect measurements. From the 'electric' point-of-view, we also consider imidazolium based ionic liquids or IL/solvent mixtures which have the highest conductivities. Some attempts to prepare ferrofluids based on imidazolium salts are already found in literature (see for example, [176]). The exact choice of the compositions will depend both on the results obtained in the former two types of ferrofluids.

5.2.3. Future Applications

The magnetothermoelectric project is just starting; therefore, it is yet premature to speculate its future performance as a thermoelectric energy material. Nevertheless, it is always instructive to have a quantitative goal in mind to help determine the ensuing research direction. As already stated, liquid thermoelectric materials suffer from poor electrical conductivity, which lowers the overall thermal-to-electric energy conversion efficiency. In general, the efficiency of a TE material η , is defined by the ratio between the electrical power output and total heat input and is expressed as:

$$\eta = \frac{\left[\frac{(T_H - T_C)}{T_H}\right] \left[(1 + ZT)^{\frac{1}{2}} - 1\right]}{\left[(1 + ZT)^{\frac{1}{2}} + \frac{T_C}{T_H}\right]} = \eta_c \frac{\sqrt{1 + ZT} - 1}{\sqrt{1 + ZT} + \frac{T_C}{T_H}} \quad (5.6)$$

where η_c is the Carnot efficiency, T_c the cold and T_H the hot temperature at the end of the sample. ZT is called the "figure of merit." ZT is a dimensionless parameter characterizing the thermoelectric materials' property and is comprised of three transport parameters:

$$ZT = S_e^2 \frac{\sigma}{\kappa} T \quad (5.7)$$

where σ is the electrical conductivity and κ the thermal conductivity. As can be seen from Equations 5.6 and 5.7, the value of η approaches the Carnot efficiency limit when ZT approaches infinity. Strictly speaking, the conversion efficiency at maximum output power (η_{MOP}) differs from η described above; however, for materials with moderate ZT values ($ZT < 1$), η_{MOP} and η are quite close (for in-depth analysis of thermoelectric device efficiency, see [177] for example). Therefore most research efforts in the field of thermoelectric materials focus on maximizing ZT in order to give the initial estimate of the efficiency of a given system.

Thus good thermoelectric materials require a large Seebeck coefficient S_e as well as a high electrical-to-thermal conductivity ratio σ/κ . At room temperature, the best performing nanostructured TE materials based on bismuth chalcogenides have reported ZT values of about 2.4 [178], while in more conventional bulk semiconductor alloys the value is limited to about 1. The electrical and thermal conductivities (σ and κ) of ionic liquids are in the order of 0.01 S/cm and 0.001 W/K/cm, respectively [179]. Therefore, for ionic liquids and colloidal suspensions to be considered credible for TE applications; *i.e.*, comparable to semiconductor based devices, their Seebeck coefficients must be 20mV/K or higher to achieve a ZT value of about 1. Given the high Seebeck coefficient already observed in TBAN/1-dodecanol mixture (7 mV/K, see above), this goal appears to be not too optimistic.

5.2.4. Concluding Remarks

The Seebeck coefficient has scarcely been measured in ionic fluids and never in ferrofluids. To the best of my knowledge, the link between the thermodiffusion of colloidal particles in general and the resulting thermoelectric potential across the carrier fluid has never been demonstrated experimentally. There are many parameters to consider and the resulting physical phenomena to understand before one can consider ferrofluids for thermoelectric energy applications. However, in certain ferrofluids it has been demonstrated that a right combination of the particle size, concentration and the ionic strength of the carrier fluid can result in the Soret coefficient of as high as 1/K. If the effective number of charge per nanoparticle is not too high, then a Seebeck coefficient of a few mV/K can be expected. From the carrier fluid's perspective, some ionic liquids (*e.g.*, EMIM based IL's) show a marked enhancement in the electrical conductivity with increasing temperature from 0.01 S/cm at room temperature to above 0.1 S/cm at 130 °C [180]. Such enhancement in the electrical conductivity can further help increase the material's thermal-to-electrical energy conversion efficiency. Therefore, a successful demonstration of enhanced Seebeck coefficients in ferrofluids as well as the cause-effect relation between the Seebeck and the Soret effects will offer a new possibility in the thermoelectric energy materials research.

References

1. For review, N. A. Frey *et al.*, *Chem. Soc. Rev.*, **38** 2532 (2009).
2. For review, Q. A. Pankhurst *et al.*, *J Phys D: Appl Phys.* **42** 224001 (2009).
3. For example, M. Johanssen *et al.*, *Int. J. Hyperthermia*, **26** 790 (2010).
4. J. L. Dormann, D. Fiorani and E. Tronc, *Adv. Chem. Phys.* **98** 283 (1997).
5. S. Bedanta and W. Kleeman, *J. Phys. D: App. Phys.* **42** 013001 (2009).
6. X. Battle, A. Labarta, *J. Phys D.* **35** R15 (2002).
7. E. Tronc, *et al.*, *J. Mag. Mag. Mat.* **221** 63 (2000).
8. O. Iglésias *et al.*, *J. Nanosci. Nanotech*, **8** 2761 (2008).
9. *Surface Effects in Magnetic Nanoparticles*, ed. D. Fiorani, Nanostructure Science and Technology Series, Springer, DOI: 10.1007/b136494 (2005).
10. J. A. Mydosh, *Spin glasses : and experimental introduction* (Taylor & Francis, London 1993)
11. K. Binder and A. P. Young, *Rev. Mod. Phys.*, **58** 801 (1986).
12. K. H. Fischer and J. A. Hertz, *Spin Glasses and Random Fields* (World Scientific Singapore 1997).
13. D. L. Stein, *Decoherence and Entropy in Complex Systems*, ed. By H. T. Elze, Springer, Lecture Notes in Physics, **633** 349 (2004).
14. E. Vincent, in *Ageing and the Glass Transition*, ed. by M. Henkel, M. Pleimling and R. Sactuary, Lecture Notes in Physics **716** 349 Springer, Berlin (2007), also available at [arXiv:cond-mat/0603583](https://arxiv.org/abs/cond-mat/0603583) (2006).
15. An-H. Lu, E. L. Salabas a,d F. Schüth, *Ang. Chemie*, **46** 1222 (2007).
16. T. Hyeon *Chem. Commun.*: 927 (2003).
17. A. K. Gupta and M. Gupta "Synthesis and surface engineering of iron oxide nanoparticles for biomedical applications" *Biomaterials* **26** 3995 (2005).
18. S. Mornet *et al.*, *Prog. Solid State Chem.* **34** 237 (2006).
19. B. Gleich and J. Weizenecker "Tomographic imaging using the nonlinear response of magnetic particles" *Nature* **435** 1214 (2005).
20. J. Philip, and Shima.P.D. B. Raj "Nanofluid with tunable thermal properties" *Applied Physics Letters* **92** 043108 (2006).
21. L. Néel, *Ann. Geophys.* **5** 99 (1949).
22. E. C. Stoner and E. P; Wolfarth, *philos. Trans. Roy. Soc. London ser. A* 240 599 (1948).
23. Here, the atomic spins are aligned ferromagnetically. It should be noted that other ordering; ferromagnetic and antiferromagnetic, are also possible, but the concept of 'superspin' due to uniformly magnetized spins is valid in all cases.
24. See for example, P. E. Jönsson, *cond-mat/0310684* (2003); P. Nordblad, *J. Phys. D: App. Phys.* **41** 134011 (2008) and references therein.
25. See for example, ref. 6 and references therein.
26. R. C. O'Handley, *Modern Magnetic Materials: Principles and Applications*, Wiley-VCH, Weinheim (2000).
27. D. Givord, Q. Lu and M. F. Rossignol, *Science and Technology of Nanostructured Materials*, ed. G. C. Hadjipanays and G; A. Prinz, Plenum, New York (1991).
28. M. Artus *et al.*, *J. Phys : Condens. Matter* **23** 506001 (2011).
29. M. Farle, *Rep. Prog. Phys.* **61** 755 (1998).
30. H. Kachkachi *et al.*, *Eur. Phys. J. B.* **14** 681 (2000).
31. Y. Labaye *et al.*, *J. Appl. Phys.* **91** 8715 (2002).
32. E. C. Sousa *et al.*, *J. Magn. Magn. Matt.* **272-276** e1215 (2004).
33. J.P. Chen *et al.*, *Phys. Rev. B* **51** 11527 (1995).
34. F. Gazeau *et al.*, *J. Mag. Mag. Mat.* **186** 175 (1998).
35. F. Bødker, S. Mørup and S. Linderøth, *Phys. Rev. Lett* **72** 282 (1994).
36. L. Néel, *C. R. Acd. Sci., Paris* **228** 664 (1949).

37. W. F. Brown, *J. Apply. Phys.* **20** 130S (1959); W. F. Brown, *J. Apply. Phys.* **34** 1319 (1963); W. F. Brown, *Phys. Rev. B*, **130** 1677 (1963).
38. E. Thellier, *C. R. Acad. Sc.*, **213** 1019 (1941); E. Thellier and O. Thellier, *C. R. Acad. Sc.*, **213** 59 (1941); E. Thellier and O. Thellier, *C. R. Acad. Sc.*, **214** 382 (1942).
39. D. J. Dunlop, *Physics Today* **65** 31 (2012).
40. C. P. Bean, *J. Appl. Phys.* **26** 1381 (1955).
41. D. Parker *et al.*, *J. Appl. Phys.* **97** 10A502 (2005).
42. For more detailed description, see J. L. dormann, L. Bessais and D. Fiorani, *J. Phys. C: Solid State Phys.* **21** 2015 (1988).
43. S. Chikazumi, *Physics of Magnetism*, (Krieger, Malabar, Florida 1964).
44. J. A. de Toro *et al.*, *J. Phys. Chem. C* **117** 10213 (2013).
45. S. Bedanta *et al.*, *Phys. Rev. Lett.* **98** 176601 (2007).
46. S. Shtrikmann and E. P. Wohlfarth, *Phys. Lett A* **85** 467 (1981).
47. H. Vogel, *Phys Z.* **22** 645 (1921) and G. S. Fulcher, *J. Am. Ceram. Soc.* **8** 339 (1925)
48. P. Prené *et al.*, *IEEE Trans. Mag.*, **29** 2658 (1993).
49. S. Mørup and E. Tronc, *Phys. Rev. Lett.*, **72** 3278 (1994).
50. S. Mørup, *Eur. Phys. Lett.* **28** 671 (1994).
51. M. El-Hilo, R. W. Chantrell and K.O'Grady, *J. Appl. Phys* **84** 5114 (1998).
52. S. Gangopadhyay *et al.*, *IEEE Trans. Magn.* **29** 2619 (1993).
53. W. Luo *et al.*, *Phys. Rev. Lett.* **67** 2721 (1991).
54. E. Vincent *et al.*, *J. Magn.Mag. Mat.* **161** 209 (1996).
55. H. Mamiya and I. Nakatani, *J. Appl. Phys.* **81** 4733 (1997); H. Mamiya, I. Nakatani and T. Furubayashi, *Phys. Rev. Lett.* **80** 177 (1998)
56. T. Jönsson *et al.*, *Phys. Rev. Lett.* **75** 4138 (1995) ; C. Djurberg *et al.*, *Phys. Rev. Lett.* **79** 5154 (1997); T. Jönsson, P. Svedlindh and M. F. Hansen, *Phys. Rev. Lett.* **81** 3976 (1998); M. F. Hansen *et al.*, *J. Phys: Cond. Matt.* **14** 4901 (2002).
57. S. Batlle, M. Garcia del Muro and A. Labarta, *Phys. Rev. Lett.* **55** 6440 (1997).
58. J. L. Dormann, D. Fiorani and E. Tronc, *J. Magn. Magn. Mater.* **202** 251 (1999).
59. P. E. Jönsson, *Adv. Chem. Phys* **128** 191(2004); P. E. Jönsson *et al.*, *Phys. Rev. B* **71** 104404 (2005).
60. M. Sasaki *et al.*, *Phys. Rev. B* **71** 104405 (2005).
61. S. Sahoo *et al.*, *Phys. Rev. B* **67** 214422 (2003); Xi Chen *et al.*, *Phys. Rev. B* **72** 214436 (2005); O. Petravic *et al.*, *J. Mag. Mag. Mat.* **300** 192 (2006); S. Bedanta *et al.*, *J. Phys. D : Appl. Phys.* **43** 4374002 (2010).
62. P. Nordblad, *J. Phys. D : Appl. Phys.* **41** 134011 (2008).
63. D. Parker *et al.*, *Phys. Rev. B* **77** 104428 (2008).
64. K. Hiroi *et al.*, *Appl. Phys. Lett.* **98** 252505 (2011); K. Hiroi, K. Komatsu and T. Sato, *Phys. Rev. B* **83** 224426 (2011).
65. D. Peddis *et al.*, *Nanotechnology* **21** 125705 (2010); D. Peddis *et al.*, *Phys. Chem. Chem. Phys.* **14** 3126 (2012).
66. S. Mørup *et al.*, *J. Magn. Magn. Mater.* **40** 163 (1983).
67. V. Jahan, S. M. S. Kenari, *American Journal of Intelligent Systems*, **1**, 1 (2011).
68. S. F. Edwards and P. W. Anderson, *J. Phys F*, **5** 965 (1975).
69. D. Sherrington and S. Kirkpatrick, *Phys. Rev. Lett.*, **35** 1792 (1975).
70. G. Parisi, *Phys. Rev. Lett.* **43** 1754 (1979).
71. G. Parisi, *J. Phys. A* **13** 1101 (1980).
72. G. Parisi, *Phys. Rev. Lett.* **50** 1946 (1983).
73. D.S. Fisher and D. A. Huse, *Phys Rev. B* **38** 386 (1988).
74. D.S. Fisher and D. A. Huse, *Phys. Rev. L* **56** 1601 (1986).
75. D.S. Fisher and D. A. Huse, *J. Phys A* **20** L997 (1987).
76. D.S. Fisher and D. A. Huse, *J. Phys A*, **20** L1005 (1987).
77. H.G. Katzgraber, M. Körner, A. P. Young, *Phys Rev B* **73** 224432 (2006).

78. V. Canella and J. A. Mydosh, *Phys Rev. B* **6** 4220 (1972).
79. D. H. Reich et al., *Phys. Rev B*, **42** 4631 (1990).
80. J. Ferré and J. Rajchenbach, *J. Appl. Phys.* **52** 1697 (1981).
81. S. Kirkpatrick and D. Sherrington, *Phys Rev. B*, **17** 4384 (1978).
82. A. T. Ogielski, *Phys. Rev. B*, **32** 7384 (1985).
83. V. Dupuis, *Dynamique Lente des Systèmes Magnétiques Désordonnées*, PhD thesis, Univ. Paris XI (2002).
84. See article attached in Section 4.1.2 and Ref. [59].
85. V. Dupuis et al., *Pramana – J of Phys.* **64** 1109 (2005).
86. E. Vincent et al., *Complex behavior of glassy systems*, ed. by M. Rubi, Lecture Notes in Physics, Springer, Berlin **492** 184 (1997).
87. J. P. Bouchaud and D. S. Dean, *J. Phys I (France)* **5** 265 (1995), M. Sasaki et al., *Eur. Phys. B* **29** 469 (2002).
88. J. P. Bouchaud et al., *Phys. Rev. B* **65** 024439 (2001).
89. A. J. Bray and M. A. Moore, *Phys. Rev. Lett.* **58** 57 (1987).
90. M. Mézard, G. Parisi and M. A. Virasoro, *Spin-Glass Theory and Beyond*, World Scient. Singapore (1987).
91. L. F. Cugliandolo and J. Kurchan, *Phys Rev. B* **60** 922 (1999).
92. P. E. Jönsson et al., *Phys. Rev B*, **70** 174402 (2004).
93. H. Yoshino et al., *Eur. Phys. J. B* **20** 367 (2001).
94. R. Kubo, *Rep. Progr. Phys.* **29**, 255 (1966).
95. T. S. Grigera and N. E. Israeloff, *Phys. Rev. Lett.* **83**, 5038 (1999).
96. See for example; L. Buisson and S. Ciliberto, *Physica (Amsterdam)* **204D**, 1 (2005); C. Maggi, R. DiLeonardo, J. C. Dyre, and G. Ruocco, *Phys. Rev. B*, **81** 104201 (2010).
97. See for example, H. Oucris and N. E. Israeloff, *Nature Phys.* **6** 135 (2009)
98. S. Joubaud, B. Percier, A. Petrosyan, and S. Ciliberto, *Phys. Rev. Lett.* **102** 130601 (2009).
99. S. Jabbari-Farouji et al., *Phys. Rev. Lett.* **98**, 108302 (2007); P. Jop et al., *J. Stat. Mech.* **2009** P04012 (2009).
100. See for example, J. P. Bouchaud, *J. Phys. I (France)* **2** 1705 (1992); G. Parisi, *Phys. Rev. Lett.* **79** 3660 (1997).
101. L.F. Cugliandolo and J. Kurchan, *J. Phys. A* **27** 5749 (1994).
102. M. Ocio, H. Bouchiat, P. Monod, *J. Phys. Lett.* **46**, 647 (1985) ; M. Alba et al., *J. Appl. Phys.* **61** 3683 (1987); Ph. Refregier and M. Ocio, *Rev. Phys. Appl.* **22**, 367 (1987).
103. D. Herisson and M. Ocio, *Phys Rev. Lett* **88** 257202 (2002); D. Hérisson and M. Ocio, *Eur. Phys. J B* **40**, 283 (2004).
104. T. Jonsson, et al., *Phys. Rev. Lett.* **75**, 4138 (1995); T. Jonsson, P. Nordblad, and P. Svedlindh, *Phys. Rev. B* **57**, 497 (1998).
105. See article presented in Section 4.2.4.
106. Y.G. Joh, R. Orbach, G.G. Wood, J. Hammann, E. Vincent, *Phys. Rev. Lett.* **82** 438 (1999); Y.G. Joh, R. Orbach, G.G. Wood, J. Hammann, E. Vincent, *J. Phys. Soc. Jpn.* **69** Suppl. A 215 (2000).
107. F. Bert, V. Dupuis, E. Vincent, J. Hammann, J.-P. Bouchaud *Phys. Rev. Lett.* **92** 167203 (2004).
108. L. Berthier and J-P. Bouchaud, *Phys. Rev. B*, **66** 054404 (2002).
109. L. Berthier and A. P. Young, *Phys. Rev. B* **69** 184423 (2004).
110. J. Kisker et al., *Phys. Rev. B* **53** 6418 (1996).
111. F. Belletti et al., *Phys. Rev. Lett.* **101** 157201 (2008).
112. L. Lundgren, P. Svedlindh and O. Beckman, *Phys. Rev. B* **26** 3990 (1982).
113. E. Vincent et al., *Lecture Notes in Physics* **492** 184 (1997).
114. G. F. Rodriguez, G. G. Kenning, R. Orbach, *Phys. Rev. Lett.* **91** 037203 (2003).
115. E. Vincent et al., *Phys. Rev. B* **52** 1050 (1995).
116. R. Massart, *IEEE Transaction on Magnetism*, **17**, 1247 (1981); *Magnetic Fluids and Application Handbook*, B. Berkowski (ed), Begell House NY (1996).

117. A. Crisanti and F. Ritort, *J. Phys. A* **36** R181 (2003).
118. V. Mosser IProc *9th Int. Conf. Sol. St. Sensors and Actuators, Transducers '97*, Chicago, USA, 16 (1997); V. Mosser *et al.*, *Proc. SPIE*, **5115** 183 (2003).
119. X. Chen *et al.*, *Physical Review B* **68** 054433 (2003).
120. S. Mørup and G. Christiansen, *J. Appl. Phys.* **73** 6955 (1993); S. Mørup, *Hyp. Int.* **90** 171 (1994), M. F. Hansen and S. Mørup, *J. Magn. Mag. Mater.* **184** 262 (1998).
121. J. M. Luttinger and L. Tisza, *Physical Review* **70**, 954 (1946).
122. J. A. Sauer, *Phys. Rev.* **57** 142 (1940).
123. J. P. Bouchaud and P. G. Zerah, *Physical Review B*, **47** 9095 (1993).
124. Y. Imry and S. K. Ma, *Phys. Rev. Lett.* **35** 1399 (1975).
125. R. Kretschmer and K. Binder, *Z. Physik B* **34** 375 (1979).
126. H. Zhang and M. Widom, *Phys. Rev. B* **15** 8951 (1995).
127. F. Borgonovi and G. L. Calerdo, *J. Stat Mech.: Theory and Experiment*, **2010** P05013 (2010).
128. D. G. Rancourt and J. M. Daniels, *Phys. Rev. B* **29** 2410 (1984).
129. S. Bedanta *et al.*, *Physical Review B* **72** 024419 (2005).
130. S. Bedanta *et al.*, *Phys. Rev. Lett* **98** 176601 (2007).
131. L. J. Heyderman *et al.*, *Appl. Phys. Lett.* **85** 4989 (2004).
132. K. Yamamoto *et al.*, *Appl. Phys. Lett.* **93** 082502 (2008)
133. K. Yamamoto *et al.*, *Appl. Phys. Lett.* **98** 072509 (2011).
134. J. Hauschild, H. J. Elmers and U. Gradmann, *Phys. Rev. B* **57** R677 (1998).
135. S. Russ and A. Bunde, *Phys. Rev. B* **74** 024426 (2006)
136. V. Russier, *J. Appl. Phys.* **89** 1287 (2001).
137. J. J. Weis, private communication.
138. I. Lisiecki *et al.*, *Advanced Materials* **15** 712 (2003)
139. I. Lisiecki *et al.*, *Chemical Materials* **19** 4030 (2007)
140. I. Isabelle Lisiecki and M.P. Pileni, *Langmuir* **19** 9486 (2003).
141. X. M. Lin *et al.*, *Langmuir* **14** 7140 (1998)
142. Note: in the work by Bouchaud and Zerah (ref. [6]), the calculated value of T_c was found to be approximately half of the experimentally observed value. Following this example, we state here the twice the T_c value calculated from the equation.
143. See article presented in Section 4.1.1.
144. P. Jönsson and J. L. Garcia-Palacios, *Physical Review B* **64** 174416 (2001).
145. I. Lisiecki and M. P. Pileni, *C. R. Chimie* **12** 235 (2009).
146. H. Yoshino and T. Rizzo, *Phys. Rev. B* **77** 104429 (2008).
147. K. A. Gschneidner, Jr., V. K. Pecharsky, and A. O. Tsokol, *Rep. Prog. Phys.* **68** 1479 (2005).
148. D. Serantes *et al.*, *Physical Review B* **80** 134421 (2009).
149. H. Zeng *et al.*, *Applied Nanoscience* **1** 51, (2011)
150. S. Hariharan and J. Gass, *Review of Advanced Materials Science* **10** 398 (2005).
151. S. A. Suslov, *Phys. Fluids*, **20** 084101 (2008)
152. S. M. Snyder *et al.*, *J. Magn. Magn. Mat.* **262** 269 (2003)
153. K. Nakatsuka *et al.*, *J. Magn. Magn. Mat.* **252** 360 (2002).
154. H. Ning *et al.*, *J. Phys. Chem.B*, **112**, 10927 (2008).
155. D. Kôhler *et al.* W. Stadelmaier, *Macromolecules*, **42** 9147,(2009).
156. A. Parola and R. Piazza, *J. Phys. Cond. Matt.*, **20** 153102 (2008).
157. A.Majee, *Effet thermoélectrique dans les dispersions colloïdale*, PhD thesis, l'Université Bordeaux I, (2012).
158. T. Völker, E. Blums and S. Odenbach, *Int. J. Heat and Mass Trans.* **47** 4315 (2004).
159. J. Lenglet *et al.*, *Phys. Rev. E* **65** 031408 (2002).
160. R. Perzynski, private communication (2013).
161. J. C. Bacri *et al.*, *Phys. Rev. E* **52** 3936 (1995).

162. T.I. Quickenden and Y. Mua, *J. Electrochem. Soc.*, **142** 3985 (1995).
163. Y. Ito, T. Nohira, *Electrochimica Acta*, **45** 2611(2000).
164. T. Ikeshoji, *Bull. Chem. Soc. Jpn.*, **60** 1505 (1986).
165. R. Hu *et al.*, *Nano Lett.*, **10** 838 (2010).
166. M. S. Romano, *et al.*, *J. Therm. Anal. Calorim.*, **109** 1229 (2012).
167. N.S. Hudak and G.G. Amatucci, *J. Electrochem. Soc.*, **45** A572 (2011).
168. M. Bonetti *et al.*, *J. Chem. Phys.*, **134** 114513 (2011).
169. M. Bonetti, S. Nakamae, and M. Roger, *Review of Scientific Instruments* **82** 064906 (2011).
170. A. Stoppa, J. Hunger and R. Buchner, *J. Chem. Eng. Data*, **2009**, 54, 472-479.
171. V.V. Chaban *et al.*, *J. of Phys. Chem. B*, **(2012)** , 116, 7719-7727.
172. N.S Choi *et al.*, *Angew. Chem*, **124** 10134 (2012).
173. N.S Choi *et al.*, *Angew. Chem. Int. Ed.* **51** 9994 (2012).
174. T.J. Abraham, D.R. MacFarlane and J.M. Pringle, *Chem. Comm.*, **47** 6260 (2011).
175. V. Zinovyeva *et al.*, *ChemElectroChem*, doi : 10.1002/celc.201300074 (2013).
176. N. Jain *et al.*, *Appl. Mat. Interfaces*, **3** 662 (2011).
177. C. Goupil *et al.*, *Entropy* **13** 1481 (2011).
178. R. Venkatasubramanian *et al.*, *Nature* **413** 597 (2001).
179. K. E. Johnson, *Electrochem. Soc. Interface* **38** (2007).
180. J. Vila *et al.*, *Fluid Phase Equilibria* **242** 141 (2006).

Research Summary :

During my Ph.D and the following post-doctoral periods, my research was focused on understanding the nature of strongly correlated electrons in oxide conductors such as high-T_c superconductors and colossal magneto-resistive compounds. The electronic conduction is anisotropic in both of these materials, controlled by their respective crystalline structures and chemical compositions. In particular, I have investigated the quasiparticle dynamics unique to the 2D structure near the superconducting transition temperature and at sub-kelvin temperature range through magnetothermal transport measurements (PhD 1995-1998 at Florida State Univ., USA and Post-doc 2000-2002 at ESPCI, Paris). In colossal magneto-resistive oxide materials, I have studied the magneto-thermopower in order to decipher the electron-phonon interaction mechanisms as a function of samples' chemical composition (post-doc 1999-2000 at CEA-Saclay). Through these experiences, I have gained valuable experimental skills and understanding of electron transport in various substances that can be applied to other fields of research.

In 2002, I redirected my research focus on another anisotropic electronic conduction, namely, 1-D conduction in DNA molecules. I joined the group of Dr. H. Bouchiat at Université Paris-XI to study the magnetic and structural properties and their relation to the electrical conduction in λ -DNA molecules. This work led to the uncovering of a surprising low temperature paramagnetic phase in these molecules which served to improve the understanding of the electromagnetic properties of DNA.

Since my arrival to the group SPHYNX (formally GMFD- magnetism, frustration and disorder group) within the SPEC/CEA Saclay in 2005, my main research subjects concern the out-of-equilibrium magnetic state of interacting ferromagnetic nanoparticles, now widely known as "superspin glass" (SSG). There are two physical characteristics of nanoparticles (np) which make them particularly interesting in the field of (super)spin glasses; namely, large individual np magnetic moments (superspins) and their associated slow spin-flip dynamics. The former allows the measurements of magnetic signal arising from a small number of np 's (a few hundred or less), rather than billions of atomic spins required in spin glasses. To this end, I have developed micro-Hall sensor based local magnetometry technique at SPEC (with D. L'Hôte) in collaboration with LSI Polytechnique (M. Konczykowski) and ITRON France (V. Mosser). Micro-Hall sensors are robust in wide magnetic field and temperature ranges and they can be brought into direct contact with samples. These features make micro-Hall sensors an ideal local probe to study the mesoscopic collective superspin dynamics in the SSG state. Through magnetic noise measurements, we were able to observe the violation of the Fluctuation-Dissipation Theorem (FDT) in the SSG state of a frozen ferrofluid. Our experimental findings on the FDT violation in an SSG was the second of its kind in magnetic systems with the only other example being a spin glass measured by the same group at SPEC some 10 years ago.

The second characteristics of nanoparticles (slow superspin dynamics) was exploited to study the growth of SSG order in ferrofluids utilizing a SQUID magnetometer. At low temperatures, superspin rotation processes become so slow that the effective time scale (the experimental time normalized to the individual spin rotation time constant) becomes comparable to the time scale explored by numerical simulations. From our magnetization relaxation measurements, the correlation lengths in the SSG state were determined. Our results allow bridging the time gap between the time frame explored by numerical simulations and that of experiments in atomic spin glasses.

In addition to the activities involving magnetic nanoparticles, I also investigate magnetic phases at very low temperatures (sub-Kelvin) in materials such as graphite intercalated compounds (BaC₆) and kagome antiferromagnets (Herbersmithite). Furthermore, I have initiated with two other researchers at SPEC an applied research project in the liquid thermoelectric energy materials development. This project was inspired by a theoretical work predicting a marked enhancement in the thermoelectric energy efficiency when nano-objects are implemented as charge and heat carriers rather than electrons/holes or ions. The thermoelectric power (Seebeck coefficient), as well as electrical and thermal conductivities are currently investigated in binary mixtures of ionic liquids and organic solvents. As of today we have obtained Seebeck coefficients on the order of thermoelectric solid semiconductors, opening a possibility to explore liquid conductors as the future generation energy materials.

Research projects and perspectives: Magnetic nanoparticle systems - Supermagnetism, Measurement Techniques and Applications

Supermagnetism describes the physics of magnetic states created by assemblies of nanometric magnetic objects; *e.g.*, *superparamagnetism* (SPM), *superspin glass* (SSG) and *superferromagnetism* (SFM). Such assemblies can come in various forms and in dimensions – ferrofluids, 3D-supercrystals, 2D-monolayer films, dispersions in solid matrices, *etc.*

I will focus my future research on the experimental investigations of emerging supermagnetic phenomena in supracrystals and ferrofluids and the development of measurement techniques dedicated to this purpose. Additionally, I intend to explore the applications of magnetic *np*'s in fields outside of magnetism, for example, in complex systems physics and in energy materials.

Superferromagnetism: Recent advances in the magnetic nanoparticle synthesis technique have enabled the creation of supracrystals where nanoparticles are self-organized in regular 3D-lattices over near macroscopic volumes. A possible consequence of such spatial ordering is the emergence of dipolar-SFM state, provided that the magnetic anisotropy-axes of individual particles are all aligned. To achieve this

goal, we have recently obtained external funding (RTRA-Triangle de la Physique 2012 and l'Institut des Systèmes Complexes de Paris Ile de France) to install a high temperature oven insert within the existing SQUID magnetometer at SPEC. This feature will allow the in-field annealing of supracrystals samples with all np anisotropy axes in parallel. With a close collaboration with Dr. I. Lisiecki (LI2M/UMPC), I intend to study the possible existence of a bulk SFM state and its associated phenomena. Some of the key issues to be addressed include: the geometrical limits separating the SFM and SSG states, and the SFM domain wall relaxation dynamics.

Superspin glasses: I will further develop local magnetization measurement techniques and protocols based on micro-Hall sensors to tackle some of the unsolved questions in (super)spin glasses. We have recently developed a new measurement stage for micro-Hall sensors adapted for the use in a pulsed-tube cryostat at SPEC. Our first project will be to measure the step-wise magnetization increase in the SSG state of ferrofluids, which is predicted to occur at mesoscopic scales when a group of correlated (super)spins become magnetized collectively.

Magnetic nanoparticles in other domains of Physics: The unique properties of magnetic nanoparticles and their interactions with their environment give rise to innovative experimental possibilities outside the field of conventional magnetism. For example, I have been developing a new experimental approach to investigate the structural glass transition in glycerol via rotational dynamics of magnetic np 's suspended within. By monitoring the nanoparticles' frequency dependent magnetic susceptibility and magnetization relaxations, one can uncover the dynamic heterogeneity of the surrounding glycerol molecules. This experiment illustrates a novel use of magnetic np 's as a probe in the physics of "complex systems" which is a unifying research theme of our group SPHYNX/SPEC.

Energy: I intend to expand my current research on the materials development for waste heat recovery to include magnetic nanoparticle assemblies. Specifically, I will study the magneto-thermo-electric effects in diluted ferrofluids. The possibility to control and manipulate the mass and heat transport processes in ferrofluids via an external magnetic field has expanded their interest for use in thermal engineering, *e.g.*, magneto-refrigeration. Less explored is the magneto-thermoelectric property of ferrofluids. Under a temperature gradient, the thermo-diffusive behavior (Soret effect) of electrically charged magnetic nanoparticles should produce an electric potential energy gradient in the carrier fluid. Taking the advantage of large Soret coefficients found in ferrofluids, we intend to demonstrate and identify novel magneto-thermoelectric conversion materials that are cost-effective and environmentally sound. This is a joint project with Dr. R. Perzynski's team at PECSA/UPMC and it has recently been awarded external financial supports (LABEX-PALM 2012 and ANR-PROGELEC 2012). Additionally, in the spirit of novel energy materials research, magnetocaloric effect near the SFM/SPM transition of supracrystals is also within the scope of my future research.

Articles dans des revues internationales avec comité de lecture

- V. Zinovyeva, S. Nakamae, M. Bonetti and M. Roger, “Enhanced Thermoelectric Power in Ionic Liquids,” *ChemElectroChem*, published on-line, DOI : 10.1002/celec.201300074 [2013].
- S. Nakamae, C. Crauste-Thibierge, K. Komatsu, D. L’Hôte, Y. Tahri, E. Vincent, E. Dubois, V. Dupuis and R. Perzynski, “Dynamic Correlation Length Growth in Superspin Glass: Bridging Experiments and Simulations,” *Applied Physics Letters* **101** 242409 [2012].
- M. Bonetti, S. Nakamae, and M. Roger, “A simply-designed cell for thermal conductivity measurements of low vapor-pressure liquids,” *Review of Scientific Instruments* **82** 064906 [2011].
- M. Bonetti, S. Nakamae, M. Roger, P. Guenoun, “Large thermoelectric power in non-aqueous electrolyte,” *Journal of Physics and Chemistry* **134** 114513 [2011].
- K. Komatsu, D. L’Hôte, S. Nakamae, V. Mosser, M. Konczykowski, E. Dubois, V. Dupuis, R. Perzynski, “Experimental Evidence of Violation of Fluctuation-Dissipation Theorem in a Superspin Glass”, *Physical Review Letters* **106** 150603 [2011].
- A. Yu. Kasumov, S. Nakamae, M. Cazayous, A. Sacuto, T. Kawasaki, Y. Okahata, and H. Bouchiat, “Effect of Pre-melting on the electrical conductivity in DNA,” *Research Letters in Nanotechnology* [2009].
- E. Wandersman, V. Dupuis, E. Dubois, R. Perzynski, S. Nakamae and E. Vincent, “Extraction of a dynamical correlation length in a superspin glass” *Euro Physics Letters* **84** 37011 [2008].
- S. Nakamae, A. Gauzzi, F. Ladieu, D. L’Hôte, N. Eméry, C. Hérold, J.F. Marêché, P. Lagrange and G. Loupiau, “Absence of superconductivity down to 80 mK in graphite intercalated BaC₆” *Solid State Communications* **145**, 493 [2008].
- F. Bert, S. Nakamae, F. Ladieu, D. L’Hôte, P. Bonville, F. Duc, J.-C. Trombe, and P. Mendels, “Low temperature magnetization of the $S=1/2$ kagome antiferromagnet ZnCu₃(OH)₆Cl₂” *Physical Review B* **76**, 132411 [2007].
- S. Nakamae, M. Cazayous, A. Sacuto, P. Monod, and H. Bouchiat, “Low temperature paramagnetism in B-DNA molecules” *Physical Review Letters* **94**, 248102 [2005].
- S. Nakamae, K. Behnia, N. Mangkorntong, M. Nohara, H. Takagi, S. J. C. Yates and N. E. Hussey, “Electronic ground state of heavily-overdoped non-superconducting La_{2-x}Sr_xCuO₄,” *Physical Review B, Rapid Communications* **68**, 100502 [2003].
- S. Nakamae, K. Behnia, L. Balicas, F. Rullier-Albenque, H. Berger and T. Tamegai, “Effect of controlled disorder on quasiparticle thermal transport in Bi₂Sr₂CaCu₂O₈,” *Physical Review B* **63** 4509 [2001].
- S. Nakamae, D. Colson, A. Forget, I. Legros, C. Ayache, J. F. Marruco and M. Ocio, “Thermoelectric power of hole doped La_{2-2x}Sr_{1+2x}Mn₂O₇ ($0.3 \leq x \leq 0.5$),” *Physical Review B*, **63** 2407 [2001].

- N. Hussey, S. Nakamae, K. Behnia, H. Takagi, C. Urano, S. Adachi and S. Tajima, “Absence of residual quasiparticles in the underdoped cuprate $\text{YBa}_2\text{Cu}_4\text{O}_8$,” *Physical Review Letters*, **85** 4140 [2001].
- Y. Tsabba, S. Reich, S. Nakamae, and J. Schwartz, “Magnetoresistance in underdoped $\text{HgBa}_2\text{Ca}_2\text{Cu}_3\text{O}_8$ films in high magnetic fields,” *Physica C* **307** pt. 3–4, 237 [1998].
- S. Nakamae and J. Schwartz, “Magnetoresistivity of Ag tape co-processed with $\text{Bi}_{1.4}\text{Pb}_{0.6}\text{Sr}_2\text{Ca}_2\text{Cu}_3\text{O}_x$ superconductor,” *Cryogenics* **36** 395 [1996].
- J. Schwartz, S. Nakamae, G. W. Raban Jr., J. K. Heuer, S. Wu, J. L. Wagner and D. G. Hinks, “Large critical density in neutron irradiated polycrystalline $\text{HgBa}_2\text{CuO}_{4+d}$,” *Physical Review B – Rapid Communications* **48** 9932 [1993].

Articles dans des conférences internationales avec comité de lecture

- S. Nakamae, C. Crauste-Thibierge, K. Komatsu, D. L'Hôte, E. Vincent, E. Dubois, V. Dupuis and R. Perzynski, “Anisotropy-axis orientation effect on the magnetization of $\gamma\text{-Fe}_2\text{O}_3$ frozen ferrofluid” *Journal of Physics D: Applied Physics* **43** 474001 [2010].
- K. Komatsu, D. L'Hôte, S. Nakamae, V. Mosser, A. Kerlain, M. Konczykowski, E. Dubois, V. Dupuis, and R. Perzynski, “Magnetic Noise of a Frozen Ferrofluid” *Journal of Applied Physics* **107** 09E140 [2010].
- S. Nakamae, C. Crauste-Thibierge, K. Komatsu, D. L'Hôte, Y. Tahri, E. Vincent, V. Dupuis, E. Dubois and R. Perzynski, “Superspin Glass Aging Behavior in Textured and Non-Textured Frozen Ferrofluid” accepted, *Journal of Applied Physics* **107** 09E135 [2010].
- A. Yu. Kasumov, A. Chepelianskii, S. Gueacuteron, H. Bouchiat, S. Nakamae, M. Cazayous, T. Kawasaki, Y. Okahata, D. Klinov, “Defects and conductivity of DNAs,” *Latest Trends on Systems. 14th WSEAS International Conference on Systems*, 360 [2010].
- K. Komatsu, D. L'Hôte, S. Nakamae, F. Ladieu, V. Mosser, A. Kerlain, M. Konczykowski, E. Dubois, V. Dupuis, R. Perzynski “Noise Measurement of Interacting Ferromagnetic Particles with High Resolution Hall Microprobes” *AIP Conf. Proc.* **1129**, 153 [2009].
- S. Nakamae, Y. Tahri, C. Thibierge, D. L'Hôte, E. Vincent, V. Dupuis, E. Dubois and R. Perzynski, “Observation of superspin glass state in magnetically textured ferrofluid ($\gamma\text{-Fe}_2\text{O}_3$)” *Journal of Applied Physics*, **105**, 07E318 [2009].
- D. L'Hôte, S. Nakamae, F. Ladieu, V. Mosser, A. Kerlain and M. Konczykowski, “A local noise measurement device for magnetic physical systems” *J. Stat. Mech.* P01027 [2009].
- S. Nakamae, C. Capan, K. Behnia, N. E. Hussey, F. Rullier-Albenque, S. Adachi, S. Tajima, C. Urano, Y. Takagi, T. Tamegai, Ch. Marin and E. Walker, “Low- and zero-energy quasiparticle heat transfer in high- T_c superconductors,” *Journal of Physics and Chemistry of Solids* **63** 1065 [2002].
- K. Behnia, S. Nakamae, F. Rullier-Albanque and T. Tamegai, “Effect of controlled disorder on thermal conductivity of Bi_2Tl_2 ,” *Physica C* **341-348** 1809 [2000].

-
- S. Nakamae, D. Colson, I. Legros, A. Forget, M. Ocio J. F. Marucco, "Hole doping effect on the electric, thermoelectric and magnetic properties of double layered manganites," *Supermaterials, NATO Science Series, Mathematics, Physics, and Chemistry*, **8** 77 [2000].
 - S. Nakamae, J. Crow et J. Schwartz, "Neutron irradiation effect on magnetization and thermal conductivity of $(\text{Hg}_{1-x}\text{Bi}_x)\text{Ba}_2\text{Ca}_2\text{Cu}_3\text{O}_8$ superconductor," *IEEE Transaction on Applied Superconductivity* **9** 2300 [1999].
 - S. C. Nakamae, J. Crow and J. Schwartz, "Anisotropic thermal conductivity of c-axis aligned $\text{Bi}_2\text{Sr}_2\text{CaCu}_2\text{O}_x$ superconductor in high magnetic fields," *Journal of Applied Physics* **83** 6786 [1998].
 - S. Nakamae and J. Schwartz, "Thermal conductivity of $\text{Bi}_2\text{Sr}_2\text{CaCu}_2\text{O}_x$ superconductors in high magnetic fields," *IEEE Transaction on Applied Superconductivity* **7** 1699 [1997].
 - S. C. Nakamae and J. Schwartz, "Magnetothermal conductivity of $\text{Bi}_2\text{Sr}_2\text{CaCu}_2\text{O}_x$ bulk superconductor in high magnetic fields," *Journal of Applied Physics* **81** 4931 [1997].
 - S. C. Nakamae and J. Schwartz, "Thermal conductivity of $\text{Bi}_2\text{Sr}_2\text{Ca}_n\text{Cu}_{n+1}\text{O}_x$ bulk superconductors in high magnetic fields," *Journal of Applied Physics* **79** 6567 [1996].
 - E. E. Burkhardt, J. Schwartz and S. Nakamae, "Investigation of the 2-dimensional analytical stability models for high- T_c superconducting tape," *IEEE Transaction on Applied Superconductivity* **52** 430 [1995].
 - E. E. Burkhardt, S. Nakamae and J. Schwartz, "Stability models for high- T_c superconducting conductors," *IEEE Transaction on Applied Superconductivity* **5** 393 [1995].
 - E. E. Burkhardt, J. Schwartz and S. Nakamae, "Analysis of superconducting magnet (SCM)-ground coil interactions for EDS Maglev coil configurations," *IEEE Transaction on Applied Superconductivity* **3** 430 [1993].
-

Conférences invitées dans des congrès internationaux

- "Superspin glass in interacting magnetic nanoparticle systems," *The French-Brazilian meeting on Nanoscience, Nanotechnology and Nanobiotechnology*, Brasilia, Brazil, 10-14 Dec. 2012.
 - "Effect of anisotropy alignment on the superspin glass ageing dynamics of frozen ferrofluids," *8th International Conference on Fine Particle Magnetism*, Uppsala, Sweden 21-24 Juin 2010.
 - "Low and Zero-Energy Quasiparticle Heat Transport in Superconductors," *Todai International Symposium on Correlated Electrons*, ISSP Kashiwa, Kashiwa, Japan, 2-5 Oct. 2001.
-

Présentations invitées

- "Superspin glass of $\gamma\text{-Fe}_2\text{O}_3$ frozen ferrofluid," Séminaire Générale, LAMPS, Université de Perpignan Via Domitia, Décembre 2010.

- “Scientific Research Environment in France,” General Physics Seminar, Department of Physico-Informatics, Keio University, Yokohama, Japan, Juillet 2009.
 - “Carrying Heat and Electricity through 1D conductors,” Research Seminar, Mechanical Engineering Department, Stanford University, Palo Alto, CA, USA, Février 2005.
 - “Low temperature magnetic property of B-DNA molecules,” Séminaire Générale de Physique, Physics Department, University of Groningen, Groningen, Netherlands, Janvier 2005.
-

Posters, Communications orales dans des conférences nationales et internationales (dans les derniers 6 ans)

- “Probing structural glass transition via slow magnetization dynamics of magnetic nanoparticles,” *Workshop on surface/interface effects in nanomagnets*, Porto, Portugal, 25-26 Oct. 2012. (oral)
 - “Superspin glass phase induced by dipole-dipole interactions in magnetic nanoparticle systems,” *Workshop on Dynamics of Nanomagnets Assemblies*, Perpignan, France, 7-8 Nov. 2011. (oral)
 - “Propriétés thermoélectriques d’une nouvelle classe de matériaux: les liquids ioniques,” *GDR Thermoélectricité*, Orsay, 11-12 Juil. 2011. (poster)
 - “Effect of anisotropy alignment on the superspin glass ageing dynamics,” *11th Joint Magnetism and Magnetic Materials/INTERMAG Conference*, Washington DC, USA, 18-22 Janv. 2010. (oral)
 - “Effect of anisotropy alignment on the superspin glass ageing dynamics of frozen ferrofluids,” *Congrès general de la Société Française de Physique*, Palaiseau, 6-10 Juillet 2009. (poster)
 - “Superspin glass state in textured ferrofluid,” *53rd Conference on Magnetism and Magnetic Materials*, Austin, TX, USA, 10-14 Janv. 2008. (oral)
 - “Nanoparticle magnetization and fluctuation detection by micro-Hall sensors,” *10th Joint Magnetism and Magnetic Materials/INTERMAG Conference*, Baltimore, MD, USA, 7-11 Janv. 2007. (oral)
 - “Determination of growing number of correlated superspins from field effect measurements,” *7th International Conference on Fine Particle Magnetism*, Rome, Italy, 9-12 Oct. 2007. (oral)
 - “Superspin Dynamics in Ferrofluids Probed by Micro-Hall Sensors,” *Quantum disordered systems, glassy low temperature physics and the glass transition*, Dresden, Allemagne, 19-24 Mars, 2006. (poster)
-

Rapports de recherches, papiers soumis, articles de vulgarisation

- S. Nakamae, “Radiation Risk after Fukushima: Know and reduce your risk using available data,” *RadioProtection Cirkus*, la portail de la radio protection pratique et opérationnelle, <http://www.rpcirkus.org/> [2011].

- S. Nakamae, M. Cazayous and H. Bouchiat, "Environmental effects on DNA molecules: the link between structural and electrical properties," a book chapter in preparation to appear in *Defects and Conductivity of DNAs*, ed. A. Yu. Kasumov, Pan Stanford Publishing Pte. Ltd. submitted in [2011].
- F. Ladieu, D. L'Hôte, S. Nakamae and E. Vincent, "Local Magnetic Microprobes: a tool for investigating the dynamics of magnetic materials," "Spin glasses; Frustration and disorder," "Frustration without disorder," "Superconductivity at very low temperature," *Scientific Reports-Service de Physique de l'Etat Condensé*, p. 45-50 [2007]

Nom : NAKAMAE **Prénom :** Sawako

Née le 3 octobre 1970 à Yokohama, Japon (nationalité japonaise), mariée, deux enfants

Fonction actuelle : Ingénieur-chercheur au CEA-Saclay, Service de Physique de l'Etat Condensé, groupe SPHYNX (Systèmes Physiques Hors-Equilibre, hYdrodynamique, eNergie et complexeXité) depuis 2005

Adresse professionnelle : SPEC/IRAMIS/DSM CEA-Saclay, 91191 Gif sur Yvette

Tel: 01 6908 7538 Fax: 01 6908 8786 Email : sawako.nakamae@cea.fr

site web : <http://iramis.cea.fr/spec/Phocea/Pisp/index.php?nom=sawako.nakamae>

Adresse personnelle : 44 rue de la Butte aux Cailles, 75013 Paris

Titres

Universitaires

1999 : Thèse de doctorat en physique de la matière condensée à Florida State University, Tallahassee, Floride, USA (directeur : Prof. Jack Crow et Prof. Justin Schwartz)

1995 : Master of Science en Physique à Florida State University, USA

1993 : Bachelor of Science en Physique de l'University of Illinois à Urbana-Champaign, USA

Parcours

Jan.-Juin 2005: Chercheur Étranger au Laboratoire de Physique du Solide de l'École Supérieure de Physique et de Chimie Industrielles (ESPCI), Paris

Sept. 2003-Déc. 2004: ATER à l'Université Paris 7 attachée au Laboratoire de Physique du Solide de l'ESPCI, Paris (dir : Alain Sacuto)

Juil. 2002-Août 2003: Post-doctorat au groupe de physique statistique à l'E.N.S. (dir : Vincent Croquette), Paris et au groupe de physique mésoscopique, Laboratoire de Physique des Solides de l'Université Paris XI, Orsay (dir : Hélène Bouchiat)

Jan. 2000-Juin 2002: Post-doctorat au Laboratoire de Physique Quantique de l'ESPCI, Paris (dir : Kamran Behnia)

Jan. 1999-Déc. 1999: Post-doctorat au SPEC, CEA-Saclay (dir : Dorothée Colson)

Activités

d'enseignement

2008-2009: Tutorat de physique du solide à l'ESPCI

2003-2004: ATER à l'Université Paris 7

1993-1994: Enseignante vacataire à Florida State University

Activités

administratives

2011-présent: Membre de Bureau, LABEX -PALM (Emergence)

2011-présent: Expert du CEA (niveau 2)

2008-présent: Correspondant Web pour le SPEC, CEA-Saclay

2008-2010: Expert extérieur pour la 28^{ème} section de CNRS

Prix

1999-2001: Intern'l Research Fellow Award, National Science Foundation, USA
 1993-1998: Woman in Physics Award, Dépt. de Physique, Florida State Univ.

Organisation de colloques, séminaires

2013: *Workshop on Optical and Electrical Properties of Nanomagnets*, Paris Oct. 24-25 (Co-organisatrice)

2012: *Workshop on Surface and Interface Effects in Nanomagnets*, Porto, Portugal Oct. 25-26 (membre de la comité d'organisation)

2011-present : Coordinateur de « Réunion SPEC » au Service de Physique de l'Etat Condensé, CEA-Saclay

Contrats de recherche

2013-2016: Coordinatrice du projet ANR-PROGELEC « TE-FLIC » *Thermoélectricité dans des ferrofluides, liquides ioniques et colloïdes*, avec le groupe de R. Perzynski, UPMC

2012: Coordinatrice du projet LABEX-PALM-Emergence «MAGTEP » *Magneto-thermoelectric power in ferrofluids*.

2012: Coordinatrice des projets Ile de France-DIM « Petit Four » et RTRA Triangle de la Physique « DipSFM » *Small oven insert for SQUID magnetometer for producing Dipolar SuperFerroMagnetism in Supercrystals of Co-nanoparticles*, avec I. Lisiecki, UPMC et A. Albouy, LPS, U-Psud.

2011-2012: CEA/DSM-Energy « Flûte » *Fluides thermoélectriques*, (partenaire)

2009-2010: Porteuse du projet RTRA-Triangle de la Physique « DynMAG » *Observation of magnetic dynamics in individual nano-objects and their assemblies via Hall microprobes*, avec M. Konczykowski, LSI Ecole Polytechnique.

Encadrements

2012: Stage de 1^{ère} année d'école ingénieur de V. Devries (l'ENS-Paris) 50%

2011: Stage de Master II de M. Woné (l'ENS-Paris) 66%

2010: Stage de 1^{ère} année d'école ingénieur de P. Ronceray (l'ENS-Paris) 100%

2008-2010: Co-encadrement d'un post-doctorant, K. Komatsu 50%

2008: Stage de Master I de Y. Tahri (UVSQ) 100%

2006: Stage de technicien de B. Perrot (Institut Catholique de Lille) 100%

Relecture

Reviewer pour les journaux scientifiques depuis 2002

- American Physical Society
- American Institute of Physics
- Elsevier
- Royal Academy of Chemistry